Valentin Ivanov

ADVANCED AUTOMOTIVE ACTIVE SAFETY SYSTEMS: Focus on Integrated Chassis Control for Conventional and Electric Vehicles with Identification of Road Conditions

URN: urn:nbn:de:gbv:ilm1-2017000475

ADVANCED AUTOMOTIVE ACTIVE SAFETY SYSTEMS:

Focus on Integrated Chassis Control for Conventional and Electric Vehicles with Identification of Road Conditions

Habilitationsschrift

zur Erlangung des akademischen Grades

Doktoringenieur habilitatus (Dr.-Ing. habil.)

vorgelegt der
Fakultät für Maschinenbau der
Technischen Universität Ilmenau

von Herrn

Valentin Ivanov, DSc PhD MechEng

geboren am 16.01.1971 in Minsk / Belarus

1. Gutachter: Univ.-Prof. Dr.-Ing. Klaus Augsburg
2. Gutachter: Prof. Dr.-Ing. Johann Reger
3. Gutachter: Prof. Dr.-Ing. Roland Kasper

Tag der Wissenschaftliche Aussprache: 03.08.2017

urn:nbn:de:gbv:ilm1-2017000475

Contents

PREFACE

The presented work summarizes actual developments of automotive active safety systems and introduces original scientific results obtained by the author during his research activities at Belarusian National Technical University, National Academy of Sciences of Belarus and Technische Universität Ilmenau in close cooperation with industrial and academic partners on international level. Certain of the introduced topics are investigated by the author in a series of individual and collaborative research projects. In particular, it concerns the fellowship "Fuzzy Environment of Tyre-Surface Interaction" of Alexander von Humboldt Foundation (2007), Marie Curie project "INTYRE" (2008-2010), DFG project "Integration of Inverse Dynamics and Fuzzy Sets for Control Processes in Mechatronic Systems" (2013), and the European FP7 project "E-VECTOORC" (2011-2014), which were carried out on research facilities of Automotive Engineering Group at Technische Universität Ilmenau under scientific coordination of Prof. Dr.-Ing. Klaus Augsburg. The author would like to thank Prof. Augsburg for his invaluable support and encouragement during the mentioned projects. The author would like also to express the deepest gratitude to his colleagues Dr. Barys Shyrokau (Delft University of Technology) and Dipl.-Ing. Dzmitry Savitski (Technische Universität Ilmenau) for their long-standing cooperation and inestimable contribution to joint research activities.

NOMENCLATURE AND ABBREVIATIONS

ABS	Anti-lock braking system
AD	Active differential
AFS	Active front steering
aLSD	active limited slip differential
ARC	active anti-roll bars
ARCS	anti-roll control system
ARS	Active rear steering
AS	Active suspension
AWS	All-wheel steering
BA	Brake assistance
CAN	Controller area network
CoG	Centre of gravity
CM	Central motor
DC	Direct current
DOF	Degrees of freedom
DYC	Direct yaw moment control
EHCU	Electro-hydraulic control unit
ESC	Electronic stability control
ESP	Electronic stability programme
FEV	Full electric vehicle
FIS	Fuzzy inference system
FWS	Active front wheel steering
GIS	Geographic information systems
GPS	Global positioning system
HCU	Hydraulic control unit
HEV	Hybrid electric vehicle
HIL	Hardware-in-the-loop
IMC	Integrated motion controller
ITS	Intelligent Transport System
IWM	In-wheel motor
LCA	Lane change assistance

LMS	Least mean squares
OBM	On-boar motor
OS	Oversteer
NHTSA	National Highway Traffic Safety Association
NVH	Noise – Vibration - Harshness
PSD	Power spectrum density
RLS	Recursive least squares
RWS	Active rear wheel steering
SA	Steering assistance
SCB	Slip control boost
SUV	Sport utility vehicle
TC	Traction control
TCS	Traction control system
TPCS	Tyre pressure control system
TV	Torque vectoring
TVbB	Torque vectoring by braking
TVD	Torque vectoring differential
US	Understeer
WSC	Wheel slip control
VCU	Vehicle control unit
V2I	Vehicle-to-infrastructure
V2R	Vehicle-to-road
V2V	Vehicle-to-vehicle
YMC	Yaw moment control

A_b	albedo value
a_x	longitudinal acceleration
a_y	lateral acceleration
B_u	control effectiveness matrix
c_{pf}	pressure ratio between the front left and front right wheels
c_{pr}	pressure ratio between the rear left and rear right wheels
c_α	cornering stiffness
e	control error
E_{perf}	objective function of the performance criteria

E_{st}	objective function of the stability criteria
EMF	electromotive force
f	function
F_d	force considering the road disturbances
F_{driver}	driver control action
F_{em}	brake force generated by electric motor
F_{hydr}	brake force generated by hydraulic brake system
F_r	rolling resistance force
F_x	longitudinal force
F_y	lateral force
F_z	vertical force
g	acceleration of gravity; weighting factor
G_x	normalized longitudinal acceleration
G_y	normalized lateral acceleration
$G(s)$	transfer function
$H(s)$	transfer function
i	current; precipitation intensity
I_w	moment of wheel inertia
J	cost function
k_{pred}	correction coefficient
k_λ	slope of friction-slip curve
K	tyre torsional spring stiffness
K_B	brake gain
K_P, K_I, K_D	PID controller gains
L	vehicle base
m	vehicle mass
m_w	wheel mass
M_z	tyre self-aligning torque
M_ψ	yaw moment of the vehicle
p_{br}	brake pressure
p_{br0}	preload brake pressure
$P_s^m{}_w$	slip power
P_w	instantaneous power of wheels

r	tyre radius (general notation)
r_{dyn}	dynamic tyre radius
s	Laplace operator; wheel slip (in fuzzy inference system)
T_{br}	brake torque
T_c	road surface temperature
T_d	equivalent torque from road disturbances
T_{dem}	torque demand
T_e	ambient temperature
T_{em}	output torque of electric motor
T_{pred}	predictive torque
T_{react}	reactive torque
T_w	drive torque
u	command variable; control demand
u^{CA}	control input vector
V	absolute vehicle velocity
V_{ch}	characteristic vehicle velocity
V_{emf}	back EMF
V_x	longitudinal vehicle velocity
V_y	lateral vehicle velocity
V_w	wheel velocity
V_λ	slip velocity
w	weighting factor, correction factor
x	offset
z	road disturbances
α	tyre slip angle
β	side slip angle
β_τ	brake force distribution coefficient
γ	friction rate; actual yaw rate
γ_{th}	control thresholds
δ	steering angle (general); offset
δ_f	steering angle of front wheels
ε	control error (in ABS algorithm from Section 2.2.3)
η	positive estimator gain

θ	truth value of fuzzy variable
θ_s	torsional angle
κ	texture microprofile
λ	wheel slip (general); texture macroprofile
λ_{ref}	reference wheel slip
λ_x	longitudinal wheel slip
λ^*	combined wheel slip
μ	tyre adhesion coefficient
μ_{act}	actual tyre-road friction coefficient
μ_{env}	friction coefficient by the environmental conditions
μ_{est}	estimated value of the tyre-road friction coefficient
μ_{prim}	primary coefficient of tyre friction
μ_x	coefficient of longitudinal tyre friction
μ_y	coefficient of lateral tyre friction
ν	course angle
ν_{PI}	proportional-integral control demand
ν_{react}	control demand for reactive torque
ξ_{driver_dem}	correction factor
ρ	moisture
ϕ	roll angle
ψ	yaw angle
ω	wheel rotational velocity; motor speed
Ω	yaw rate (in ABS algorithm from Section 2.2.3)
$\in$	control threshold
ℓ	observer gain

LIST OF FIGURES

LIST OF TABLES

INTRODUCTION

Improvement of vehicle safety is still an urgent problem in modern society. In accordance with data of the Global Road Safety Partnership [1], about 1.3 million people are killed and from 40 to 50 million people are injured every year in road accidents. The resulting direct and indirect economic damages can be yearly estimated as > US$ 518 billion (as estimated by World Health Organization in 2000) that costs governments up to 3% of their Gross National Product. This situation attracts considerable attention both of public and private sectors as well as policy-makers. In particular, the European Road Safety Action Plan fixed the target of "halving the overall number of road deaths in the European Union by 2020 starting from 2010" [2]. To reach these and other targets for better road safety, a number of effective measures is being proposed. They concern essentially improvement of road infrastructure, advanced training of road users, technologies of Intelligent Transport Systems (ITS), and efficient engineering solutions for vehicle safety.

The latter measures can be considered as the most impactful way to enhance the safety, and this factor justifies intensive investments in research and development of relevant automotive systems and devices. The design of vehicles deals, in this respect, with passive and active safety. *The passive safety* refers to the constructional features of the vehicle, which determine probability and character of damages in the case of a road accident. The passive safety measures as safety belts and airbags aim at protection of the driver and the passengers from severe crash injuries. *The active safety* relates to probability of the accident occurrence and depends on brake efficiency, stability, handling and other attributes of vehicle dynamics. The importance of active safety in terms of controllable vehicle dynamics can be confirmed by Toyota's data [3] estimating that 20% of serious accidents are caused by the loss-of-control driving situations. Among them, 2/3 of critical situations are related to such factors as wheel blocking at braking, skidding of driving wheels, change of road surface conditions and inadequate steering manoeuvres. A negative influence of the listed factors could be essentially minimized or eliminated by the operation of active systems.

Modern vehicles are being equipped with different automotive control systems, which are responsible for maintenance of the active safety. Figure 1 illustrates progress in development of commercial automotive active safety systems. Nowadays, in accordance with UN/ECE

Regulation No. 13, many classes of vehicles are obliged with the mandatory installation of anti-lock braking systems (ABS) and electronic stability control (ESC). This is due to the fact that already the first variants of active safety systems have shown a material effect. For instance, Table 1 presents corresponding statistical data from different international sources.

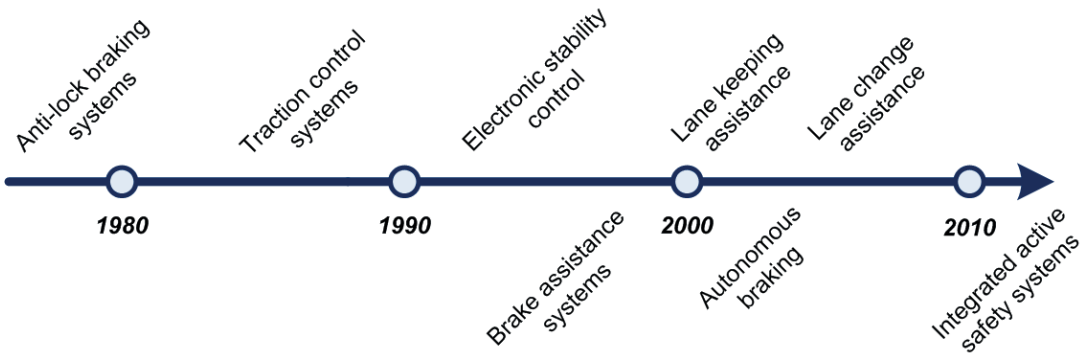

Figure 1 - Commercial implementation of active safety systems

Table 1: Effectiveness of ESC systems

Effect	Value	Country, analysed period
Fatal crash reduction by ESC for: ▪ Run-off-road accidents ▪ Single-vehicle accidents ▪ Rollovers	Cars / Light transport vehicles 36% / 70% 36% / 63% 70% / 88%	USA, 1997-2004 [4]
Accident rate reduction by ESC for: ▪ Single car accidents ▪ Head-on collisions	 ~35% ~30%	Japan, 1995-2000 [3]
Accident rate reduction by ESC for: ▪ Serious crashes ▪ Crashes with fatalities	 11% 25%	UK, 2000-2005 [5]
Overall ESC effectiveness in accident rate reduction on: ▪ Icy roads ▪ Wet roads ▪ Dry roads	 20% 9% 5%	UK, 2000-2005 [5]
Accident rate reduction by ESC for: ▪ Car crashes of all severities ▪ Car rollover crashes of all severities	 27.6% 55.6%	New Zealand & Australia (five selected states), 2001-2008 [6]
Accident rate reduction by ESC for: ▪ Single vehicle accidents ▪ Multi-part accidents	 ~40…50% (estimated) ~10% (estimated)	EU, until 2006 [7]

An analysis of recent research review literature as well as technological trends allows concluding that further development of active safety systems is closely connected with three main areas:

- new sensor technique and elements of road infrastructure for measurement and estimation of parameters of tyre-road interaction and vehicle dynamics;
- integration of active chassis and driveline subsystems to target an advantage in simultaneous improvement of safety, energy efficiency and other factors of vehicle performance;
- the use of electric powertrains in vehicle traction, braking and stability control that requires re-designing the architecture of active safety systems.

In the light of stated introductory information the structure of the presented work is defined as follows. *Chapter 1* introduces fundamental subjects of ground vehicle dynamics, which influence active safety of the vehicle. In particular, relevant sections consider (i) interaction of the rolling tyre with the road surface as well as (ii) longitudinal and lateral vehicle dynamics. Also Chapter 1 gives a survey on functionality of active safety systems from viewpoint of their control architecture. The content addresses sequentially the brake, traction and stability control systems. *Chapter 2* is concerned with methods and tools for definition of tyre-road interaction parameters as the most important information for algorithms of active safety systems. The identification of tyre-surface friction is particularly discussed. *Chapter 3* gives the prospects for enhancement of active safety through implementation of the integrated vehicle dynamics control. Special attention is given here to new variants of system architecture using active chassis subsystems. *Chapter 4* is devoted to active safety systems for electric vehicles. Both state-of-the-art and several recent original solutions are being described.

1. AUTOMOTIVE ACTIVE SAFETY SYSTEMS: BASIC INFORMATION

1.1. Active Safety in Context of Tyre and Vehicle Dynamics

The cause of many critical situations at driving is the vehicle motion close to physical limitations. These limitations bear on both tyre-road interaction dynamics and vehicle dynamics in general. Next paragraphs introduce the main tyre and vehicle dynamics parameters used in active safety control algorithms.

1.1.1. Tyre friction and slip

A tyre is in the effect the final control object of any active safety system. Regardless of the type of the vehicle manoeuvre, required control actions correct practically the brake or traction torques applied to tyres. As result of an external torque application, slip processes occur by the interaction of the tyre with the road surface. Many fundamental studies on tyre friction have deeply investigated the nature of the wheel slip. In this regard the works of Clark [8], Grosch [9], Kummer [10], Moore [11], Persson [12] deserve a particular attention. Despite existing variety of theoretical approaches, most of studies consider that phenomena in the contact of the deformable rolling tyre with the road surface belong to processes of external friction, where the tyre grip as well as energy dissipation in the tyre-road contact are defined by adhesion and hysteresis (deformation-related) friction processes [13], [14]. An excess of shearing stresses over adhesion forces in the tyre-road contact causes the slip of rubber elements. Because of the slip, the longitudinal vehicle velocity V_x is inconsistent with the circumferential velocity of the tyre $\omega \cdot r$. This difference defines the slip velocity V_λ:

$$\begin{aligned} V_\lambda &= V_x - \omega \cdot r_{dyn} \text{ (braking mode)} \\ V_\lambda &= \omega \cdot r_{dyn} - V_x \text{ (traction mode)} \end{aligned}, \tag{1.1}$$

where ω is the wheel rotation velocity, r_{dyn} is the dynamic tyre rolling radius. In a dimensionless form the slip can be written as

$$\lambda = V_\lambda / V_x \ . \tag{1.2}$$

One of the most important tyre characteristics used in control algorithms of automotive active safety systems is the dependence of longitudinal coefficient of tyre friction μ_x from the slip (the coefficient μ_x can be calculated as ratio of longitudinal and normal tyre forces F_x/F_z). Figure 2 shows the tyre adhesion coefficient in relation to the slip. The same qualitative behaviour is also valid for the coefficient of tyre friction μ_x.

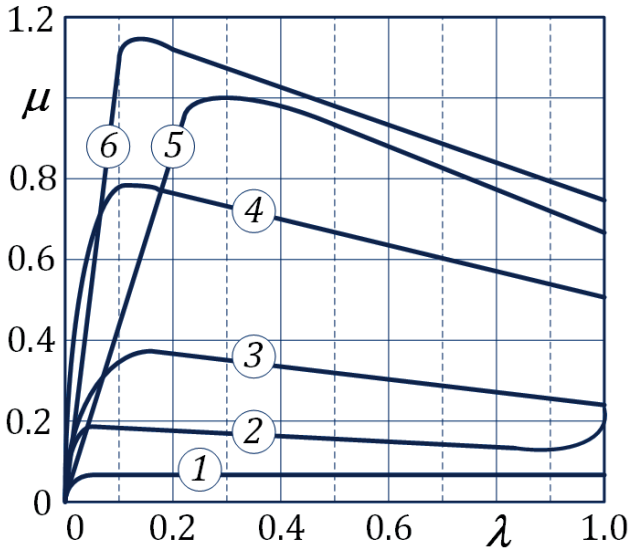

Figure 2 - Generic tyre friction - slip curves.
1 - glaze ice, 2 - snow, 3 - wet cobbled roadway, 4 - wet worn-out asphalt, 5 - dry cobbled roadway, 6 - dry concrete road

Referring to Figure 2, the friction-slip curves have initially a near-linear gradient. The tyre rolling in this area with small values of slip is favourable for vehicle stability. However, maximum braking or traction performance takes place in the extremum area of corresponding friction-slip curve. After the maximum the coefficient of friction decreases. The post-extremum part corresponds to the most adverse conditions of vehicle motion. In this area the tyre can rapidly come to the full slip $\lambda=1$ that means the wheel blocking at braking or the wheel spin at vehicle acceleration. This can lead to skidding of the vehicle and influences negatively on vehicle stability, handling, driving comfort and tyre wearing. Hence, the first target of the active safety control can be as follows: ***To keep the tyre rolling as close as possible to the slip values corresponding to the maximum of friction coefficient***.

Major challenge for the formulated safety control target consists in definition of the maximum of friction coefficient and in proper tracking of relevant reference slip. It is evident from

friction-slip curves on Figure 2 that the position of the friction maximum is significantly varied depending on type of road surface. Moreover, in some cases as the ice road, the extremum of the curve cannot be sharply defined. The drift of maximum friction coefficient or corresponding reference slip area is also subjected to various factors. Based on results of known studies, Table 2 summarizes the most relevant influences.

Table 2: Influence of various factors on tyre friction and slip

Factor	References	Maximum friction	Reference (optimal) slip
Increase of wheel load	[15], [16]	decreased	decreased
Increase of tyre inflation	[15], [17], [18]	mixed drift (decreased / increased)	increased
Growth of water film on wet road	[19], [20]	decreased	marginal influence
Higher initial velocity at braking	[15]	decreased	marginal influence
Increase of velocity in a traction mode	[16], [21]	decreased	not indicated
Decrease of surface temperature on ice	[22]	increased	marginal influence
Increase of dry surface temperature	[23]	decreased	not indicated
Increase of tread stiffness	[24]	increased	decreased
Wearing of tread	[25]	decreased	not indicated

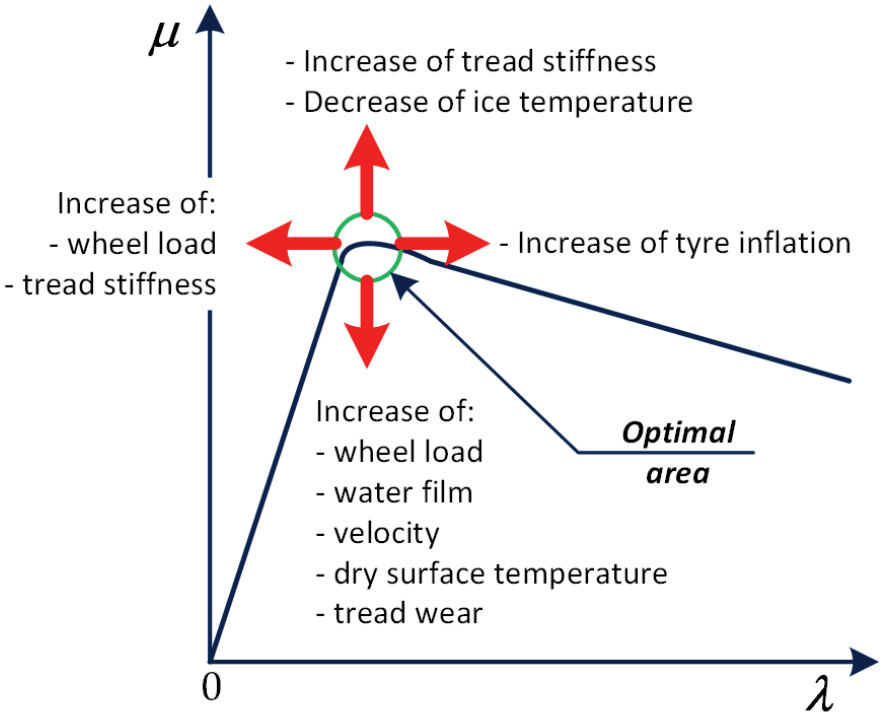

Different factors can also simultaneously affect tyre dynamics during the driving with continuous shifting of optimal tyre-slip area that complicates active safety control. Therefore, the control strategies of active safety systems should include reliable mechanisms of tyre friction estimation and slip target adaptation.

1.1.2. Tyre cornering properties

Tyre cornering dynamics has a crucial influence on vehicle stability and handling. In this regard a required component of control strategies of many active safety systems is the estimation of such parameters like tyre slip angle α and lateral coefficient of tyre friction μ_y. Analysis of research literature shows that different methodologies are proposed for description and modelling of tyre cornering properties. A major contribution to this topic has been done in particular in studies of Fiala [26], Pacejka [27], Peng et al. [28], Sakai [29], and Segel [30]. The process of tyre cornering calls for the slip of rubber elements in tyre-road contact in lateral direction. As a result, the tyre trajectory velocity deviates from longitudinal axis of wheel heading on a certain slip angle α, Figure 3a). In this case the tyre is rolling with the combined slip, which can be deduced from velocity terms shown in Figure3b)-c). Using Eqs. (1.1-1.2) for the general slip λ, the longitudinal λ_x and combined slip λ^* can be written as

$$\lambda_x = \lambda \cdot \cos\alpha \ , \tag{1.3}$$

$$\lambda^* = \sqrt{\lambda^2 + 2\cdot(1-\cos\alpha)\cdot(1-\lambda)} \ . \tag{1.4}$$

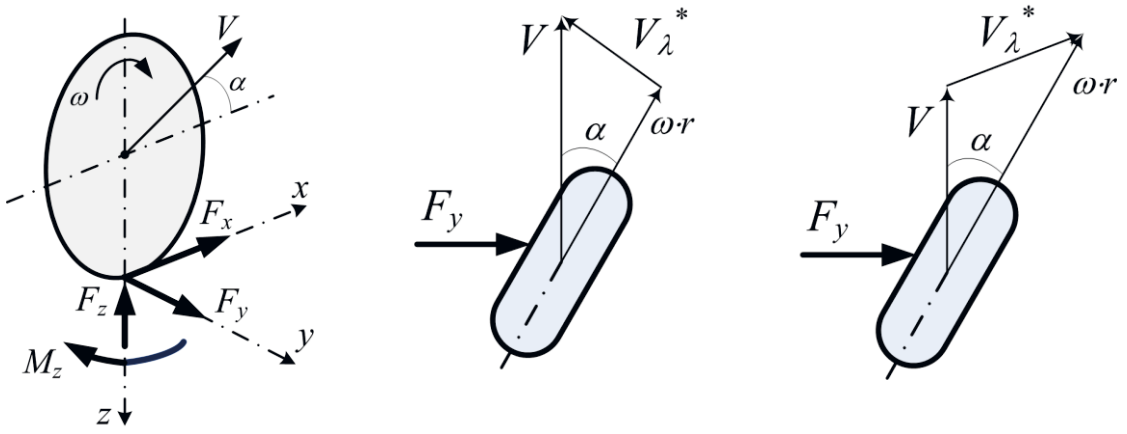

a) b) c)

Figure 3 - Tyre cornering: definition of side slip (a) and velocity terms in braking (b) and traction (c) modes

The main characteristics of lateral tyre dynamics are relations between the lateral coefficient of tyre friction μ_y, the slip and the slip angle, Figure 4. By analogy with the μ_x-parameter, the coefficient μ_y is defined as ratio of the lateral and normal tyre forces F_y/F_z. It can be seen from Figure 4(b) that the $\mu_y(\alpha)$-dependence has initial linear gradient also known as the tyre cornering stiffness c_α:

$$c_\alpha = d\mu_y / d\alpha \,. \tag{1.5}$$

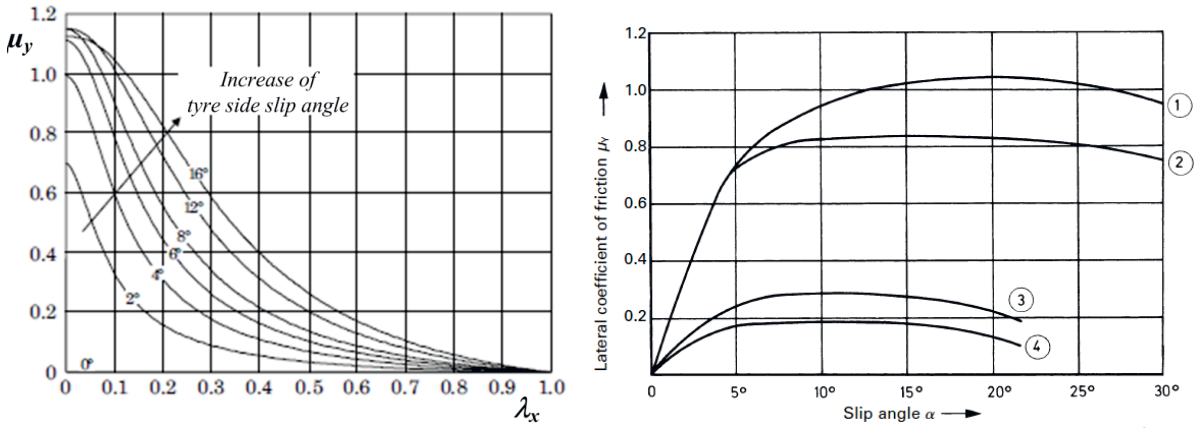

a) b)

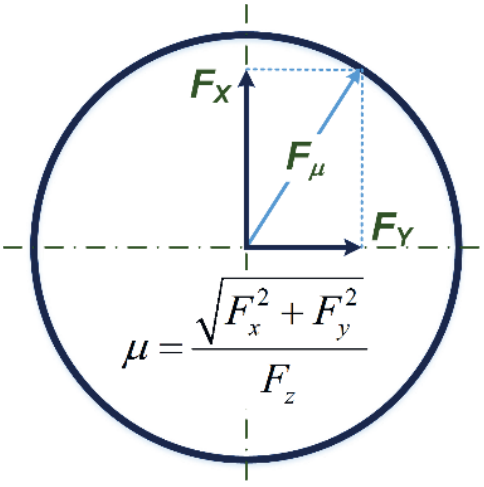

c)

Figure 4 – Characteristics of lateral tyre dynamics
a) Relation of lateral coefficient of friction and longitudinal slip (re-edited from [31]);
b) relation of lateral coefficient friction and side slip angle (reproduced from [32]), 1 - dry, rough concrete, 2 - dry, smooth concrete, 3 - snow cover, 4 - rough ice cover);
c) bottom left –relation of longitudinal and lateral forces in the form of the Kamm's circle

The growth of the tyre side slip angle has a negative influence on the vehicle safety, even by low values of the longitudinal slip. Firstly, this calls for increase of the lateral coefficient of

friction μ_y that reduces simultaneously maximum realizable longitudinal tyre-road contact force. Secondly, the $\mu_y(\alpha)$-curves are being turned at high α-values from linear into non-linear area, where the non-steady-state vehicle cornering takes place. Thus, another target of automotive active safety control is ***to set limits on growth of tyre lateral slip***.

As in the case of longitudinal tyre dynamics, the main parameters of lateral dynamics like the maximum lateral coefficient of tyre friction and the tyre cornering stiffness are influenced not only by the type of road surface but also by different operational factors, Table 3. This sets important adaptation requirements to lateral force estimators and models of tyre lateral dynamics used in algorithms of active safety control systems.

Table 3: Influence of various factors on parameters of lateral tyre dynamics

Factor	References	Maximum lateral friction	Cornering stiffness
Increase of wheel load	[33], [34], [29]	decreased	increased
Increase of tyre inflation	[33]	not indicated	decreased
Increase of velocity	[21]	decreased	decreased
Increase of surface temperature	[23]	decreased	decreased
Increase of ambient temperature	[33]	not indicated	decreased

1.1.3. Vehicle stability

The vehicle stability belongs to the most complex attributes handled by active safety systems. Fundamental works of Karnopp [35], Mitschke [36], Zomotor [37] and other authors introduced a comprehensive analysis of vehicle stability parameters and distinguished the directional stability and roll stability of the vehicle. *The directional stability* is a characteristic of the vehicle (i) to keep the course demanded by the driver control and (ii) to stabilize the direction of motion against external disturbances. In the case of vehicle manoeuvres with distinct lateral dynamics the vector of vehicle velocity V is deviated from the longitudinal X-axis of the earth-fixed coordinate system XY on a certain course angle ν (Figure 5). The course angle is the sum of the yaw angle ψ and the vehicle side slip angle β:

$$\nu = \psi + \beta \ , \tag{1.6}$$

where ψ is the angle between longitudinal axes of the earth-fixed XY and vehicle-fixed xy coordinate systems. Due to deformation processes in tyre-road contact and tyre side slip, the vector of velocity V is deviated from the x-axis on the additional angle β.

The vehicle side slip angle β and the derivative $d\psi/dt$ (yaw rate) are used as the main control indicators of active safety systems responsible for the vehicle stability control. The β-variable is generally a less sensible indicator and can be limited during the control process in relation to reference values depending on the vehicle velocity, road conditions and other factors. The yaw rate $d\psi/dt$ is widely used in algorithms of active safety control systems because this parameter can be measured directly by corresponding on-board sensors. However, the definition of the reference yaw rate dynamics is a comprehensive task requiring consideration of tyre cornering properties and response characteristics of the vehicle. Figure 6a) shows typical response characteristics used in analysis of yaw rate dynamics. In particular it can be seen from the analysis of step input of lateral force that tyres with higher cornering stiffness can provide lower growth of yaw rate during the manoeuvre, Figure6a. The understeer or oversteer behaviour of the vehicle can be also evaluated through yaw rate, Figure 6b). However, the difference in cornering stiffness of front and rear wheels is the main influencing factor on understeer/oversteer behaviour. A detailed discussion of these issues can be found in handbooks of Milliken and Milliken [38], and Wong [39].

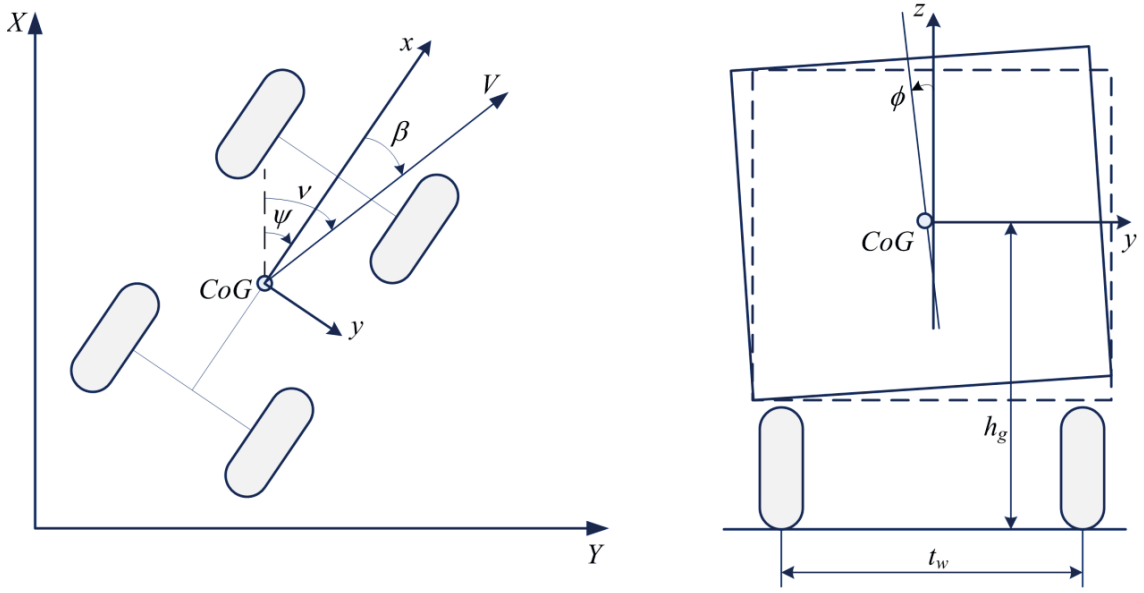

Figure 5 - Parameters of directional and roll stability
CoG - centre of gravity, β - vehicle side slip angle, ψ - yaw angle, ν - course angle, ϕ - roll angle

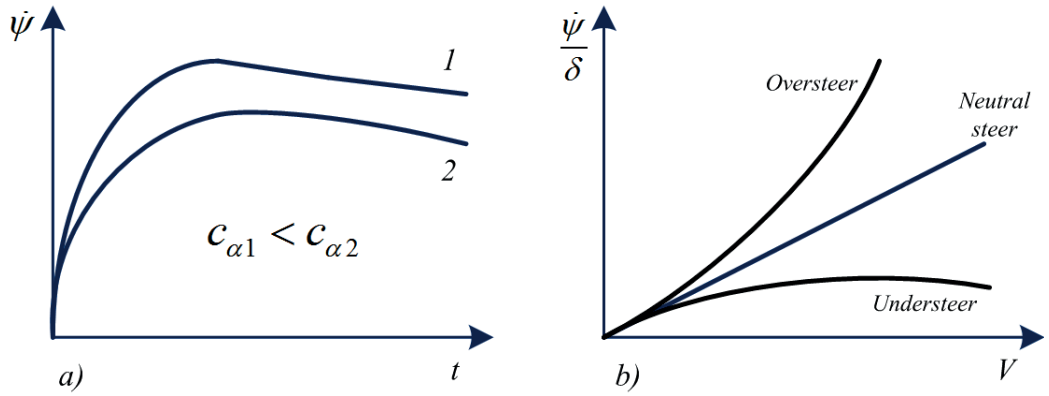

Figure 6 - Generic yaw rate dynamics: Yaw rate responses to a) step input of lateral force and b) steering input (steering angle δ)

Other domain of vehicle stability is connected with roll dynamics. *The roll stability* is a characteristic of the vehicle to stabilize the vertical position against external disturbances, e.g. inertial forces influencing the vehicle body at turning manoeuvres. The main parameter of the roll stability is the roll angle (Figure 5). The growth of the roll angle during turning manoeuvres can cause the vehicle rollover. The ϕ-value can be used in algorithms of vehicle stability control systems as an additional indicator for the optimization of control gains or for the limitation of desired yaw rate [40]. The definition of the roll angle in vehicle models is a complex task requiring taking into account different design and operational factors like suspension kinematics, gyroscopic forces caused by wheel rotation, forces in suspension links, nonlinear character of suspension stiffness, et al. Detailed consideration of the roll dynamics is especially required in stability controllers of sport utility vehicles (SUV), commercial vehicles and buses.

1.1.4. Summary

- Main factors of tyre and vehicle dynamics, which have relation to unsafe/unstable vehicle motion and are subjected to the active safety control, are the wheel slip, tyre friction in longitudinal and lateral domains, side slip angle and yaw rate.
- The key functions of active safety systems, like the wheel slip control or the vehicle stability control, should include mechanisms for adaptation to road conditions and vehicle operational conditions.
- Measurement of some parameters of tyre and vehicle dynamics with on-board sensors available on serial-production vehicles is difficult or even impossible (tyre friction, slip velocity, vehicle side slip angle), therefore the active safety controllers have to use corresponding real-time estimators / observers.

1.2. Diversity of Active Safety Systems

1.2.1. General classification

Automotive industry is proposing nowadays many serial variants of active safety systems distinguished by their functionality. In addition, relevant research and technological studies introduce further conceptual solutions in this area. Figure 7 presents a simplified classification that reflects diversity of active safety systems in context of different domains of vehicle dynamics. Next paragraphs explain the main elements of the proposed classification.

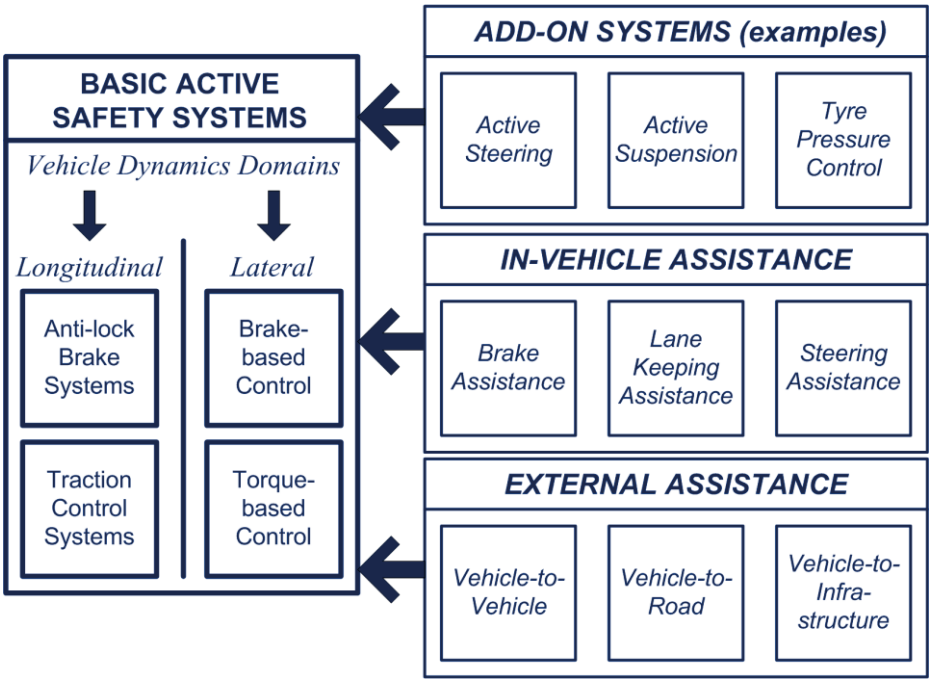

Figure 7 - General classification of active safety systems

Anti-lock braking systems and traction control (TC) systems are responsible for avoiding of critical driving situations related mainly to the *longitudinal* direction of vehicle motion, in particular, through the wheel slip control. The control of the vehicle stability focused on *lateral* dynamics is generally realized with two kinds of systems. The brake-based control systems like ESC correct the vehicle trajectory with the help of selective braking of individual wheels, e.g. by way of motor torque reduction or actuation of the friction brakes. The torque-based control supports the directional stability of the vehicle through redistribution of driving wheel torques, for instance, with the active differential control or the torque vectoring (TV).

Reliable and robust active safety control requires an integration of systems from different domains. This trend to the system integration is of vital importance for the automotive safety enhancement. Figure 7 explains possible variants of the system integration. The integration with *add-on systems* implies the gaining of additional effects from various active chassis and powertrains systems; in doing so, such active systems have usually specific functionality to improve one or another of the vehicle characteristics. For instance, the active front / rear steering can principally improve vehicle handling and driver comfort and can be also integrated with ESC. This brings additional benefits for the directional stability control [41]. The active camber control enhances manoeuvrability, and its integration with the ESC or the active suspension contributes to the directional and rollover stability [42]. Other example relates to the dynamics tyre pressure control. This system aims at the reduction of rolling resistance losses and has for the moment a limited application. However, its integration with ABS and ESC can have a positive influence on the braking performance and steady-state lateral dynamics of the vehicle [43], [44]. The integration with *add-on systems* is the most promising direction in the development of active safety control. Chapter 3 will discuss this matter in more details.

Other variant of integration relates to *in-vehicle assistance systems*. A modern vehicle has various human-machine interface devices aimed at the support of driver actions, especially during complex or dangerous manoeuvres. One of relevant examples is the combination of the brake assistance and ABS functions. In particular, many brake assistance systems can analyse the brake demand through the brake pedal travel sensor. The anti-lock brake system can also use information about brake pedal dynamics for subsequent adaptation of controlled brake pressure to the driver behaviour. Another example is the integration of ESC functions with the lane keeping assistance and the lane change assistance. Both assistance systems contribute to proper accomplishment of manoeuvres with distinct lateral dynamics by the driver that is of benefit for the vehicle stability control.

Active safety systems can obtain the radically new functionality through communication with *external assistance* related to road infrastructure and, especially, ITS. For example, the vehicle-to-vehicle communications make possible a feed-forward adaptation of the vehicle control strategy to critical situations expected from the analysis of behaviour of neighbouring vehicles in a traffic flow. The vehicle-to-road communications allow using information from on-road sensors in controllers of active safety systems (Chapter 2 will introduce relevant examples). From viewpoint of prospective technologies, a fundamentally new engineering approach to the

design of active safety systems can be also provided through unmanned driving, where a global controller of an autonomous or semi-autonomous vehicle fully integrates functions of the brake, traction and stability control.

Further sections discuss recent advances of introduced classes of active safety systems.

1.2.2. Basic active safety systems

A. Systems for longitudinal vehicle dynamics control

Anti-lock braking and traction control systems are responsible for active safety control in relation to longitudinal dynamics of vehicle motion. The main ABS functions are: (i) to prevent excessive wheel slip at braking; (ii) to secure vehicle stability and controllability at braking in any road conditions; (iii) to maximize the brake performance and the tyre friction utilization. The main TC functions are (i) to prevent excessive slip of driving wheels in traction mode, e.g. during vehicle take-off; (ii) to optimize the wheel traction forces during motion on irregular surfaces like roads with slopes or uphill / downhill roads. Because TC systems have limited functionality from viewpoint of active safety, further paragraphs are dedicated to problems of the brake control.

The anti-lock braking systems are in serial production from early 1970s and, therefore, they have well-established technologies and control design principles. The largest share of the ABS market for passenger cars belongs to the variants with relay valves as actuators. Such ABS design implements generally the relay on-off controller logic with the simultaneous use of the wheel slip and the deceleration as control parameters. This logic is generally realized in the form of the rule-based control with appointed thresholds [45]. To give an example, one may refer to the study [46] describing ABS algorithm with the wheel slip and acceleration offsets used to formulate the control logic. The offsets are

$$x_1 = \lambda - \lambda^*, \qquad x_2 = \dot{\omega} \cdot r - a_x^* \tag{1.7}$$

where λ^* and a_x^* are the slip ratio and wheel acceleration corresponding to maximum of $\mu(\lambda)$-curve. Figure 8 introduces the ABS logic operating with the described offsets. It can be seen

that the system can come up to five-phase automation mode by the corresponding specification of command variables and control thresholds. However, the full stability of the system can be guaranteed only when the μ-slip curve has a distinct extremum, and this extremum is being unchanged during the braking manoeuvre.

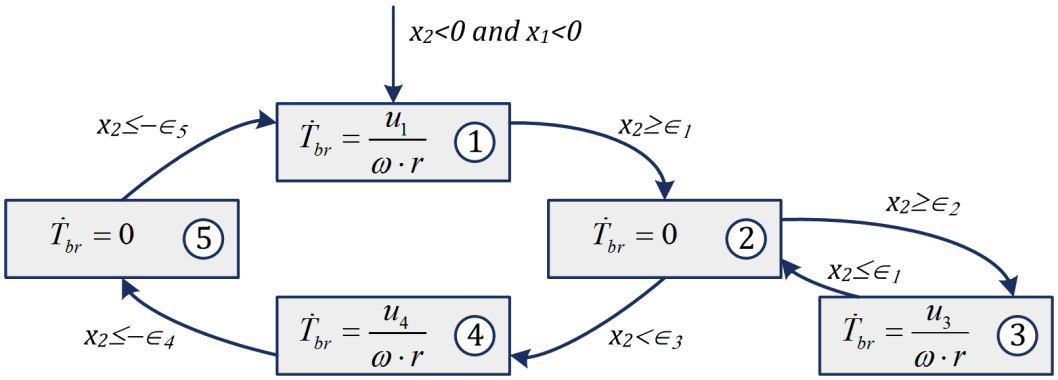

Figure 8 - Five-phase ABS logic (adapted from [46]); T_{br} - brake torque; u - command variables; $\in$ - control thresholds

Analysis of recent research and technical literature shows that modern brake-by-wire technologies are awakening interest in new approaches to the brake-based safety control [47], [48], [49]. This is especially relevant to electro-hydraulic brake systems with a decoupled architecture, where the controller unit sets up the demanded pressure in the hydraulic brake callipers in accordance with the brake pedal position and / or the brake pedal force. Advantages of such systems include fast system response time, tuneable brake pedal feel characteristics, and, as for electric vehicles, a better possibility for sharing of brake functions with an electric drivetrain. From viewpoint of the ABS design, proportional actuators of brake-by-wire systems allows realization of continuous control processes, which are significantly different from the previously introduced discrete method for the ABS with relay valves. The essence of the continuous ABS approach is that the brake torque modulation is following reference wheel slip dynamics without crisp control thresholds. Continuous controllers can be realized with different methods. For example, the study [50] discusses the model-based wheel slip control with the local linearization and gain-scheduling based on the linear-quadratic regulator for electromechanical brake actuators. The work [51] describes another model-based wheel slip control approach using a reference slip calculator and PI-controller with anti-windup strategy for the brake torque. As differentiated from the rule-based control, the continuous brake torque modulation is favourable to the wheel operation close to the optimum slip area without essential

oscillations of the brake torque. This is advantageous not only for vehicle safety but also for the control stability and driver comfort at braking. Figure 9 provides a corresponding comparative example for the braking of SUV on low-μ road with two ABS variants [52]. It can be seen that the continuous ABS secures shorter stopping time and minimal deviations of wheel velocities from a reference value.

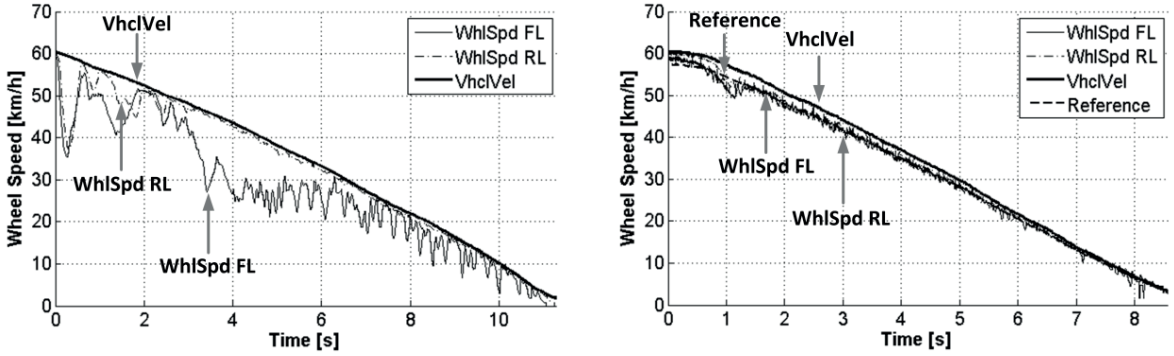

Figure 9 - Comparison of rule-based (left) and continuous (right) ABS operation. VhcVel - vehicle velocity; WhlSpd - wheel speed; FL, RL - front left and rear left wheels [52]

The continuous ABS approach is also reasonable for electric vehicles, where the brake torque modulation is possible by the use of individually controlled in-wheel or on-board electric motors operating in a regeneration mode. It allows a better utilization of fast-response dynamics of electric motors for purposes of the brake control. This matter will be discussed in Section 4 in more details.

B. Systems for lateral vehicle dynamics control

Active safety systems associated with lateral vehicle dynamics, like ESC or TV, are controlling the brake or driving torque individually for each wheel in order to keep the vehicle motion in safe limits in terms of yaw rate and sideslip angle. Therefore, the information about these parameters is crucial for lateral vehicle dynamics controllers. The availability of yaw rate sensor on serial vehicles is beneficial for the control algorithms observing and processing the yaw-based control parameters. However, the use of the vehicle side slip as the control parameter is more difficult due to lack of corresponding on-board measurement tools. For this reason, many algorithms calculate the vehicle side slip through estimators / observers [53], [54], [55].

Two different approaches to the architecture of active safety systems can generally realize both yaw rate and vehicle sideslip control. In the case of *the brake-based control* the generation of brake torques on individual wheels corrects the vehicle motion to keep the required vehicle trajectory. ESC systems apply this approach. *The torque-based control* supposes redistribution of driving torques between front/rear or left/right wheels to achieve the required yaw motion and maintain the vehicle side slip in safe limits. Such methods are realized in torque vectoring systems and active differentials. Next paragraphs introduce some examples of brake- and torque-based vehicle stability control.

Modern ESC systems have usually a very comprehensive architecture covering formulation of control signals for actuators, estimation of vehicle dynamics parameters, fail-safe functions etc. However, a key element is in fact the controller defining the correcting yaw moment M_ψ on the vehicle to keep the yaw rate or the side slip angle in required limits. As it can be shown in a general case from Figure 10, the braking of a selected wheel takes place when the actual yaw rate is above the reference yaw rate. As a result, it reduces the lateral force on the selected wheel and causes the moment M_ψ correcting the yaw motion of the vehicle. Figure 11 explains a simplified procedure of the relevant *brake-based* yaw control.

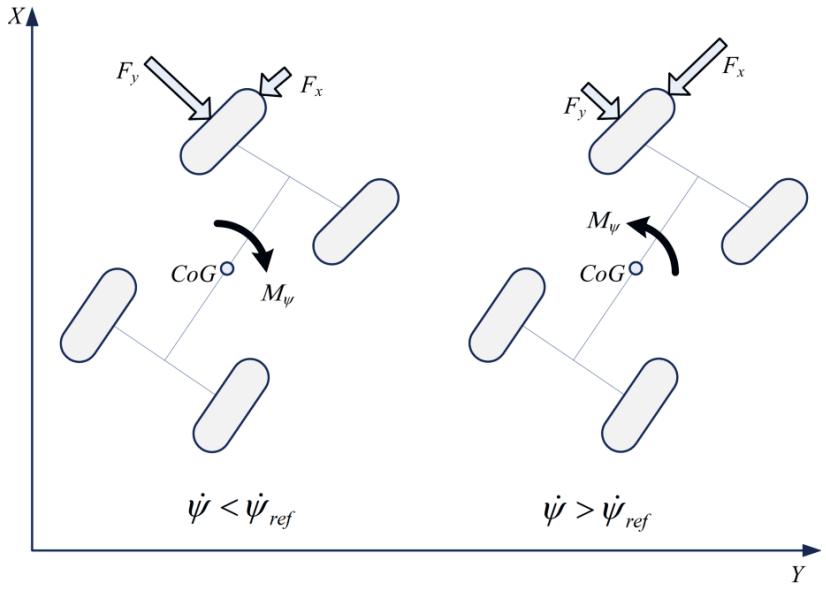

Figure 10 - General principle of correcting yaw moment generation

In accordance with Figure 11, the estimated value of the tyre-road friction coefficient μ_{est}, the vehicle velocity V_x and the front wheel steering angle δ_f allow generating the reference yaw rate

for actual driving conditions $(d\psi/dt)_{ref}$ from the vehicle model. Then the reference yaw rate is compared with the actual yaw rate value $d\psi/dt$, which can be obtained directly from the yaw rate sensor installed on the vehicle. Following the schemes from Figure 10, a single wheel (front right or front left) to be controlled is being selected on the next step. For the selected wheel, the reference slip generator computes the value of λ_{ref} corresponding to the demanded correcting yaw moment of the vehicle. The wheel slip controller allocates the demanded brake torque T_{dem} to be realized by the brake system on the corresponding wheel in order to generate the correcting yaw moment of the vehicle. In more complex situations, several wheels can be simultaneously controlled with individually tuned values and rates of corresponding brake torques. The *brake-based* stability control systems can also use the motor braking in certain control situations.

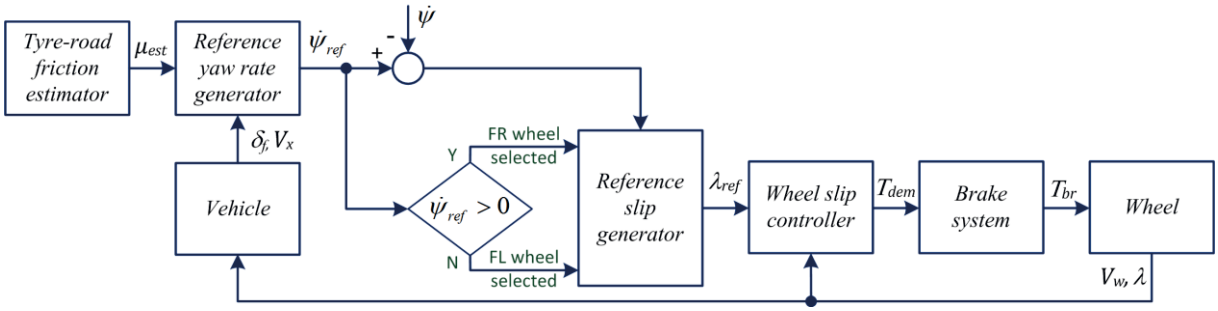

Figure 11 - Example of brake-based yaw moment control layout

The variant of another architecture of the *brake-based* stability control system is depicted on Figure 12. This system uses both the yaw rate and the side slip angle as the control parameters and can be realized through diverse control methods. There are many other control methods, which are known from published studies and can be applied for the *brake-based* stability control systems. Their analysis lies outside of the targets of the presented work. However, some examples illustrating practical implementation of the *brake-based* ESC will be later given in Chapters 2 and 3.

The generation of the vehicle yaw moment correcting the redundant yaw rate or side slip angle can be realized not only through braking but also by corresponding redistribution of driving torques between individual wheels. However, such *torque-based* stability control is mainly relevant to all-wheel drive vehicles with active inter-axle and inter-wheel differentials or to electric vehicles with individual in-wheel and on-board motors. The related torque vectoring

systems are appropriately discussed in particular in [56], [57], [58], [59] for vehicles with active differentials and in [60], [61], [62] for electric vehicles. The main idea behind the *torque-based* vehicle stability control is to distribute torques with the aims both of keeping the vehicle stable and increasing the traction efficiency. Different strategies are being proposed for this purpose. For instance, the following methods are known from [63], [64]:

- *Constant torque distribution* – driving forces are distributed between the right and left rear wheels while their distribution between the front and rear wheels is kept constant.
- *Slip-based torque distribution* - driving forces are distributed between the wheels in accordance with the appointed left/right or front/rear wheel slip difference.
- *Torque distribution in proportion to the vertical load* – optimization of the ratio of the vertical road on a wheel to the total load on all wheels.

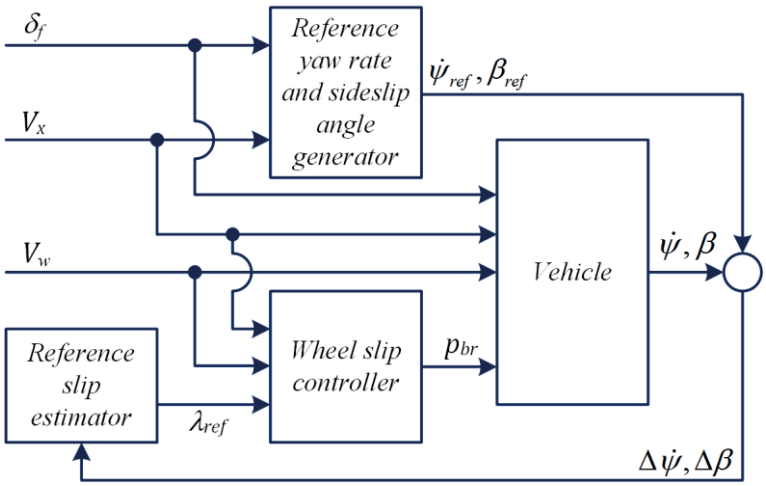

Figure 12 - Example of stability control system architecture (adapted from [65])

The *torque-based* control allows not only correcting the vehicle yaw dynamics but also influencing the vehicle agility by changing understeer / oversteer characteristics. As indicated on Figure 13, individual wheel torque control can reduce the understeer gradient and extend its linear region. In doing so, vehicle responsiveness is enhanced and the stability limit for steady-state cornering is extended. Also the torque-based control increases the maximum level of lateral acceleration. In general, this change improves the lateral performance of the vehicle. The *torque-based* control of the lateral vehicle dynamics has a high potential for electric vehicles with individually controlled motors for each wheel. Such powertrain configuration grants more

flexibility to the system architecture that allows to support the vehicle safety and handling and simultaneously to improve overall energy efficiency of the electric vehicle.

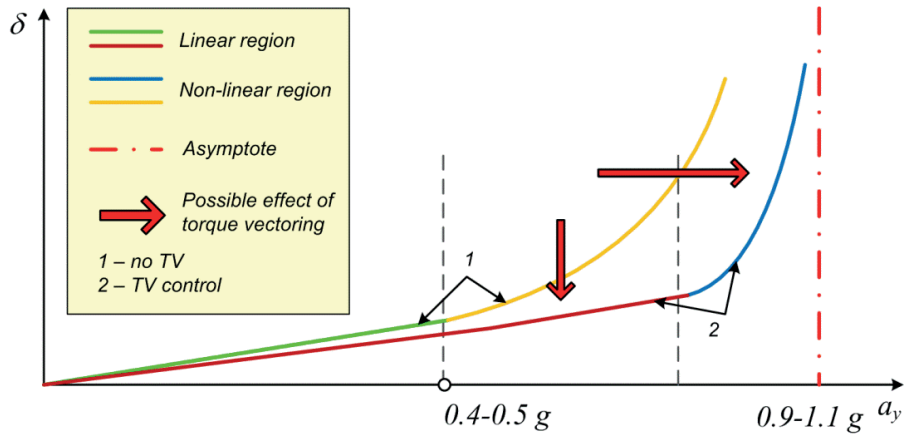

Figure 13 - Modification of vehicle understeer through torque vectoring

1.2.3. Add-on systems

One of important trends in modern vehicle design is the application of semi-active and active chassis systems instead of traditional passive systems. This is particularly true for suspension, steering and systems influencing the wheel kinematics (e.g. camber or toe angle) and tyre properties (e.g. tyre pressure). Active chassis systems not only improve the vehicle performance features such as ride comfort, steerability, or handing but also contribute to safety enhancement. Next sections give a brief overview of relevant application cases.

A. Active steering

There are several variants of the active steering that can support the vehicle safety through an integration with basic systems introduced in Section 1.2.2: active front steering [66], [67]; active rear steering [68]; all-wheel steering [69]. Usually the mentioned systems have electro-hydraulic or electro-mechanical implementation, including steer-by-wire design [70], [71].

One of the most widespread combinations in this regard is the integration of the yaw dynamics control and the active steering on the front wheels only [66], [72], [73]. Such an integration can reduce the driver's loading by complex manoeuvres with critical lateral dynamics. Additional benefits for the stability from the AFS are observed in situations with external disturbances like

the side wind or driving/braking on split-μ road. Recent studies give much attention for the integration not only the AFS but also the active rear steering (ARS) and the all-wheel steering (AWS) control. A comparative investigation in this regard has been presented in [74], [75] for AFS/YMC, ARS/YMC and AWS/YMC configurations. It was demonstrated by the simulation of lane change maneuvers that (i) the integration with AFS gives benefits in minimization of the side slip angle and more precise path following, (ii) the ARS/YMC is efficient for the situations with deterioration in the rear wheel cornering stiffness, and (iii) the AWS/YMC integration can be characterized by high stability limits with high responsiveness.

The integration of the torque-based yaw moment control with the active steering is specifically promising in context of electric vehicles. In particular, the study [76] introduced a hybrid electric vehicle with the integrated control of the AFS and the axial motors with the inter-wheel differential generating individual wheel torques. Such a control architecture has demonstrated a potential to reduction of side slip and yaw rate both of oversteer and understeer vehicle in the simulation of J-turn and single-lane change maneuvers. Another architecture has been investigated in [77] and [78], where a full electric vehicle is equipped with in-wheel motors. The integration covered the joint operation of the electric motor torque control with the AFS and the AWS. Both variants have been tested on the experimental vehicle and demonstrated, in particular, the robustness to cornering stiffness variation.

B. Controllable suspension

A controllable - both semi-active and active - suspension influences vertical dynamics of the vehicle to improve first of all the ride comfort. However the controllable suspension can also bring certain positive effects to the roll stability through coordinated operation with other active safety systems [79], [80], [81], [82]. For example, the study [83] investigated the brake-based yaw moment control with the active steering and the active suspension represented by the active roll bars and controlled magnetorheological dampers. The functional tests of the discussed combination for a midsize rear wheel drive car are demonstrated that the inclusion of active suspension elements allows essential reduction of the time of brake system control activation. This can be considered as beneficial in terms of (i) lesser losses of the vehicle velocity during the manoeuvre and (ii) a certain increase of the energy efficiency due to lower demand in the operation of the brake actuators. Several studies pay attention to the influence of the suspension control on longitudinal vehicle dynamics [84], [85] . Here a particular effect can be observed

for conditions of a rough, uneven surface. For instance, the work [86] investigated the braking of a sport utility vehicle on two types of rough terrain. The integration has concerned ABS and a semi-active $4S_4$ suspension unit. Considering braking from 80 km/h to 10 km/h, the optimal integration variants allowed reducing the stopping distance as shown on Figure 14.

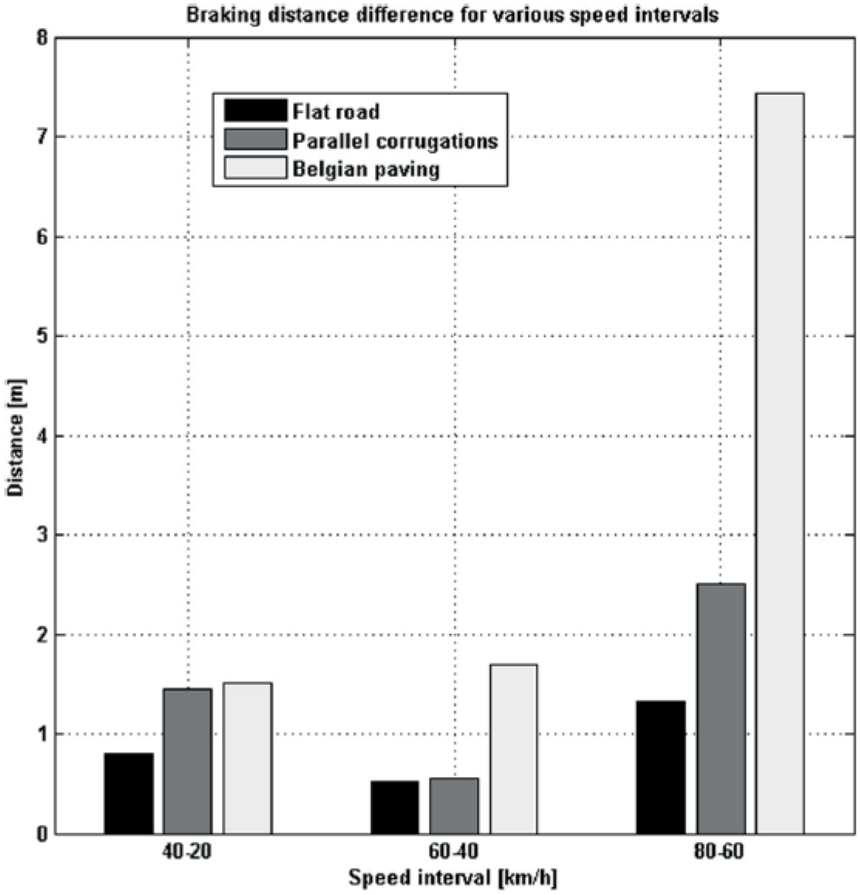

Figure 14 – Effect of optimal suspension configuration on stopping distance reduction (reproduced from [86])

Active suspension is also often used in multi-actuated / over-actuated vehicles. The study [87] described corresponding example, where a combined operation of the AS, the AFS and the wheel slip control (active brakes) serves to control the yaw and roll stability. The simulation of fish-hook manoeuvres for the vehicle equipped with the proposed system architecture has showed that a certain reduction of the side slip angle and the yaw rate can be reached as compared with the brake-based vehicle stability control. One more example is introduced in [88] for the all-wheel drive hybrid electric vehicle. The vehicle architecture integrated the AFS, the ESC, and the individual wheel torque control and, the anti-roll control system (ARCS). The study performed benchmark of different control configurations by example of the simulation of

a sine-with-dwell manoeuvre from 80 km/h and showed that the inclusion of the ARCS reduced the maximum roll angle and the maximum roll velocity, Figure 15. However, this inclusion did not improve the system performance in terms of the yaw stability criteria (maximum yaw rate and maximum side slip angle).

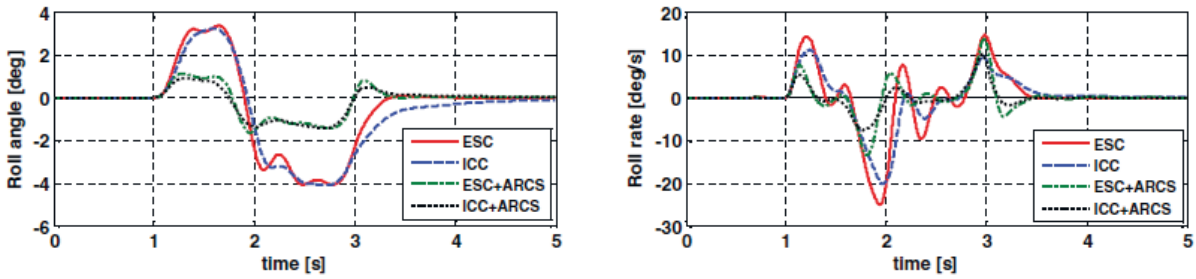

Figure 15 – Roll angle and roll rate by different system configurations (reproduced from [88])

C. Active tyre / wheel systems

Some recent technologies are proposing new types of chassis actuators and active chassis systems, which influence the wheel kinematics or specific tyre parameters and can be also used as add-ons to the basic active safety systems. The relevant examples in this regard are the active camber control and the tyre pressure control systems (TPCS).

The active camber control [42], [89], [90] allows to improve the vehicle handling and safety through extension of lateral tyre friction utilization and better manoeuvrability. In particular case, when the camber control system actuates the rear axle, the mentioned effects are being achieved through the increase of the rear wheel cornering coefficient. In terms of the vehicle design, the active camber can be considered as an add-on element to active suspension with contribution, within certain limits, to rollover stability improvement.

Another example of add-on system relates to tyre pressure variation. Several research and industrial studies have confirmed the fact that the adaptation of tyre pressure can essentially influence vehicle dynamics. For example, the work [91] corroborated by way of experiments the relationship between tyre pressure and longitudinal tyre stiffness that can be applied to the ABS/TCS control where the forecasting or reconstruction of tyre friction–slip dependencies is required. Experimental tests of the test truck detected also the clear-cut relationship between the braking stiffness and the tyre pressure both on asphalt and snow surfaces: deflated tyres

guarantee higher braking stiffness [92]. In the context of lateral dynamics, several research works indicates that (i) lower tyre inflation pressure produces understeer tendency at low and medium forward speeds and oversteer tendency at high speeds [93]; (ii) deflated tyres can ensure more stable motion at some operational conditions [94]; (iii) tyre pressure influences the transient handling response, roll stiffness and slip angle [93]; (iv) the deflated tyres can better transfer lateral contact forces at low wheel loading [95]. Hence, certain improvement of longitudinal and lateral vehicle dynamics performance can be achieved through targeted individual dynamic inflation and deflation of tyres. Such an approach is being realized now in concepts of tyre pressure control systems, which are subjected to the integration with ABS, ESC and active suspension [43].

1.2.4. Assistance systems

Depending on implemented informational and communicational technologies, assistance systems can be divided into in-vehicle and external groups, as proposed on Figure 7. By an *in-vehicle assistance* is meant that the driver assistance system receives information from sensors and devices installed on the vehicle. In the case of an *external assistance* the information channels between the driving environment and the vehicle are used in addition. For the most part the assistance devices should inform of warn the driver with audio, visual or tactile signals about coming or expected critical situation during the driving. However, certain of the discussed assistance tools can be connected to basic active safety systems to improve their control performance and reliability due to additional information channels.

The most widespread *in-vehicle* systems realize functions of the brake assistance, steering assistance, and lane change assistance. The known brake assistance (BA) devices can be realized with different degrees of the driver intervention [96], [97], [98]. For instance, some BA systems support the driver in particular manoeuvres as parking. More advanced BA systems change the brake system dynamics when an extreme, dangerous situation is recognized, e.g. the gradient of the brake pressure increase becomes higher even by a gentle actuation of the brake pedal. This function has to be consistent with the ABS strategy. Another example is the steering assistance (SA). The SA uses external information about the driving environment and analyses the manoeuvre emergency taking into account the actual driver demand on the steering wheel. When a critical situation is expected, the SA system can both warn the driver and partially activate relevant vehicle systems. For instance, the SA functions can use the actuators of ESC

and ARS as described in [99]. The ESC functionality can be also extended with lane change / keeping assistance (LCA). A LCA system analyses the road and warns the driver when a critical departure from the required trajectory takes place [100], [101]. Hence, two main features are true for all discussed devices: (i) detection and analysis of external (road) environment, for example, using radar technique; (ii) providing additional informational channels for active safety systems that increases their ability for predictive, feedforward control.

An *external* assistance concern vehicles having a possibility to communicate or interact with other traffic objects and driving environment. By the external assistance is meant that on-board active safety systems can use complementary vehicle dynamics data received from vehicle-to-vehicle (V2V), vehicle-to-road (V2R) and vehicle-to-infrastructure (V2I) communication sources [102], [103]. It should be also mentioned that the listed communications are indispensable attributes of automated driving. Therefore, many studies dedicated to active safety control with the external assistance are subjected to autonomous vehicles. In particular, with the V2I communication the vehicle can receive the data from global positioning (GPS) and geographic information systems (GIS) [104]. These data can be used for the identification and prediction of road profile and vehicle path tracking that supports the ESC operation. Another example is the optical road monitoring as element of V2R [105]. This allows recognizing low-friction road conditions and preparing ABS, ESC or other safety systems for preemptive actuation, when required. Various roadside sensors within V2R can be also used for off-board estimation of vehicle velocity that is useful for speed adaptation functions in active safety systems [106].

1.2.5. Summary

- Up-to-date basic active safety systems for longitudinal and lateral vehicle control have well-established principles for building the system architecture to guarantee the performance within requirements prescribed by regulation documents; further improvement of operational performance of basic active safety systems can be related to implementation of new types of fast-response actuators (e.g. electric motors for braking and stability control) that also opens ways to new safety control methods.

- Promising trend is the use of add-on chassis control systems to support the main active safety control functions; however, a clear value analysis is required to define a reasonable configuration of integrated safety control.
- Functional robustness of active safety systems can be improved by the use of additional information about the parameters of vehicle motion and driving environment provided by in-vehicle and external assistance systems.

1.3. Justification of Next Chapters

Within the framework of Chapter 1, classification and design of active safety systems have been discussed. A special attention has been given to the brake and vehicle stability controllers as key elements of safety system architecture. It was also shown that a correct definition of tyre and vehicle dynamics parameters has crucial importance for the controller design. However, further development of active safety technologies is characterized by a number both of challenges and opportunities that requires deep investigations in particular research areas. Analysis of recent related research studies and technological innovations allows definition of several topics, which are of crucial importance for coming generations of active safety systems, Figure 16. These topics can be classified into three groups discussed below.

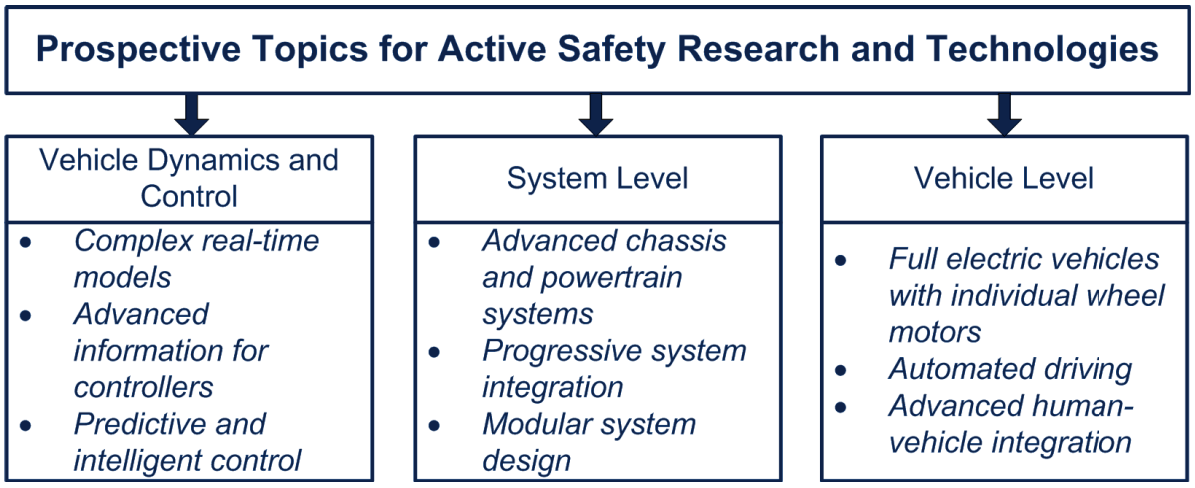

Figure 16 - Prospective topics for active safety

In the area of ***vehicle dynamics and control*** one of the main challenges is the development of *complex real-time models* describing the behaviour of the vehicle and its components. For the most part the control algorithms of active safety systems are using semi-empirical tyre models like Pacejka or Dugoff tyre model, linearized (bicycle) vehicle reference models for the lateral dynamics, look-up tables for various vehicle characteristics as well as many other analytical tools, which can be characterized in the aggregate as a simplified description of complex processes accompanying the vehicle motion. Such simplified approaches were reasonable up to now because of constrained processing resources of electronic control units and limited set of sensors available on a vehicle. Modern on-board electronics allows to overcome these

boundaries to a certain extent. As a result, advanced real-time models will become more and more widespread. In particular, this concerns physical tyre models as FTire and MF-SWIFT, or vehicle models with high degrees of freedom.

Next challenge relates to *advanced information for controllers*. As indicated above, a conventional car possessed so far only few sensors for the estimation of motion dynamics parameters. This situation is being radically changed now, and the vehicle becomes further possibilities to receive information from additional on- and off-board sources as radars, navigation devices, roadside sensors et al. Therefore, new variants of controller architecture can be proposed for active safety systems with a target to use available in-vehicle and out-of-vehicle informational channels with maximum efficiency for failsafe and robust control. The use of advanced information is also closely related to the development of systems based on *the predictive and intelligent control*. Previous generations of active safety systems have used the post-factum control philosophy as a rule. The modern vehicle as a component of V2X communication has a possibility to monitor driving environment in different ways - from near-to-body areas through radar sensors up to the whole route profile via geo-positioning services. Hence, some critical situations for the vehicle motion can be forecasted. As a result, a demand for active safety controllers with forecasting logic and preemptive control actions will be continuously increased. Here many opportunities for computational intelligence methods are in sight.

On the ***system level***, the trend is to extend the active safety control with *advanced chassis and powertrain systems* as mechatronic X-by-wire systems, active systems controlling tyre kinematics and other system examples mentioned in Section 1.2.3. This creates prerequisites for the *progressive system integration* from simple cooperative variants (e.g. integration of ESC and active steering for purposes of lateral stability control) to more complex cases, where the optimal control on several chassis and powertrain systems has to be implemented for safety enhancement with simultaneous improvement of other vehicle characteristics as energy efficiency and driving comfort. In the context of vehicle components, further challenges are connected with *modular system design*. Here the modularity means that several active systems can be integrated in one unit (mainly near to the wheel / inside the wheel hub) for reduction of power and communication channels and a better realization of individual wheel control of forces and torques.

On the **vehicle level**, new paradigms of active safety control are expected first of all with relation to *automated driving*. On the one hand, semi-autonomous and fully autonomous vehicles can essentially prevent critical situations because of (i) extended information supplied by V2X communication and (ii) minimization of wrong actions of the driver. But on the other hand, the active safety control for automated driving requires more comprehensive strategies for failsafe operation. Another challenging direction concerns *advanced human-vehicle integration*, where the active safety control becomes new functions of adaptation to the driver style / type. This is required for a better prevention of wrong driver actions and for keeping the hazard perception by the driver on the safe level. Such a human-vehicle integration has demand for additional driver-related sensors as well as for extension of control strategies with the self-learning and identification procedures. Finally, new opportunities for active safety systems are being opened for *electric vehicles with individual wheel motors*. Individual in-wheel / on-board motors can be considered in fact as universal actuators because they are able to realize not only the traction control but also the brake control with ABS functionality, torque-based lateral dynamics control, and even the vertical dynamics control (motor-based ride dynamics control).

This short overview of prospective topics for active safety points to ample opportunities for the theoretical and experimental investigations. Further sections of the presented habilitation thesis will be concentrated on specific research topics from three groups of problems discussed above. There are: *Identification of road and driving environment parameters; Integration of various safety systems for purposes of the cooperative vehicle dynamics control; Adaptation and re-design of active safety control for electric vehicles*. These topics have been selected not only based on the author's research experience but also with taking into account their urgency for coming active safety systems.

2. IDENTIFICATION OF ROAD CONDITIONS FOR ACTIVE SAFETY SYSTEMS

2.1. Overview of Methods for Definition of Tyre-Road Interaction Parameters

2.1.1. About applicability of tyre models for active safety controllers

Definition of tyre parameters is an important component of computing processes in active safety system controllers. Here semi-empirical and empirical approaches like the Magic Formula (MF) model find most often use for the calculation of tyre forces and moments. However, simulation of tyre dynamics covers many other model variants, which can be potentially implemented in vehicle controllers. Several studies have proposed classifications of tyre models for better understanding their applicability to automotive control systems. In particular, the work [107] recommends to differentiate tyre friction models, which are suitable for real-time systems, by algebraic, statistical and observer-based methods as well as by deterministic and stochastic optimization methods. Another classification in relation to domains of vehicle dynamics is given in [108]:

- Longitudinal tyre-road friction models, for instance, piecewise linear model, Burckhardt model, Rill model [109], Dahl model [110], LuGre model [111];
- Lateral tyre-road friction model as linear proportional model, nonlinear proportional model [112], analytical models based on the single-track vehicle model [113];
- Integrated analytical tyre-road friction models, for instance, MF model, Kiencke model [31], 3-D LuGre-type model [20];
- Sensor-based tyre-road friction monitors as an observer of slip slope [114] or an observer of the maximum of friction-slip-curve [115] based on the wheel velocity information, estimators of lateral friction coefficient with accelerometers [116] and others.

The work [117] has investigated specific tyre models in context of real-time systems. For this purpose, the classification has been given, which includes knowledge models (white box), representation models (black box), and hybrid models (grey box). The mentioned study has concluded that sufficiently precise description of tyre friction limits both in steady and transient

state conditions with reasonable computational time can be provided by (i) Pacejka's MF model and (ii) the nonlinear tyre model based on a quasi-steady state concept and taking account for the effective slip ratio and the updating relaxation lengths [118]. The real-time usability can be further improved by the interpretation of the hybrid tyre models in the form of multidimensional look-up tables.

Analysis of recent studies shows that the combination of estimation technique with semi-empirical tyre models is dominating now in active safety system controllers. Another approach deserving more and more attention both by researchers and system developers relates to the integration of on-board estimators of tyre parameters with information provided by sensor fusion, which can utilize sensing of vehicle, road and environmental parameters for a better identification of driving situation. Overview of relevant estimators and various sensors for the assessment of tyre parameters is introduced next.

2.1.2. Traditional estimators of tyre parameters

Tyre parameters estimators, e.g. for maximum of tyre-road friction coefficient μ_{max}, are finding a wide utility in algorithms of active safety systems. As it can be seen from Figure 2, the μ_{max}-value corresponds to the extremum of μ-λ-curve described as $d\mu/d\lambda=0$. Because some road surfaces cannot guarantee a sharply defined extremum of μ-λ-curve, more reasonable approach consists in assessment of the slope of the curve $k_\lambda=\Delta\mu/\Delta\lambda$. Initially the slope k_λ has near-to-linear character, therefore the subsequent detection of an essential deviation from the linearity points to the approaching of the extremum area. This effect lies in the background of estimators, which assess indirectly the maximum of tyre-road friction through the slope k_λ. The relevant computing methods have different complexity depending on the sensor involved in estimation procedures.

In the simplest case the estimation can be based on signals from the wheel velocity sensors only. For instance, such an example is considered in [119], where the estimator uses the torque balance for the 1-DOF vehicle model, Figure 17. The torque balance of the 1-DOF model is

$$T_w - T_{br} - I_w \cdot \dot{\omega} - F_r \cdot r_{dyn} - F_x \cdot r_{dyn} = 0 \ , \tag{2.1}$$

where T_w is the drive torque, T_w is the brake torque, I_w is the moment of wheel inertia, F_r is the rolling resistance force. In addition to Eq. (2.1), the tangential (longitudinal) tyre force F_x can be theoretically limited by tyre friction conditions:

$$F_x \leq \mu_x \cdot F_z \cdot r_{dyn} \ . \tag{2.2}$$

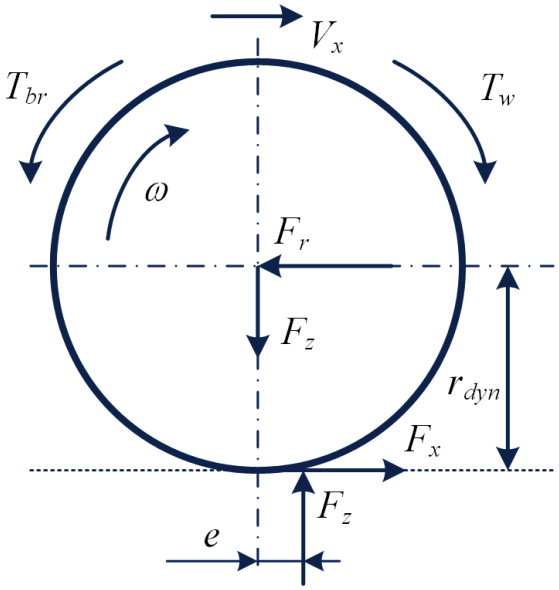

Figure 17 - 1-DOF vehicle model

Following the study [119], Eq. (2.1) can be rewritten as:

$$I_w \cdot \dot{V}_w = F_x \cdot r_{dyn}^2 - T_{br} \cdot r_{dyn} + F_d \cdot r_{dyn}^2 \ , \tag{2.3}$$

where $V_w = \omega \cdot r_{dyn}$ is the linear wheel velocity, F_d is the force considering the road disturbances. Then the wheel deceleration is

$$\ddot{V}_w = -\frac{k_\lambda \cdot r_{dyn}^2}{I_w} \cdot \dot{V}_w + w \,, \tag{2.4}$$

where w is the factor considering disturbances from the road and brake torque fluctuations:

$$w = \frac{F_d}{dt} \cdot r_{dyn}^2 - \frac{dT_{br}}{dt} \cdot r_{dyn} \,. \tag{2.5}$$

The analysis of Eq. (2.4) shows that the k_λ-value can be estimated through the break point frequency for the wheel deceleration, for example, with the least square method, Figure 18.

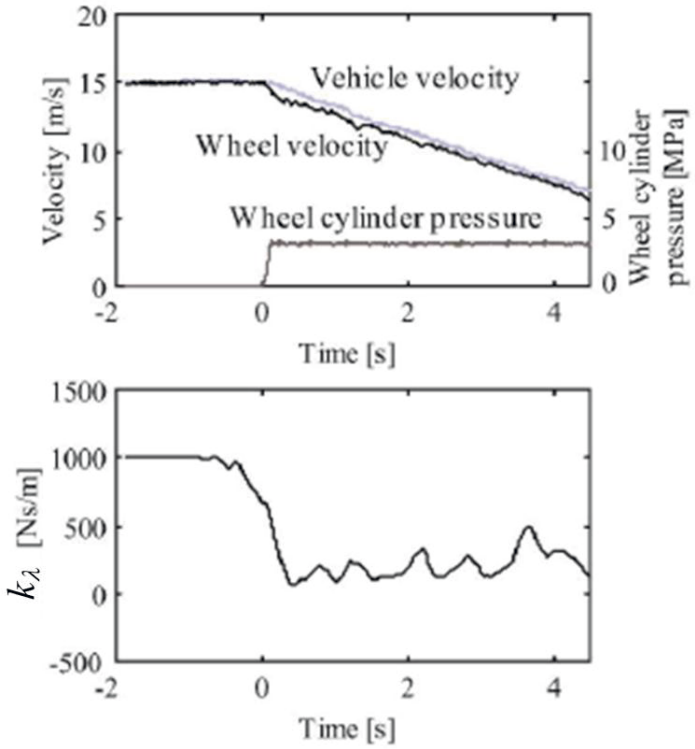

Figure 18 - Estimated k_λ-value during a braking manoeuvre (reproduced from [119])

An alternative approach is proposed in [120], where k_λ is estimated through the power spectrum density (PSD) of the wheel velocity, Figure 19, and the tyre rotational vibration model:

$$\begin{cases} I_{w1} \cdot \dot{\omega}_1 = -K \cdot \theta_s \\ I_{w2} \cdot \dot{\omega}_2 = K \cdot \theta_s + F_x \cdot r_{dyn} + T_d \end{cases}, \tag{2.6}$$

where $I_{w1,2}$ are moments of inertia at the tyre rim and belt sides correspondingly, $\omega_{1,2}$ are rotational velocities at the tyre rim and belt sides correspondingly, K is the tyre torsional spring stiffness, T_d is the equivalent torque from road disturbances, θ_s is the torsional angle. The linearization of the system (2.6) with the accounting for the slope k_λ allows to propose a simplified expression for the perturbation of the torque from the longitudinal force $T_w = F_x \cdot r_{dyn}$:

$$\Delta T_w = k_\lambda \cdot \Delta\omega_2 \cdot r_{dyn}^2 . \tag{2.7}$$

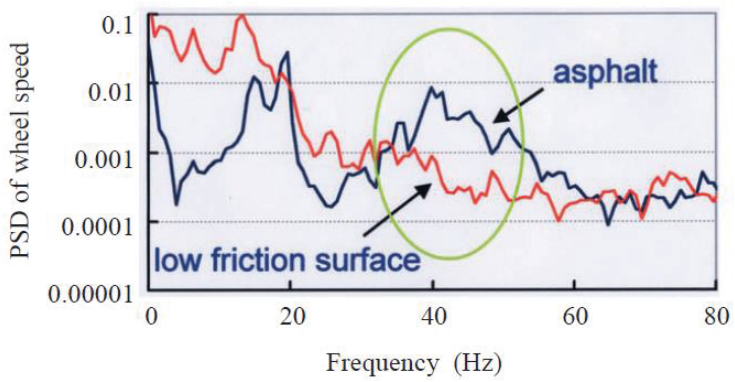

Figure 19 - Examples of power spectrum density of wheel velocity for different surfaces [120]

Considering further the transfer functions from the torque T_d to the velocity ω_1

$$G(s)=\frac{K}{I_{w1}\cdot k_\lambda \cdot r_{dyn}^2 \cdot s^2 + K\cdot(I_{w1}+I_{w2})\cdot s + K\cdot k_\lambda \cdot r_{dyn}^2}\ , \tag{2.8}$$

a hypothesis has been proposed in [120] that the strength of the resonance frequency of $G(s)$ depend on the $k\lambda$-value, therefore the slope $k\lambda$ can be estimated through the analysis of frequency characteristics of the wheel velocity. It should be mentioned that such approach is quite sensitive to the quality of sensor signals. In addition, its robustness is not sufficiently investigated for a variety of possible road and operational conditions.

The use of the slope $k\lambda$ for the road friction identification is also considered in studies [114] and [115] through the application of the linear regression with time-varying parameters:

$$\lambda(t)=\mu\cdot\frac{1}{k_\lambda}+\delta(t)\,, \tag{2.9}$$

where δ is an offset assuming that the slip is not zero when the normalized longitudinal tyre force is equal to zero:

$$\delta=\lambda\big|_{\mu=0}\ . \tag{2.10}$$

For the tyre friction assessment through the expression (2.9), the Least Mean Squares, Recursive Least Square or the Kalman filter can be particularly applied.

The described procedures are sensible to the quality of wheel velocity signals and requires advanced elements in the estimator architecture to recognize properly an eventual sudden change of the road surface during the estimation process. In this connection, more robust and comprehensive methods with the use of additional sensors are proposed in various studies. In particular, several sensor configurations for tyre-road friction estimators are discussed in [121]: (i) engine and brake torque signals from the vehicle CAN and GPS signal; (ii) engine and brake torque signals from the vehicle CAN and longitudinal accelerometer; (iii) engine and brake torque signals from the vehicle CAN and longitudinal and vertical accelerometers; (iv) longitudinal accelerometer and GPS signal. In particular for the configuration (i), the procedure of tyre-road longitudinal force estimation can be derived from the 1-DOF vehicle model (see Eq. (2.3)) with the following observer equations:

$$I_w \cdot \dot{\hat{\omega}} = T_w - T_{br} - \hat{F}_x \cdot r_{dyn} + \ell \cdot \tilde{\omega}\,, \tag{2.11}$$

$$\dot{\hat{F}}_x = -\eta \cdot \tilde{\omega}\,, \tag{2.12}$$

where η is the positive estimator gain, ℓ is the observer gain, and the estimation errors are

$$\begin{aligned} \tilde{\omega} &= \omega - \hat{\omega} \\ \tilde{F}_x &= F_x - \hat{F}_x \end{aligned}\,. \tag{2.13}$$

The mathematical formulation of related estimation algorithms in [121] is based on a recursive least-squares parameter identification. The estimator concept (2.11)-(2.13) using the information about engine and brake torque signals has a number of disadvantages related to reliability and latency of CAN data. Several studies considered other solutions with direct sensor measurements of parameters related to the wheel torque. For example, the work [122] proposed a simple model based formulation of the tyre friction coefficient from the 1-DOF and 3-DOF vehicle models and the hydraulic model of the brake system:

$$\mu = \frac{I_w \cdot \dot{\omega}_{fl} + \dfrac{-m \cdot r_{dyn} \cdot a_x - I_w \left(\dot{\omega}_{fl} + \dot{\omega}_{fr} + \dot{\omega}_{rl} + \dot{\omega}_{rr} \right)}{1 + c_{pf} + 2 \cdot \beta_\tau \cdot c_{pr}}}{m \cdot r_{dyn} \cdot \left(\left(1 - \dfrac{a}{L} \right) \cdot g - \dfrac{h_g}{L} \cdot a_x \right)}\,, \tag{2.14}$$

where indices *fl, fr, rl* and *rr* correspond to the front left, front right, rear left and rear right wheels, c_{pf} are the pressure ratio between the front left and front right wheels, c_{pr} are the pressure ratio between the rear left and rear right wheels, β_τ is the brake force distribution coefficient related to geometry of brake cylinders. The pressure ratio in Eq. (2.14) can be deduced based on the pressure sensor signals in the brake system. The use of brake pressure sensors has also some limitations affecting the precision of estimation procedure. In particular, the study [123] investigated the real-time maximum friction coefficient estimator with the longitudinal tyre force estimator, where the brake torque is one of the estimator components and is calculated as

$$T_{br} = K_B(p_{br} - p_{br0}). \tag{2.15}$$

The parameter K_B in Eq. (2.15) is the brake gain, p_{br} is the actual brake pressure, p_{br0} is the push-out (or preload) brake pressure in the brake cylinder. Analysis of experimental results given in [123] has shown that estimation procedure with the use of the brake pressure sensors is characterized by certain delays and transient processes, Figure 20. Some drawback of this approach consist in uncertain character of p_{br0}-value, which is hard to define accurately.

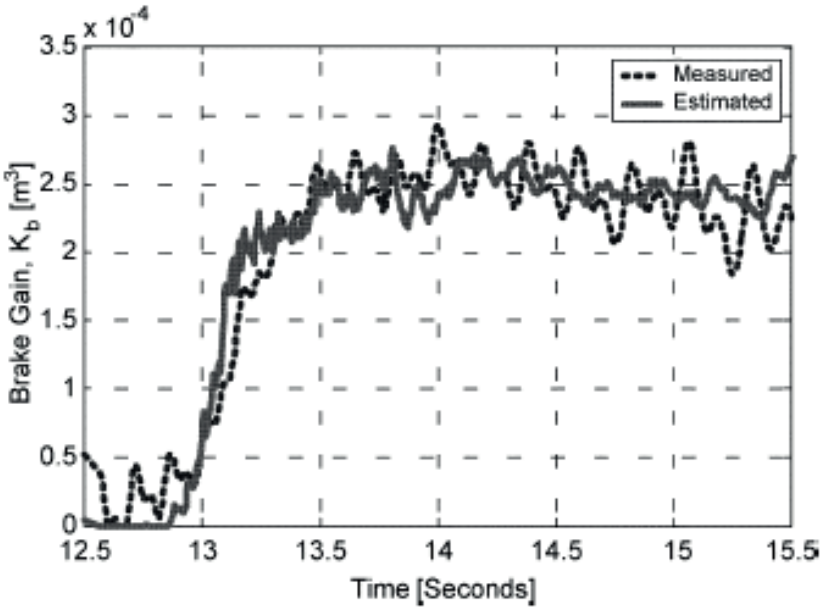

Figure 20 - Example of brake gain estimation from [123]

Several studies are known, which apply a more complex sensor technique. The researchers of Honda [124] have used a combination of (i) strain gauges to measure axial forces of the wheel

and (ii) six-component dynamometer installed on the wheel hub. The use of the wheel dynamometric hub, which is advanced with the bearings equipped with the dynamic load sensors, is also mentioned in the study of Renault [125]. With these sensors, predictive values of the tyre-road friction coefficient can be obtained, Figure 21, and further applied to the phenomenological estimator (as for Eq. (2.9)) based on the Kalman filter. However, the commercial active safety systems on mass-production cars cannot implement nowadays the dynamometric sensors due to technological limitations. Such measurement devices are generally used in the estimator design for the validation and verification purposes [126]. It should be mentioned that the quality of friction coefficient identification obtained with these devices can be not sufficient for active safety systems control tasks (see signal deviations on Figure 21). Moreover, known studies in this area discuss rarely the boundary conditions and confidence parameters for this kind of measurements.

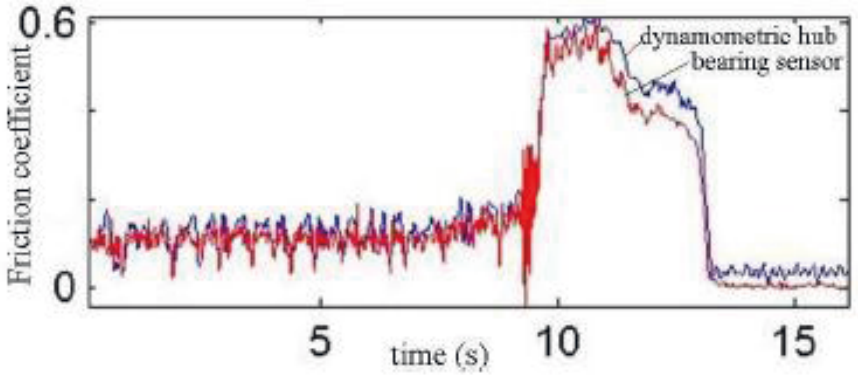

Figure 21 - Example of friction coefficient measurement from [125]

Previous paragraphs have mentioned the application of recursive methods as well as the Kalman filtering [127] for the estimation of the tyre parameters. Several other methods are also known in this regard from the analysis of research publications:

- Model-based estimation with the use of sensors available in ESC system [128];
- Diagnosis-based estimation within an algebraic framework, in particular, with use of the Dugoff tyre model and sensors available in ESC system [129];
- Maximum likelihood and recursive maximum likelihood approach [130];
- Adaptive observers, in particular, Lyapunov or Luenberger adaptive observers [131];
- Neural networks, for example, Radial Basis Function neural networks with the use of LuGre tyre model [132], or Multi-Layer Perceptrons networks with the use of tyre brush model [133];

- Sliding mode observers [134], [135];
- Advanced Kalman filters, for example, with Bayesian hypothesis selection [136] or fuzzy identification methods [137].

Performance of any estimation technique depends strongly on the set of sensors and measurable signals available for the observation of required vehicle dynamics parameters. Recent technologies make it possible to use not only standard ABS/ESC equipment like wheel speed sensors, accelerometers or yaw rate sensors but also advanced measuring devices including external on-road sensors. Different methodologies for definition of corresponding tyre parameters are discussed in next section.

2.1.3. Use of road information for definition of tyre parameters

Progress in ITS technologies motivated the development of new road infrastructure devices, which can also support the operation of active safety systems by providing the information about road surface. However not only on-road but also advanced on-vehicle sensors are now able to detect road surface conditions for further utilization of this information in automotive control systems. Relevant methods are generally based on processing of (i) acoustic, (ii) vibration and (iii) optical phenomena. Several examples of corresponding applications are introduced below.

(i) The variant of on-board system based on real-time *acoustic* analysis of tyre-road noise has been investigated in [138]. The test vehicle is equipped with the microphone, Figure 22a, to measure noise from tyre-road interaction, Figure 22b. The processing of noise-related parameters like frequencies in different domains should allow to identify at least the dry and wet asphalt concrete as well as a transition between these surfaces. Some disadvantages of this approach consist not only in a limited number of identified cases but also in low response time: results from [138] indicate that 0,2 sec and more is required to detect the change of road surface. Several other studies give particular attention for acoustic-based road identification using the ultrasonic technique [139], [140]. Such an approach can receive in future a wider application with embedding of low-cost ultrasonic sensors directly on vehicles. More surfaces can be classified through the processing of traffic noise with the statistical methods. The corresponding approach from [141] is based on the close-proximity method, which uses the parameters of

macrotexture of surface and the traffic noise in near field conditions. The results of the study [141] indicated the recognition of five different asphalt mixes, Figure 23, with the precision rate higher as 90%. As differentiated from previous example, this method uses on-road devices for noise measurement. Therefore, the road-to-vehicle communication is required, when the detected type of road surface should be utilized in an on-board controller. Particular attention should be given to the fact that robustness of the discussed approach cannot be guaranteed in the case of interference of noise from tyre-road interaction and from external noise sources.

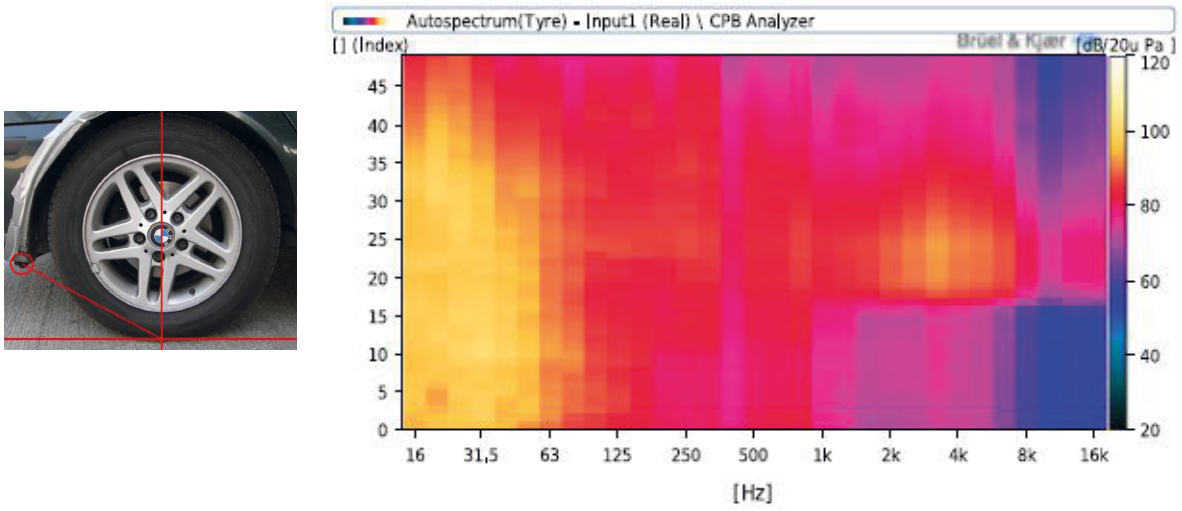

(a) (b)

Figure 22 - Acoustic identification of road surface: microphone location (a) and example of unweighted tyre-road noise (b) during a dry-wet-dry transition (reproduced from [138])

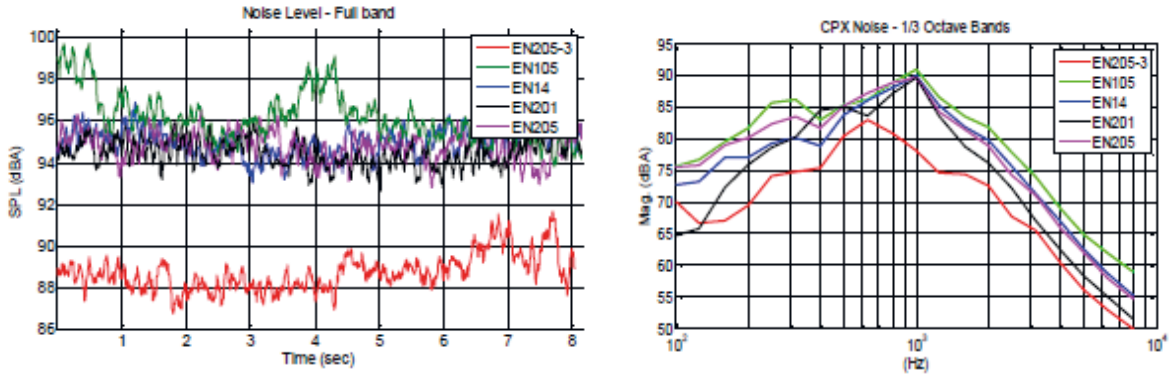

Figure 23 - Noise evolution and noise spectra for five different road tracks analysed for the vehicle speed of 80 km/h (reproduced from [141])

(ii) The systems identifying the road surface type from *vibration* parameters have generally on-board implementation. For example, the work [142] proposes the road identification by

measuring the accelerations of the vehicle body and the wheel. The vibration analysis of frequency spectrum, Figure 24, based on wavelet transform, Fast Fourier Transformation and training using the radial basis function network classifier allowed identifying both rough (blacktop) and fine (mattess) surfaces. In spite of good possibilities to measure wheel vibrations with accelerometers, it should be mentioned that lack of efficient processing methods restrains the application of vibration-based road identification in active safety systems.

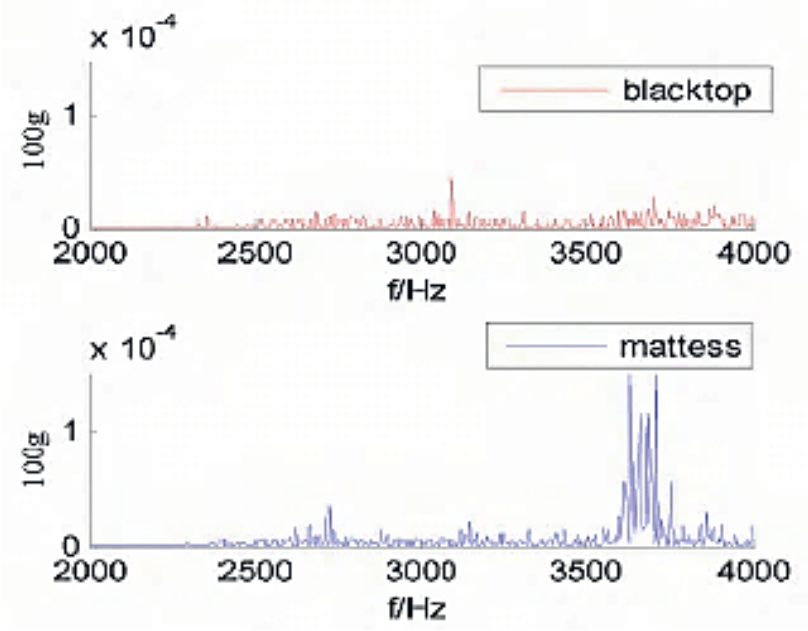

Figure 24 - Frequency spectrum of wheel vibration in domain 2-4 kHz (reproduced from [142])

(iii) *Optical* information can be also used for the detection of parameters of vehicle-road interaction. In particular, a laser displacement sensor and CCD camera found applications to measure the camber angle and slip angle [143]. Several studies are known, where the road surface can be identified with the use of image processing. For example, the work [144] has considered the assessment of polarization intensity of road surface images captured by ITS-related sensor technique. It was shown that water on the road can be recognized by the ratio of horizontal polarization image intensity to vertical polarization image intensity for each pixel of the image. The snow road can be recognized by texture analysis using the co-occurrence matrix. With this approach, the results of identification of five types of surfaces ("dry", "wet", "slushy", "icy" and "snowy") were presented. Generally, the use of the image processing is very limited now for real-time applications due to computing time, precision, and other factors. Nevertheless, the potential of this method is being increased continuously with emerging of new image processing technologies and cheap on-board cameras having sufficient performance.

An alternative approach is discussed in [145], where the on-board system includes a halogen light, a spectrometer, and the special "Road Eye" sensor consisting of laser diodes and photodiodes. Practically the method assesses the reflectance of surfaces obtained in an angular spectrally related measurement. The results of road tests, Figure 25, confirmed that surfaces with distinct properties (dry asphalt, ice, snow) can be detected from the analysis of reference and absorbing wavelengths. However, the mentioned study did not discuss applicability of this system for the identification of road surfaces with different wetness grade.

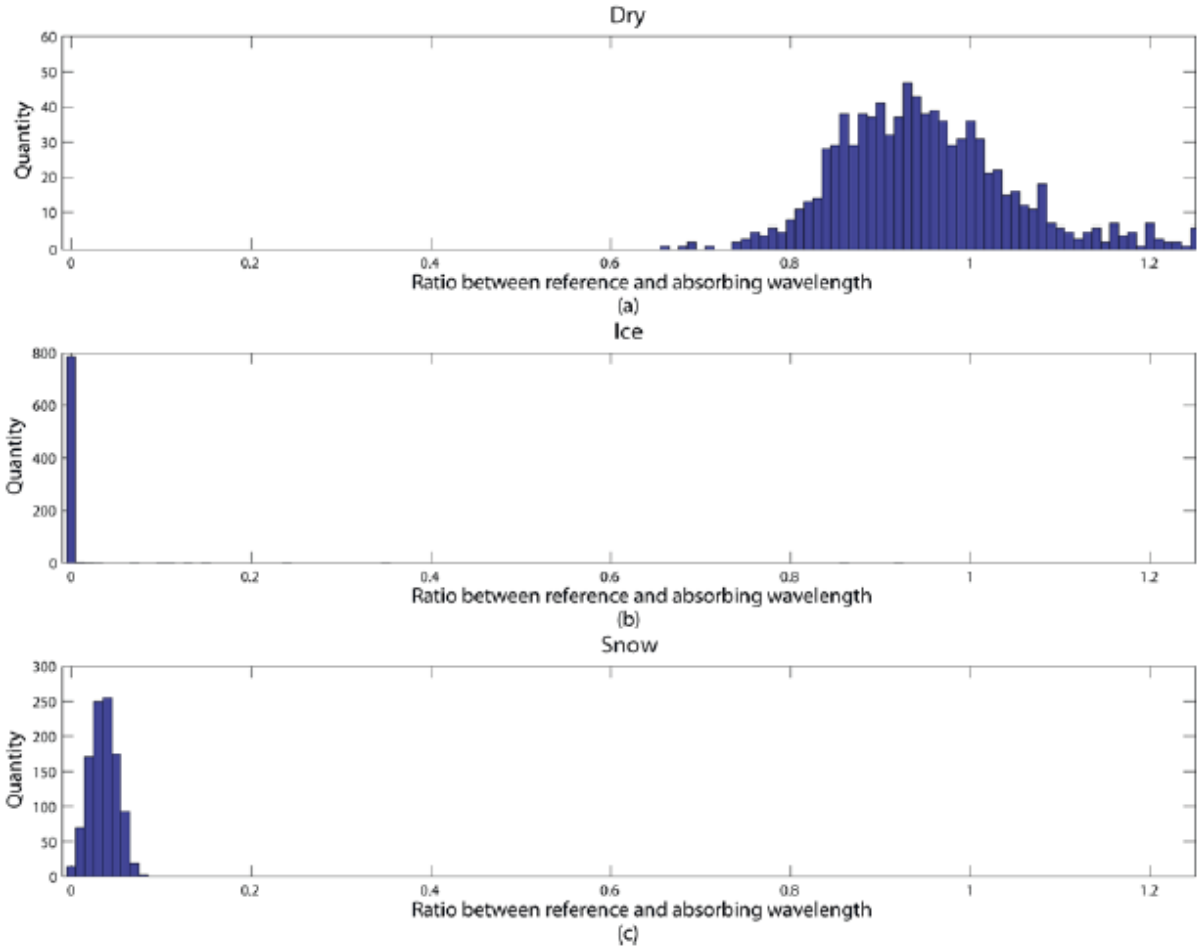

Figure 25 - The ratio distributions of real-life measurements with the "Road Eye" sensor installed on the test vehicle. Y-axis: Quantity of measurements (reproduced from [145])

Several developments propose integration of different sensors and measurement methods for identification and estimation of tyre-road interaction parameters. An example of the corresponding system concept is described in [146], Figure 26, where the combination of traditional vehicle sensors with additional optical and acoustic sensors has been used for the road wetness detection.

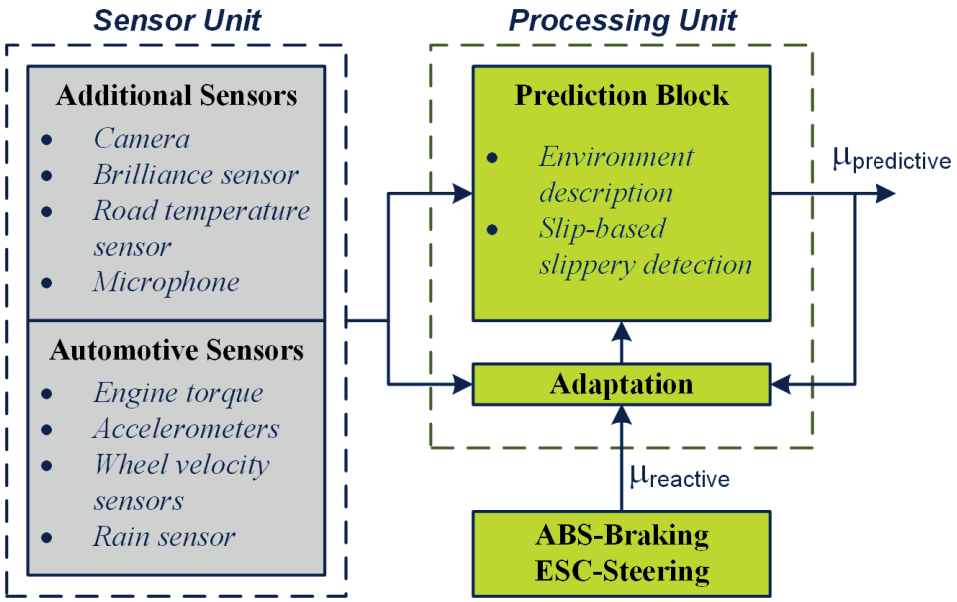

Figure 26 - Concept of integrated system for road friction identification (re-edited from [146])

Analysis of recent technologies of active safety systems, especially for vehicles as components of Intelligent Transportation Systems, shows that sensor fusion becomes more and more importance for the computing of tyre-road interaction parameters. Next section will discuss a variant of corresponding tyre-road identification system.

2.2. Particular Case of Identification of Tyre Parameters Using On-Board and On-Road Information

2.2.1. General approach

The methods of the identification of tyre parameters, which will be further introduced, have been developed by the author within the framework of several research projects carried out at Technische Universität Ilmenau: "Fuzzy Environment of Tyre-Surface Interaction" funded by Alexander von Humboldt Foundation, and "Interface of Intelligent Control Philosophy and Mechatronics Technology for Tyre-Surface Interaction" funded by the European Commission under Marie Curie International Incoming Fellowship. Major results of these projects have been published in [147], [148], [149], [150], [151], [152], [153]. The corresponding identification method received the European patent EP2089260 [154].

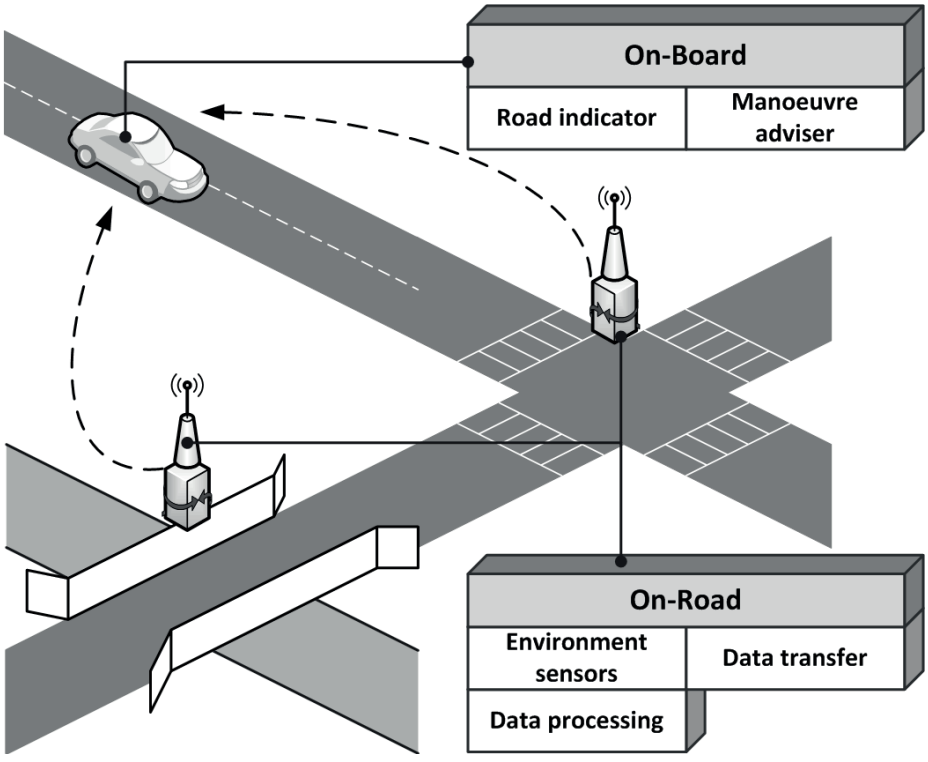

Figure 27 - Concept of surface analyser [155]

The prototype system under consideration consists of the *on-road* and *on-board* parts, Figure 27. The *on-board* part includes elements and devices interpreting the received road information for the vehicle control and driver assistance. The functions of the *on-road* part are detection and

prediction of actual friction conditions of the road surface. This part unites a complex of devices, which can be implemented in the road infrastructure:

- *Environment sensors* detect the texture of road surface, the temperature of ambient air and road surface, the moisture, the ice-point temperature, and the precipitation intensity;
- *Data processing* device is a processor computing physical parameters of the road. The computed data should be handled in numerical and linguistic forms to ensure their easy-to-use interpretation both for vehicle control systems and human machine interface;
- *Data transfer* provides wireless communication for the computed road surface characteristics from the surface analyser to the vehicle.

The proposed architecture of surface analyser can be also adapted to off-road conditions for the identification of tyre-soil/ground parameters. Taking into account surface classification tasks, the logic of the described system can be proposed on the basis of computational intelligence methods. This is further discussed by the example of fuzzy methods.

2.2.2. Fuzzy identification system for tyre-surface interaction parameters

One of key challenges for advanced active safety systems is the forecasting of possible changes in driving environment. This allows developing the control strategies with preemptive, feed-forward elements. However, the forecasting and identification of tyre-road interaction parameters comes up against the problem of uncertainty. Two kinds of vague situations take place here: numerical and linguistic uncertainty. *Numerical uncertainty* refers to unexpected oscillations of tyre-road friction coefficient. The concept of *linguistic uncertainty* is applicable to situations, when the system recognises correctly the changing an output variable (for instance, tyre-road friction or tyre force) but is not able to treat proper this information for the control algorithm. For example, the tyre-road friction drops during the manoeuver from *0,8* to *0,2*. The value of $\mu = 0,2$ can refer equally to the iced road or to the surface with a high water film. Knowing the surface type, the advanced active safety system can predict the propagation of a critical driving situation and performs feed-forward control actions.

The tyre friction identification system under discussion can handle both numerical and linguistic uncertainty and is based on fuzzy sets. This approach has been chosen first of all due to its good applicability both to the short-term and long-term dynamic processes in tyre-rod

contact. In addition, fuzzy models allow primarily deducing dynamic variables not only from the direct but also from the indirect indicators. The proposed three-layer cascade model of tyre friction is shown on Figure 28.

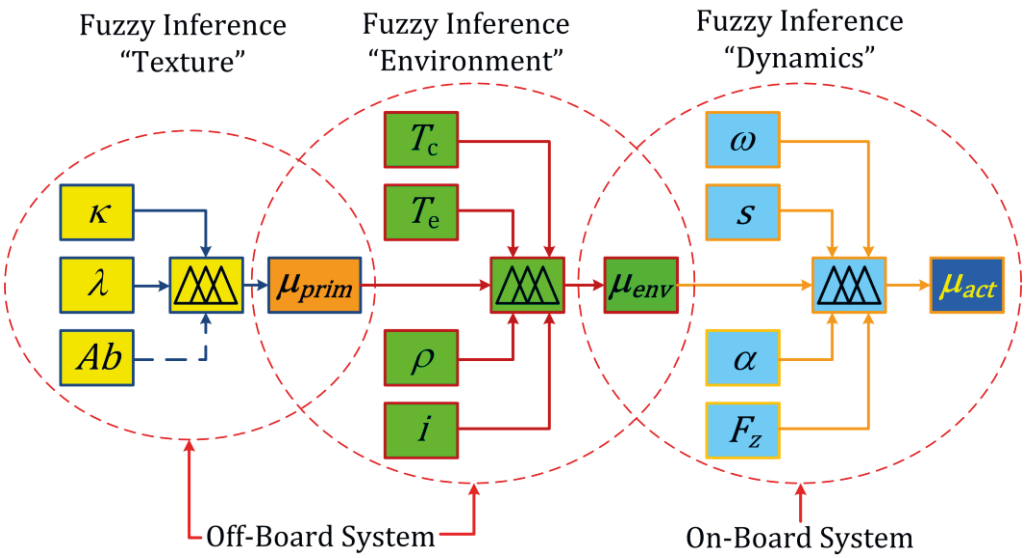

Figure 28 - Information structure of fuzzy tyre-road friction model [149]

The first fuzzy inference system (FIS) "Texture" operates with a set of input variables as the height of microprofile κ and macroprofile λ, and an optional variable describing the reflection properties of the surface, for example, the albedo value Ab. The output variable of the fuzzy inference system "Texture" is the primary coefficient of rolling friction μ_{prim} for a particular road surface type. This FIS performs the initial road identification, and the value of μ_{prim} can be next corrected in compliance with actual environmental conditions. For this purpose, the parameter μ_{prim} is simultaneously the input variable for next fuzzy inference system "Environment". Other input variables are the road surface temperature T_c, the ambient temperature T_e, the moisture ρ, and the precipitation intensity i. The output variable is the friction coefficient by the environmental conditions μ_{env}. Such an approach allows short-term prediction of the road friction. It allows anticipating a number of situations that may occur with environmental factors changing the value of the primary friction coefficient μ_{prim}. This parameter can be already used in algorithms of active safety systems.

Nevertheless, it makes sense to refine the μ_{prim}-value in accordance with the actual vehicle motion dynamics. This function is being carried out by the third FIS "Dynamics" realised as an on-board controller. It is assumed that the parameter μ_{env} is being transmitted from the ITS

infrastructure to the vehicle and is one of the fuzzy input variables, together with the wheel velocities ω, the wheel slip s, the side slip angle α, and the normal wheel loading F_z. Using all the listed input variables, the FIS "Dynamics" deduces the actual tyre-road friction coefficient μ_{act}. During the straight-line manoeuvres the parameter μ_{act} can be considered as the specific longitudinal tyre force μ_x. By other driving situations the system can deduce both the μ_x and the specific lateral tyre force μ_y from the μ_{act}–value.

Creating a fuzzy inference system, the introduction of fuzzy sets is required on the first step. Figure 29 gives an example of their description for the FIS "Texture. This description is based on statistical data, collected by the author, and data from [156]. Two limitations have been applied for this example: the close range of the μ_{prim}-coefficient is considered for the dry surface with various road compounds; the albedo value is not taken into account as one of the input variables. If the whole μ_{prim}-range should be covered, then the fuzzy description from Figure 29c) can be used. If more precise definition is required, then certain area of friction values can be represented more exactly. Figure 29d) gives the variant of advanced membership functions for the dry road. This variant can increase the accuracy of calculations but the linguistic indicators as "concrete", "asphalt" or the similar one are not applicable in such a case.

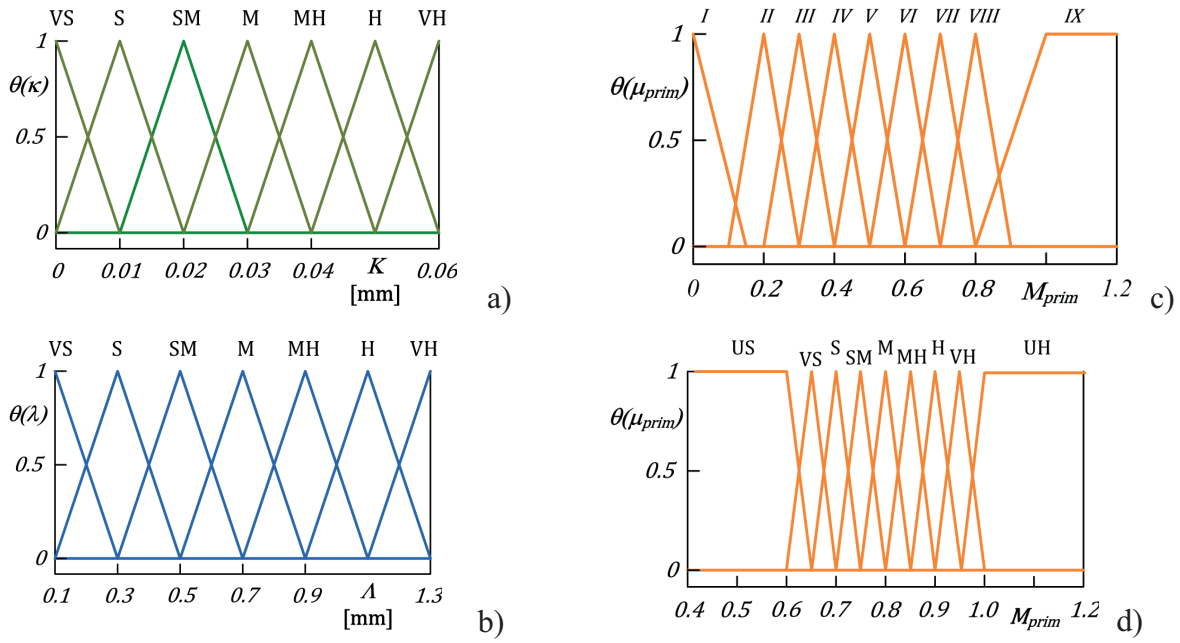

Figure 29 - Description of variables in fuzzy inference system "Texture"
Legend: US – ultra small; VS – very small; S – small; SM – small-to-medium; M – medium; MH – medium-to-high; H – high; VH – very high; UH – ultra high;
I – ice, II – snow, III – highly wet road, IV – contaminated road, V – slightly wet concrete, VI – slightly wet asphalt, VII – dry concrete, VIII – dry asphalt, IX - enhanced dry asphalt

After that the rule base should be created. Figure 30 shows example of the rule base surface covering 16 rules. More information about can be found in [149], [153] and [157].

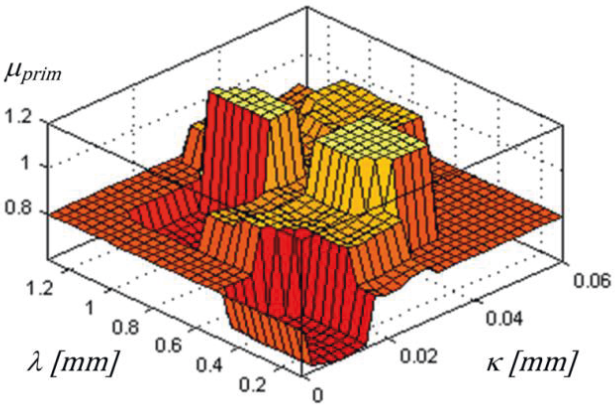

Figure 30 - Example of fuzzy surface rules

On the next step, the FIS "Environment" specifies the road friction level in accordance with actual environmental conditions and generates the corresponding linguistic attribute of the road type. Here the fuzzy description of the environmental parameters depends from the climatic area. For illustrative purposes, Figures 31 a) and b) show examples of fuzzy input variables. The FIS "Environment" requires a volumetric rule base because of large amount of possible combinations of input variables. Figure 32 displays two examples of fuzzy rules surface fragments for an optimised rule base.

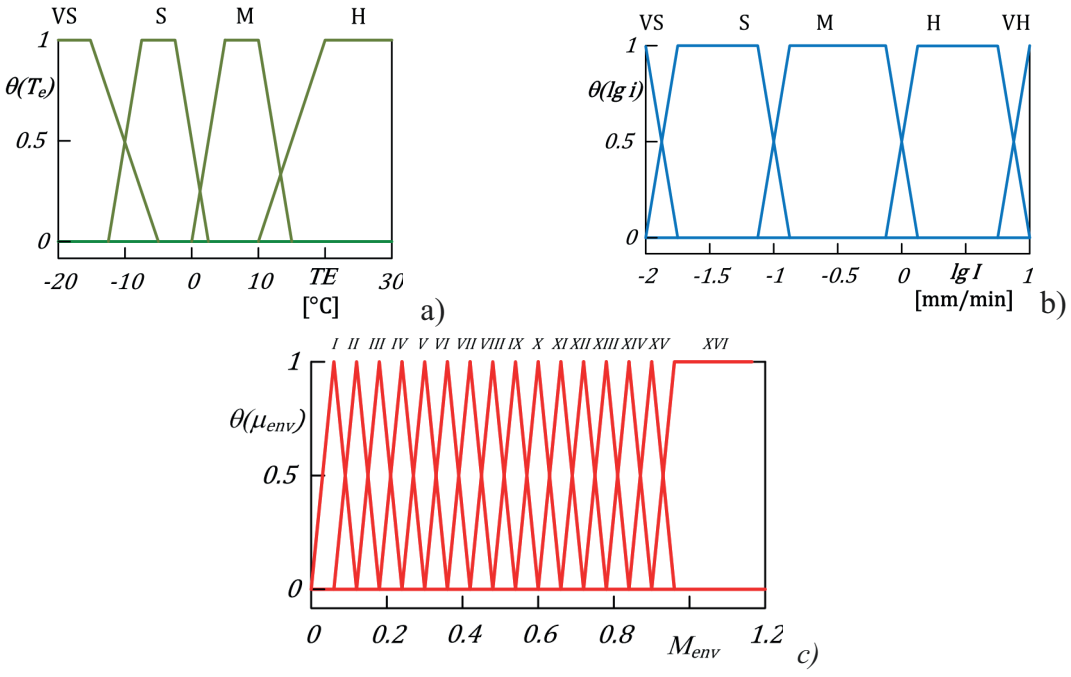

Figure 31 - Description of variables in fuzzy inference system "Environment"

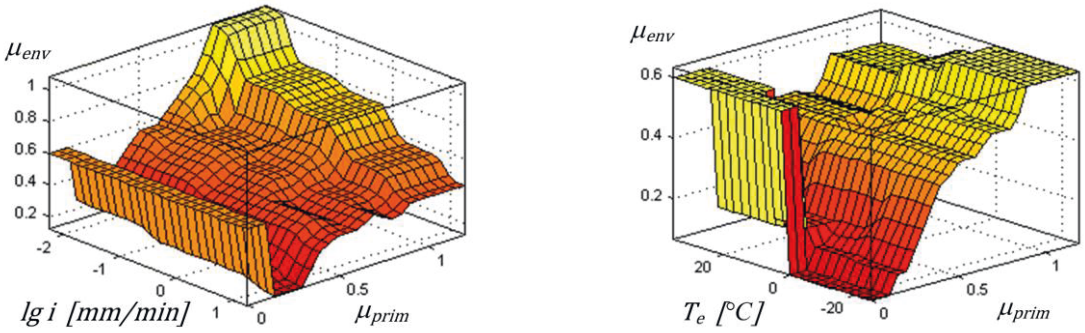

Figure 32 - Fragments of surface of fuzzy rules for the fuzzy inference system "Environment"

Table 4: The variants of linguistic attributes with regard to the description from Figure 31c)

I	I_A: high water film on polished road surface (aquaplaning tendency); I_B: wet ice
II	II_A: high water film on rough road surface (aquaplaning tendency); II_B: wet ice
III	III_A: smelting ice on road surface ('about zero' temperature); III_B: fresh snow; III_C: high water film on rough road surface (aquaplaning tendency)
IV	IV_A: snow by frost; IV_B: pressed snow
V	V_A: pressed snow; V_B: smelting snow; V_C: highly contaminated road
VI	VI_A: contaminated road
VII	VII_A: highly wet concrete (puddles); VII_B: highly wet asphalt (puddles)
VIII	VIII_A: highly wet asphalt (puddles); VIII_B: highly wet concrete (puddles)
IX	IX_A: wet asphalt; IX_B: wet concrete
X	X_A: slightly wet concrete; X_B: slightly wet asphalt
XI	XI_A: slightly wet asphalt; XII_B: slightly wet concrete
XII	XII_A: dry concrete
XIII	XIII_A: heated dry asphalt (bitumen smelting); XIII_B: rolled cement concrete
XIV	XIV_A: dry asphalt; XIV_B: dry asphalt concrete; XIV_C: rolled cement concrete
XV	XV_A: dry enhanced asphalt concrete
XVI	XVI_A: dry road with environmentally-related enhanced friction

The definition of linguistic attributes of the road type is the next main task for the FIS "Environment". For this purpose, the following approach is proposed. (i) The system calculates firstly the numerical value of the environmental coefficient of road friction μ_{env} using only "featureless" linguistic attributes like numbers from *"I"* to *"XVI"* on the Figure 31c). (ii) Considering the actual combination of environmental factors and previously computed value of the primary coefficient of rolling friction μ_{prim}, the system generates the linguistic attribute corresponding to the expected surface type. Some most useful attributes in relation to the fuzzy

description from Figure 31c) are given in Table 4. (iii) The calculated μ_{env}-value together with the linguistic attribute is transmitted to the FIS “Dynamics”.

The FIS “Dynamics” computes the actual coefficient of the road friction μ_{act} by means of the transformation of μ_{env}-value. In effect this procedure allows the reconstruction of the combined longitudinal and lateral tyre friction characteristics in relation to the wheel slip and slip angle as well as to the fluctuations of wheel loading and velocity rate. Some essential details of the discussed fuzzy inference system "Dynamics" are given in [152] and [157], and its practical realization will be illustrated in next section.

2.2.3. Application example

This section introduces the application of the proposed fuzzy identification procedure for purposes of electronic stability control and is mainly based on results presented in [147]. Figure 33 illustrates the ESC-architecture used in this study. The system under discussion has been tested on the hardware-in-the-loop test rig, Figure 34, at facilities of Automotive Engineering Group, Technische Universität Ilmenau. The test rig includes hardware components of the brake system and the hydraulic control unit (HCU). The HCU has a structure similar to conventional controllers of ESC systems. The vehicle model used in the controller has 12 DOF. The HIL experiments are performed for the bus software simulator (full mass 10270 kg, tyres 235/75 R 17.5) for three case studies: (i) straight-line braking on homogeneous road; (ii) dropping of friction during straight-line braking; (iii) lane-change maneuver. The parameters of the bus brake systems and brake hardware components, which are installed on the test rig from Figure 34, have been harmonized by using the scaling factors in the software simulator.

(i) Straight-line braking on homogeneous road. This case study relates to the braking on two surfaces of different kinds but with the similar coefficient of friction $\mu_{env} = 0{,}2$. The first situation corresponds to ice (linguistic attribute *III_A* from Table 4), Figure 35, the second situation refers to the asphalt road with high water film (linguistic attribute *III_C* from Table 4), Figure 36. It should be pointed out that the friction coefficient in the case of high water film increases slightly during braking. This effect can be explained in terms of the physical processes changing the contact patch area. The system responds to both types of surfaces with different control strategies and control thresholds. Table 5 compares the simulation results.

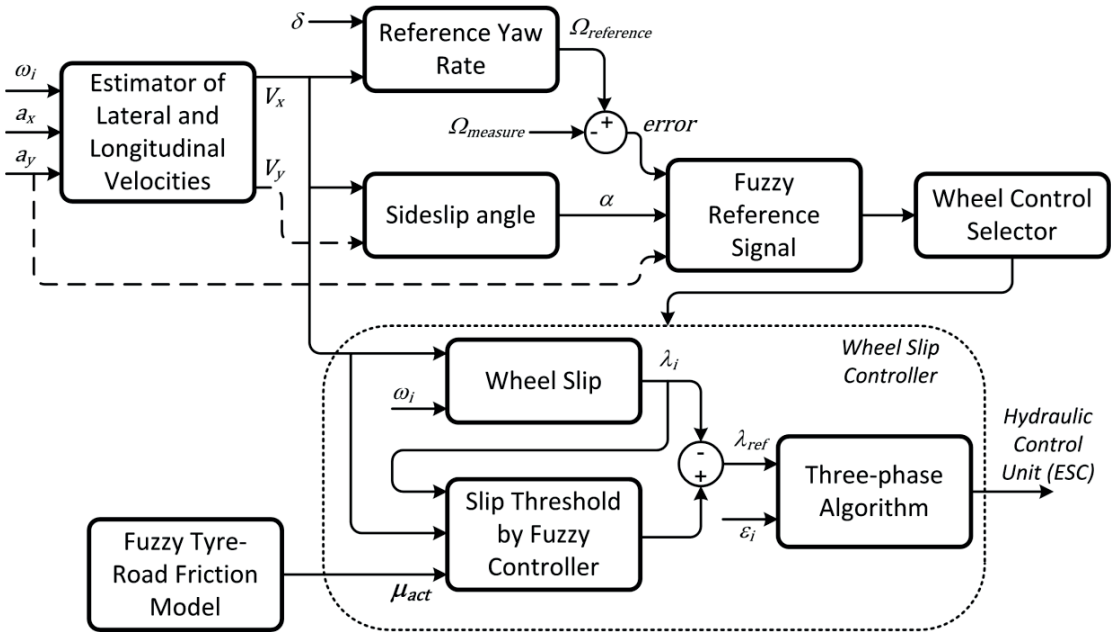

Figure 33 - Architecture of advanced ESC system

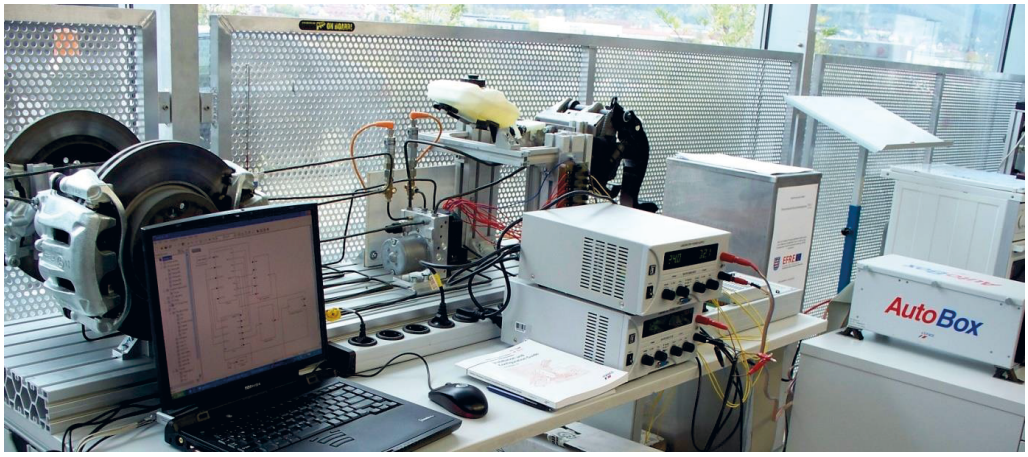

Figure 34 - HIL brake test rig of the 1st generation at Automotive Engineering Group, Technische Universität Ilmenau

Table 5: Results of HIL simulation for straight-line braking

Parameter	Ice	High water film
Brake distance, m	73,99	64,04
Maximal achieved wheel slip value front wheel, front / rear wheels	0,525/0,314	0,550/0,267
Average wheel slip value, front/rear wheels	0,127/0,123	0,109/0,121
Average brake torque before the pressure release phase, Nm front/rear wheels	1940/2240	variable
Average brake torque reduction before the pressure build-up phase, Nm, front/rear wheels	970/1565	variable
Average number of pressure swapping during one operation cycle, front/rear wheels	3/4	3/5

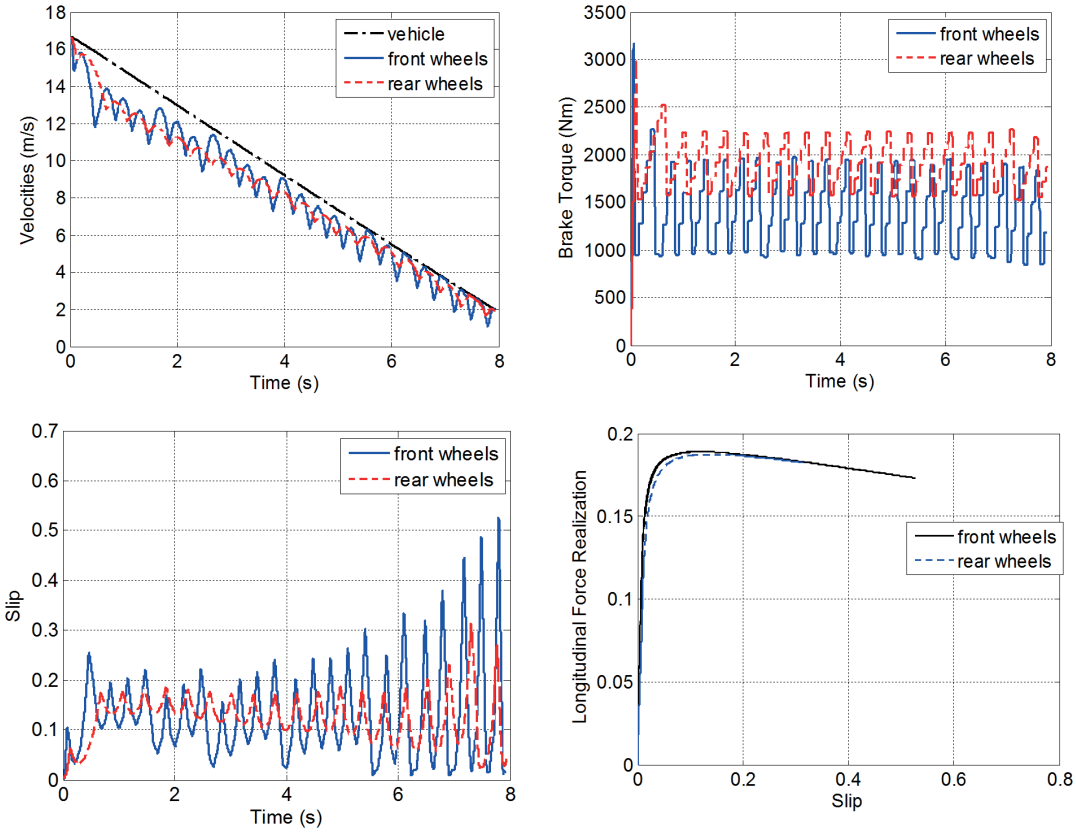

Figure 35 - Results of HIL simulation of straight-line braking on ice

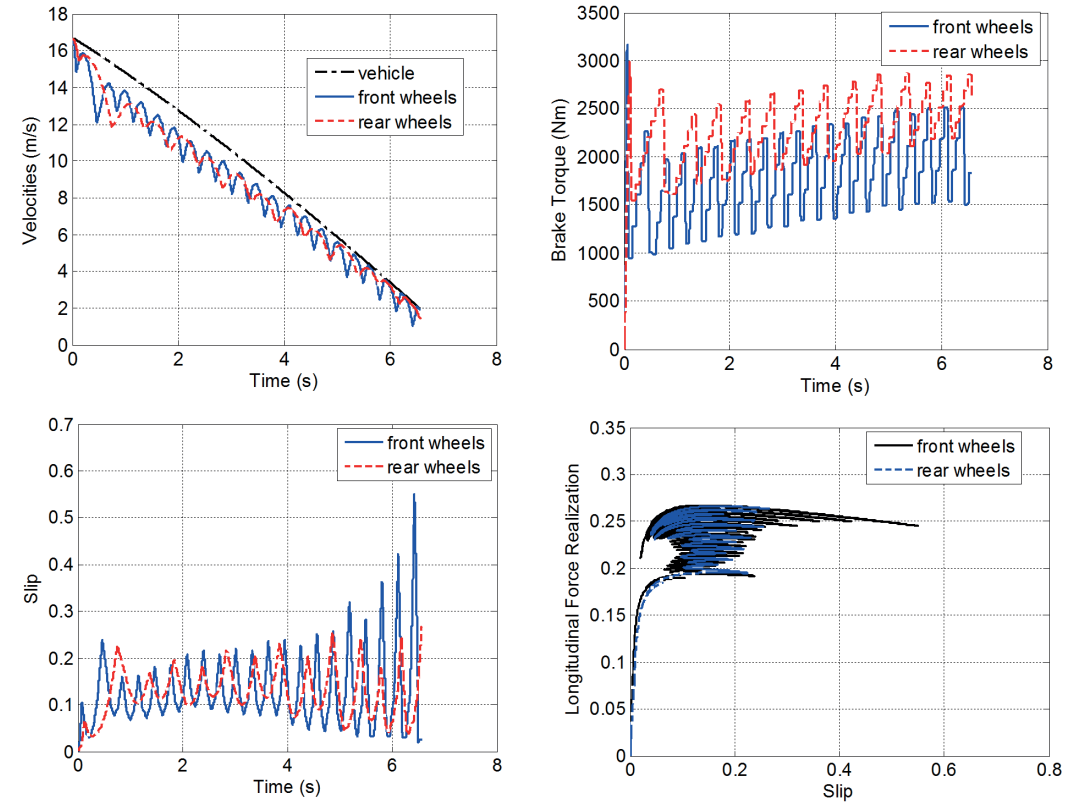

Figure 36 - Results of HIL simulation of straight-line braking on asphalt with high water film

(ii) Dropping of friction during straight-line braking. In this case, the vehicle decelerates at the beginning on the asphalt surface with $\mu_{env} = 0,8$ (linguistic attribute *XIV_A* from Table 4). Then the system detects a sharp reduction of friction and identifies that it is caused by the icy road surface (linguistic attribute *III_A* from Table 4). It can be seen from the simulation results in Figure 37 that the controller performed adaptation of the control thresholds to ensure stable braking without wheel blocking.

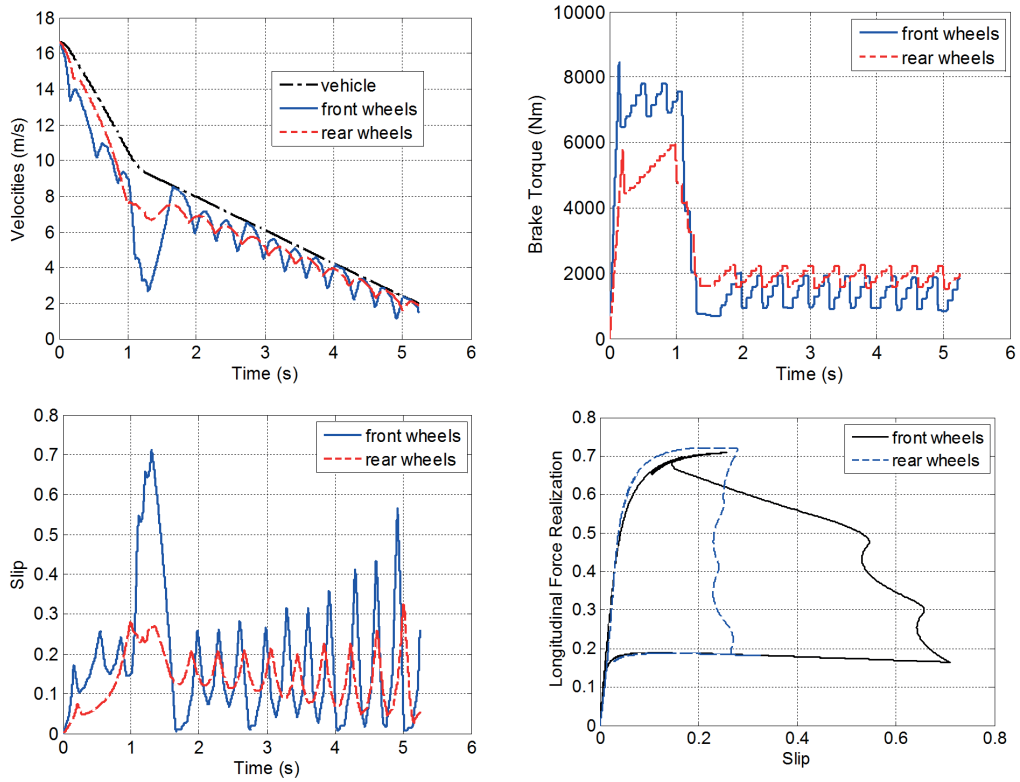

Figure 37 - Results of HIL simulation of straight-line braking with reduction of friction

(iii) Lane-change maneuver. Figure 38 illustrates the simulation results for a lane-change maneuver on ice (linguistic attribute *III_A* from Table 4). It can be seen that the vehicle keeps the trajectory with the reduction of the yaw rate amplitude, the lateral acceleration and the vehicle side slip angle. For comparative purposes, the lane-change simulation on the HIL test rig was also done for the vehicle motion on the asphalt road with high water film (linguistic attribute *III_C* from Table 4). Table 6 summarizes results for both surfaces. An analysis of driving on the highly wet road shows that the control system keeps the main stability-related parameters (yaw rate, vehicle side slip angle) close to the results for the icy surface. Here the environmental coefficient of friction $\mu_{env} = 0,2$ is similar for both surfaces, but for the wet road the actual friction coefficient during the maneuver was slightly increased up to $\mu_{act} = 0,27$.

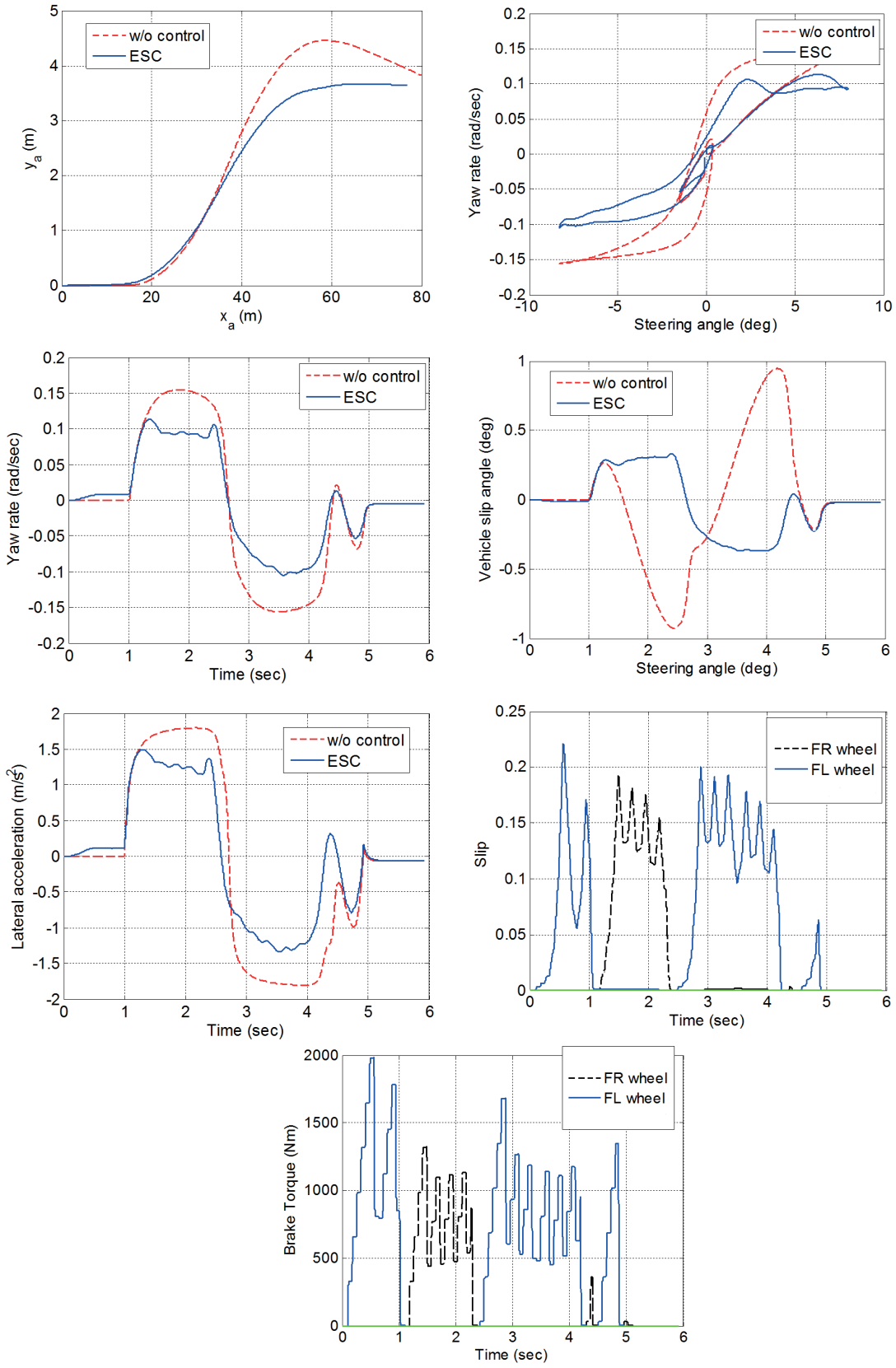

Figure 38 - Results of HIL simulation of the lane-change maneuver
Indices: FR – front right wheel, FL – front left wheel

Table 6: Results of HIL simulation of lane-change maneuver

Parameter	Ice	High water film
Maximum amplitude of yaw rate, rad/s	0,218	0,265
Average yaw rate, rad/s	0,066	0,078
Maximum achieved wheel slip value - front left wheel - front right wheel	 0,221 0,192	 0,280 0,205
Maximum amplitude of vehicle side slip, deg	0,699	0,843
Average vehicle side slip, deg	0,220	0,249
Maximum amplitude of lateral acceleration, m/s^2	3,606	3,335
Average lateral acceleration, m/s^2	1,254	1,028
Average brake moment before the pressure release phase, Nm - front wheel - rear wheel	 1983 1323	 2013 2313
Average brake moment reduction before the pressure build-up phase, Nm - front wheel - rear wheel	 500 460	 600 550

In such a manner, the ESC performed the adaptation of the control strategy to identified road type. In particular, higher brake torques are realized and the control thresholds are adjusted to be in line with the increased wheel slip on the surface with high water film.

2.2.4. Summary

The following conclusions can be made based on case study results:

- Combined use of information from on-board and on-road sensors makes feasible the tyre-road friction identification with taking into consideration physical parameters of the contact surface and the driving environment;
- Proposed approach to tyre-road friction identification extends the functionality of the active safety control through recognition of road conditions that can be efficiently used for the tuning of control algorithms of ABS, ESC and other active safety systems;
- Reasonable implementation of introduced method relates to active safety systems integrated with the vehicle-to-road and vehicle-to-infrastructure communications.

2.3. Chapter Summary

Chapter 2 overviewed methods used in active safety systems for the definition of tyre-road interaction parameters, in particular, for the friction coefficient. Their analysis can be summarized as follows:

- Both model-based and sensor-based deduction of tyre friction parameters is receiving now wide implementation in controllers of active safety systems;
- Application of physical and multi-body tyre models in the controllers is limited by requirements to real-time operation, therefore (semi-)empirical models are preferential in many contemporary systems. However, integration of active safety control systems related to different domains of vehicle dynamics can call for the implementation of more complex tyre models to increase the control robustness;
- Research studies propose various methods for tyre friction estimators, but clear benchmarking criteria for applicability of different estimation tools are still rarely explored;
- A promising technological area is to use acoustic and optical sensors for road type identification or tyre friction definition that supports active safety controllers with additional informational channels;
- Of special attention is also estimation of tyre-road parameters with the use of combined on-board and on-road sensor information. Such a methodology becomes more and more recognition due to the development of vehicle-to-road and vehicle-to-infrastructure technologies.

3. INTEGRATED ACTIVE SAFETY SYSTEMS

3.1. Impact of System Integration on Active Safety

Development of an integrated active safety systems responsible for simultaneous improvement of braking, handling, stability, ride comfort and other vehicle functions and properties is one of the most challenging research areas in the vehicle dynamics control. Basic works in this area have originated in the middle of 1980s. In particular, the study [158] introduced results of the project *Trilby* initiated by General Motors, where a global integration architecture for various vehicle subsystems has been developed, Figure 39.

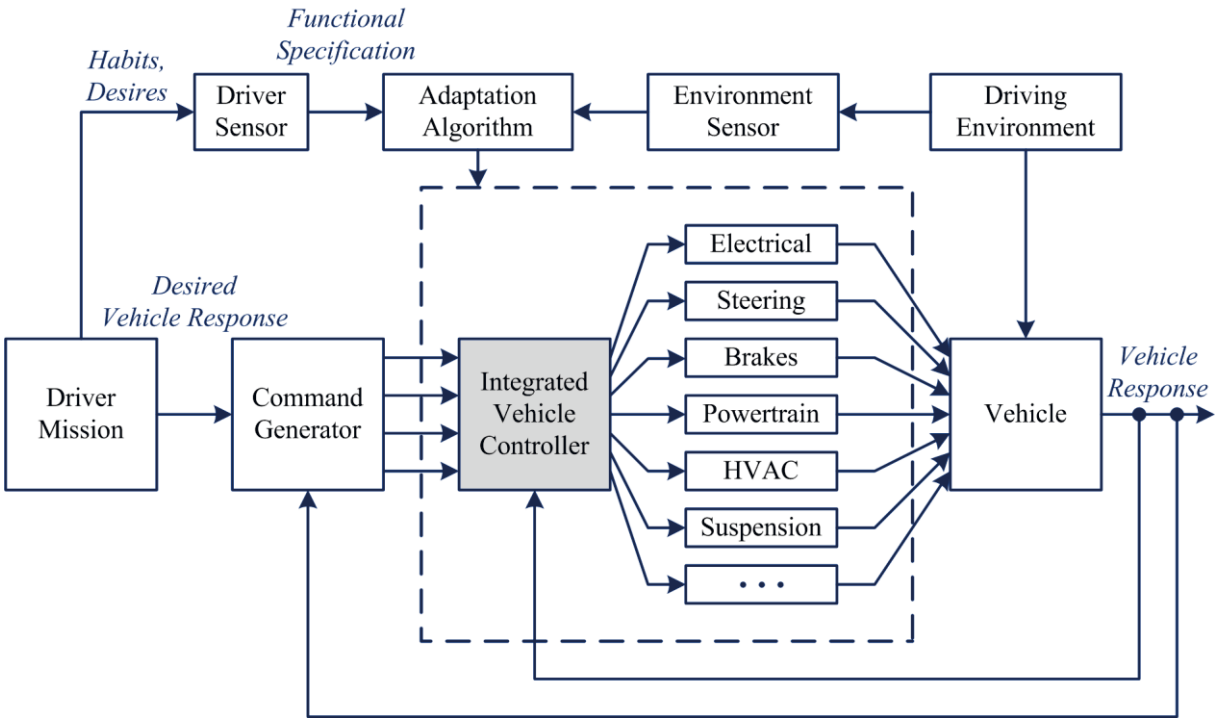

Figure 39 - Integrated control with driver and environmental adaptation (reproduced from [158])

The main goal behind the system integration from viewpoint of active safety improvement is to increase the utilization of tyre-road friction and to enlarge the area of stable vehicle motion. It can be illustrated with the longitudinal / lateral acceleration (g-g) diagram. In particular, researchers from Toyota investigated influence of several control systems on different regions of g-g diagram, Figure 40, and then illustrated a combined effect that can be expected from the system integration [159], Figure 41. It can be seen from this picture that combination of the

active steering with the traction / braking control increases safe steering limits at high longitudinal acceleration / deceleration. Simultaneously integration of the active steering and the active suspension enlarge safe steering limits at high lateral acceleration that is advantageous for rollover prevention. Generally, an ideal integrated vehicle dynamics control system could provide the full utilization of tyre traction for actual friction conditions (the outer circle on Figure 41).

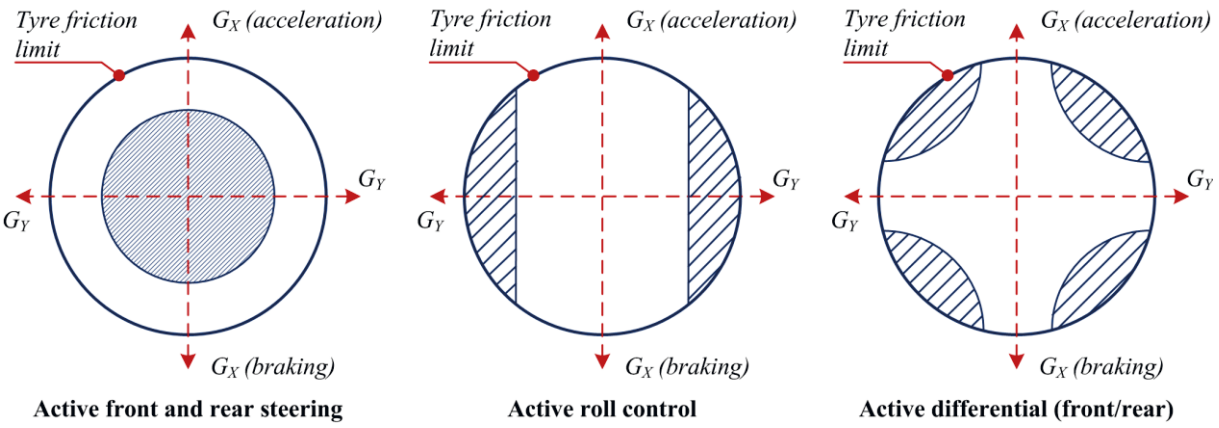

Figure 40 - Effective range (shown as hatched regions) of different control systems (adapted from [160])

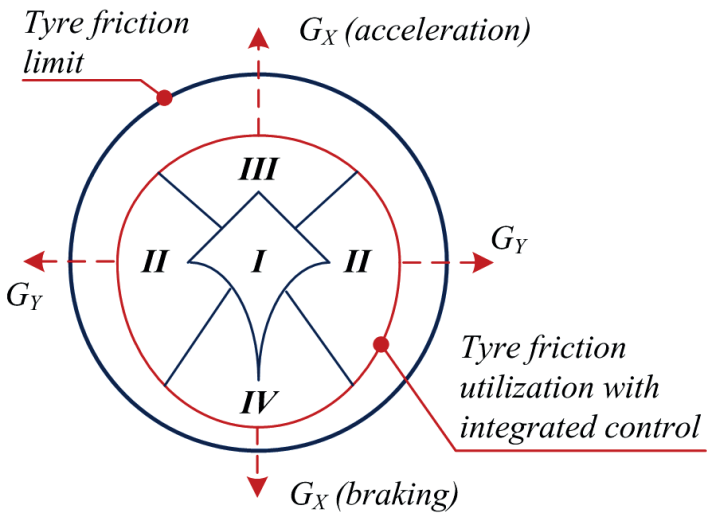

Figure 41 - Connection of integrated control and acceleration limits. Regions: I - without control; II - integration of active suspension and active front and rear steering; III - integration of traction control and active front and rear steering; IV - integration of anti-lock braking control and active front and rear steering

Many academic and industrial studies investigated different combinations of active chassis and powertrain systems. In this regards, most of known variants of integrated active safety control

has the main goal to improve vehicle stability, at least in particular critical situations. For instance, solutions are developed where the ESC system is being integrated with the active steering [72], [161], [66], the torque vectoring [162] and another active chassis systems like the active roll control, the active differentials and others [163], [164]. Nevertheless, any variant of system integration has some limitations from viewpoint of global energy efficiency, failsafe operation, processing time etc. In particular, Trächtler in [165] has shown that demand for systems integration to ensure the system compatibility is varied between individual subsystems, Figure 42. This statement can be also confirmed with the results of the study of Mitsubishi Motors investigated the influence of integration of the ABS, the active differential, the active steering and the ESC on the cornering performance [166]. Following this study, Figure 43 indicates that subsystems show quite different performance from viewpoint of stability and handling. Another relevant research has been introduced in [167], where the generation of correcting yaw torque from eight subsystems is investigated for the passenger car at different driving manoeuvres. Figure 44 displays an essential difference between individual subsystems in yaw dynamics compensation that points out to the demand on a careful analysis of subsystem combination for every driving maneuver.

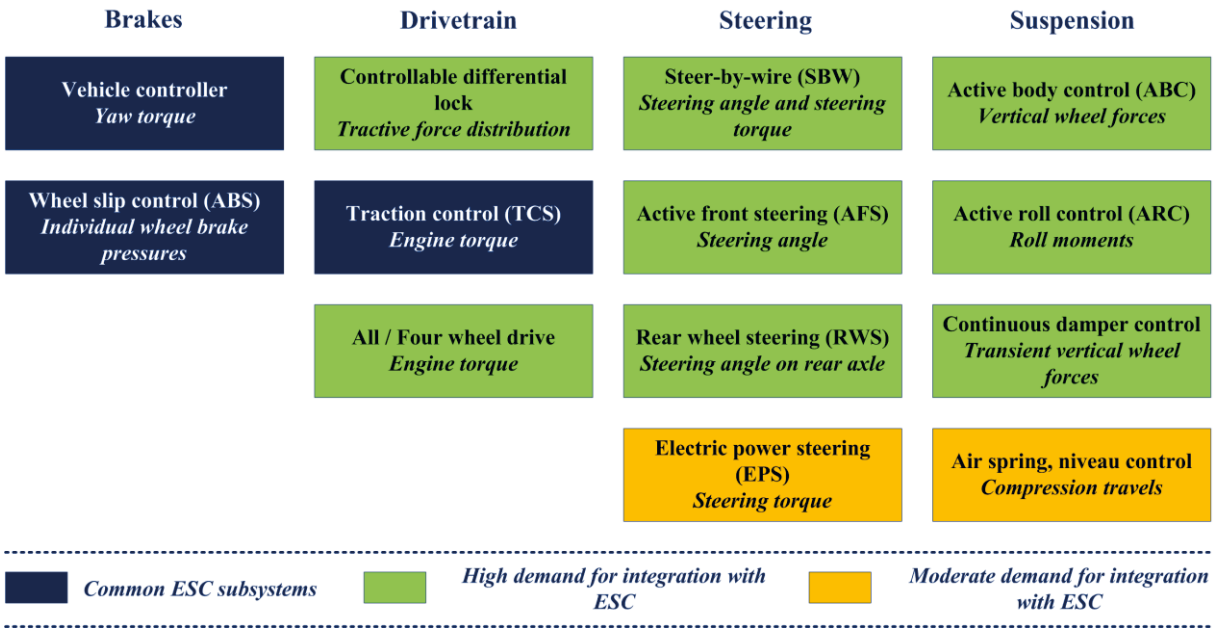

Figure 42 - Possible integration of subsystems for ESC (adapted from [165])

Hence, real definition of mechanisms of subsystem integration within an integrated vehicle dynamics controller as well as the control boundaries for each subsystem is a very complex

task. This requires not only a proper consideration of participating subsystems but also minimization of possible conflicts between the improvement of one vehicle property (e.g. stability) and the deterioration of another feature (e.g. energy efficiency) during the control process. Some relevant variants of integration of vehicle dynamics control / active safety systems are discussed in next section.

		In improving cornering	In restraining cornering
During acceleration	Longitudinal differential limiting control	–	★
	Lateral torque vectoring control	★★★	★★
	Braking control	★	★
During deceleration	Longitudinal differential limiting control	–	★
	Lateral torque vectoring control	★★	★
	Braking control	★★	★★★

★: Control effect

Figure 43 - Comparison of cornering effects from different subsystems (reproduced from [166]*)*

System / Potential		AFS	ARS	ARC	ESC	TVbB	aLSD	TVD
Straight Line Driving		13.000	12.000	-	11.000	4.000	-	4.500
Handling Region	OS	17.000	5.000	600	9.000	-	1.500	3.000
	US	5.000	16.000	600	5.000	6.000	-	2.500
Max. Lateral Acceleration	OS	2.500	1.500	2.000	10.500	-	1.000	1.500
	US	-	7.000	2.300	6.000	7.500	-	1.700

Figure 44 - Overview of systems yaw torque potential in Nm (reproduced from [167]); AFS - active front steering, ARS - active rear steering, ARC - active anti-roll bars, ESC - electronic stability control, TVbV - torque vectoring by braking, aLSD - active limited slip differential, TVD - torque vectoring differential, OS - oversteer conditions, US - understeer conditions

3.2. Overview of Integrated Active Safety Controllers

3.2.1. Classification of integrated systems

The integration of active chassis and powertrain systems can be considered in relation to three domains of vehicle dynamics, Figure 45. From this standpoint the integrated control can specifically address longitudinal, lateral and vertical motion of the vehicle or can have cross-domain applications. By the cross-domain application is meant that integrated systems are targeting simultaneously an improvement of the performance in terms of parameters related to vehicle dynamics in XY-, XZ-, YZ- or even XYZ-frame of reference. This classification was proposed by the author in [168].

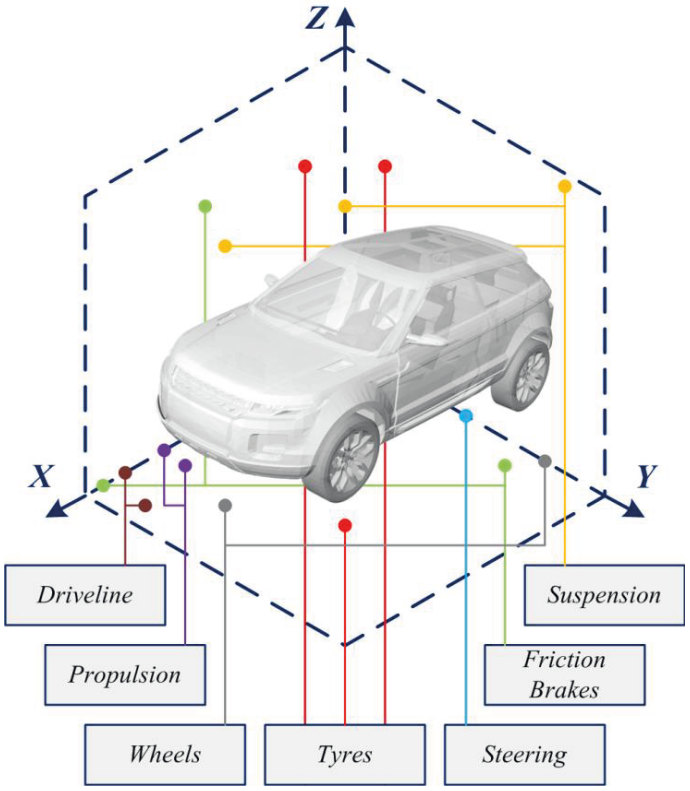

Figure 45 - A frame of reference of ground vehicle dynamics

The *X-integration* means a combined operation of systems for the purposes of longitudinal vehicle dynamics control, e.g. the braking or traction control. A case in point is the electric vehicle brake system integrating conventional friction brakes and electric motors operating in a regeneration mode. Next example is a variant of the traction control uniting the motor

management and active differential. For the X-integration, the most important performance criteria are the utilization of longitudinal friction of tyres μ_x, minimization of tyre energy dissipation and wheel slip power losses.

The *Y-integration* is attributed to the system cooperation for improvement of the lateral vehicle dynamics control. It concerns, for example, the combination of the active steering and the brake-based or torque-based yaw moment control. The integration performance in this case is assessed through parameters related to the vehicle side slip angle β and yaw rate $d\psi/dt$.

The *Z-integration* implies a joint operation of systems influencing the vertical vehicle dynamics. The coordination of the active suspension and the dynamic tyre pressure control can be considered in this context. Different indicators of ride comfort like the vertical acceleration and the vehicle body vibration frequency can characterize the performance of corresponding integrated systems.

The *XY-, XZ- or YZ-integration* supposes such a system combination that influences simultaneously two corresponding domains of vehicle dynamics. For instance, the brake control and active suspension can illustrate the XZ-integration; the active roll control and torque vectoring / electronic stability control belong to the YZ-integration. The system performance in such cases has to be assessed with integrated criteria uniting particular parameters of longitudinal, lateral or vertical vehicle dynamics.

Finally, the *XYZ-integration* cover all domains of vehicle dynamics. This class relates mainly to over-actuated / multi-actuated vehicles and deals with control tasks to find an optimal vehicle performance at any safety- and efficiency-critical manoeuvres. At that, the performance criteria can cover simultaneously vehicle stability, ride comfort, braking and traction efficiency, minimization of power losses, et al.

3.2.2. Design variants of integrated active safety systems

This section introduces several typical and reasonable examples of the integration of chassis and powertrain systems to enhance the active safety.

X-integration class: Brake and suspension control. The integration of the brake and suspension control from viewpoint of longitudinal vehicle dynamics enhances the braking performance, especially under conditions of rough, uneven surfaces, deformable grounds as well as by uphill and downhill braking. Road unevenness has an adverse influence on the tyre-surface contact: the contact is becoming a high grade of inhomogeneity that reduces the utilization of tyre friction. Moreover, road disturbances can affect the signal quality of the wheel speed sensors required for the ABS. As a consequence, most of known ABS algorithms are being deactivated in off-road conditions. These shortcomings can be avoided with the combined operation of the brakes (ABS control) and suspension control. General control scheme under discussion is shown on Figure 46. The global control task in this case is to minimize the control error e between the actual λ and reference λ_{ref} wheel slip at braking. The reference wheel slip is selected in the area corresponding to the maximum tyre-road friction for actual surface conditions (see Figure 2). The integrated controller produces the control demand u, which is splitting up between the actuators. The brake actuators produce the brake torque to be applied to the wheel. The suspension actuators change the lifting and pitching forces on the wheel to compensate road disturbances z. To eliminate the road disturbances, a certain transfer function $H(s)$ can be applied to generate the corrected control demand u^* (a corresponding approach is discussed, for example, in [85]).

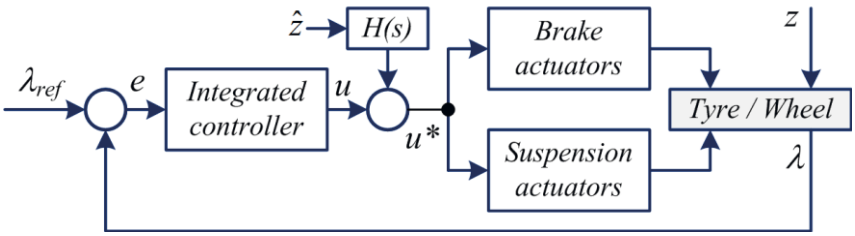

Figure 46 - Structure of integrated brake and suspension control [168]

The effect on the braking performance from the combination of the suspension and braking is demonstrated in research literature for different suspension systems. In particular, one of the first relevant studies [84] has investigated the ABS and the suspension equipped with electro-hydraulic actuators. The simulation of the car braking on the wet asphalt demonstrated that the stopping distance can be reduced by 7-8% with the integrated control as compared with the conventional ABS braking. Integration of the braking and suspension control is more reasonable for the vehicles operating in off-road conditions. This can be confirmed with results

of the study [86] investigating the braking of a sport utility vehicle on two types of rough terrain with the integration of the ABS and the semi-active $4S_4$ suspension unit. Considering braking from 80 km/h to 10 km/h, the optimal integration variants allowed reduction of the stopping distance on 1,9 m for the road with the parallel corrugations and on 9,0 m for the Belgian pavement.

Y-integration class: Active steering and brake-based yaw dynamics control. The active influence on yaw dynamics can be basically realized through the control on wheel torques and steering wheel angles. Hence, possible integration variants can involve combinations of the brake-based yaw control (electronic stability control, yaw moment control YMC), the torque-based yaw control (torque vectoring), the active front and rear steering (AFS, ARS), and the active all-wheel steering (AWS). An example of such a combination has been investigated by Nagai and his co-authors in [66] for the controller architecture illustrated on Figure 47. Here a model-matching controller based on the 2-DOF model of the lateral vehicle dynamics is used. It includes feedforward and feedback parts for the generation of predictive and reactive components of (i) additional steering angle $\Delta\delta_f$ to be realized by the AFS and (ii) correcting yaw moment M_ψ to be realized by the ESC. The feedback part was proposed on the basis of the optimal control technique. The results from [66] did not display an essential effect from integration during the lane change or J-turn manoeuvres. However, a considerable improvement of the vehicle dynamics has been obtained for the situation with the side wind disturbance.

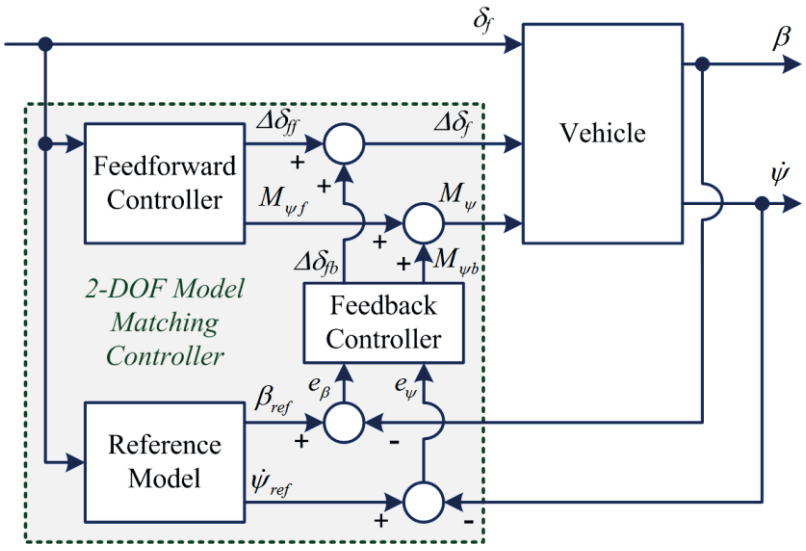

Figure 47 - Block diagram of integrated active front steering and direct yaw control system (adapted from [66])

More effect can be expected in the case of integration of the ESC with the active steering for both vehicle axles that was illustrated by Mokhiamar and Abe in [75]. Their study proposed the controller architecture based on the sliding mode and model-based methods with possibility to activate separately the active steering for front, rear or all wheels, Figure 48. Corresponding simulation results confirmed that the AWS provides not only better tracking of the reference vehicle path but also can guarantee better lateral vehicle dynamics in general, Figure 49.

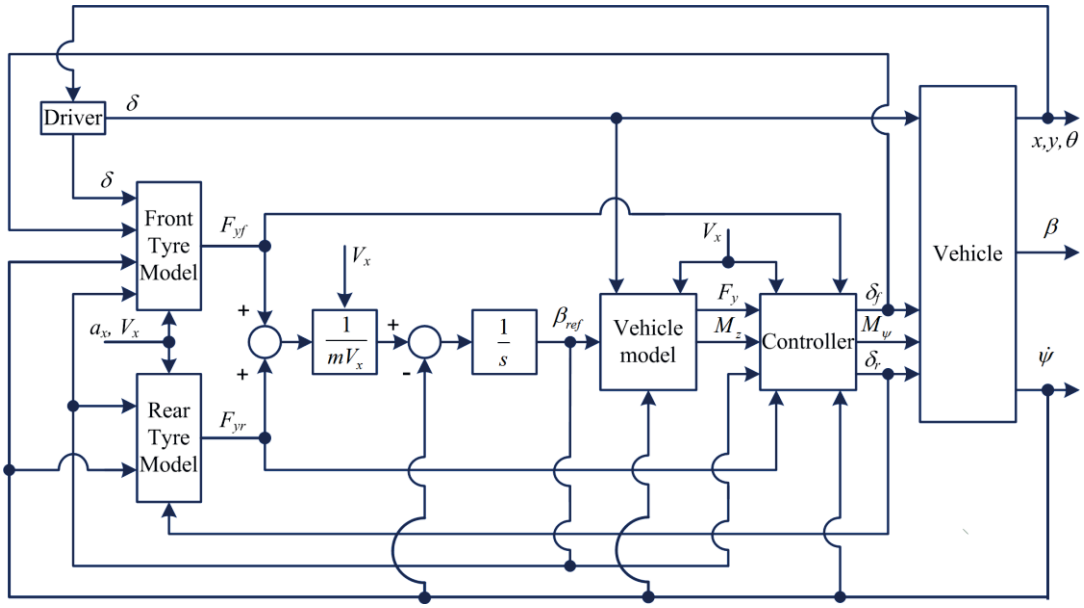

Figure 48 - Integrated controller for integration of ESC with active front and rear steering systems (adapted from [75])

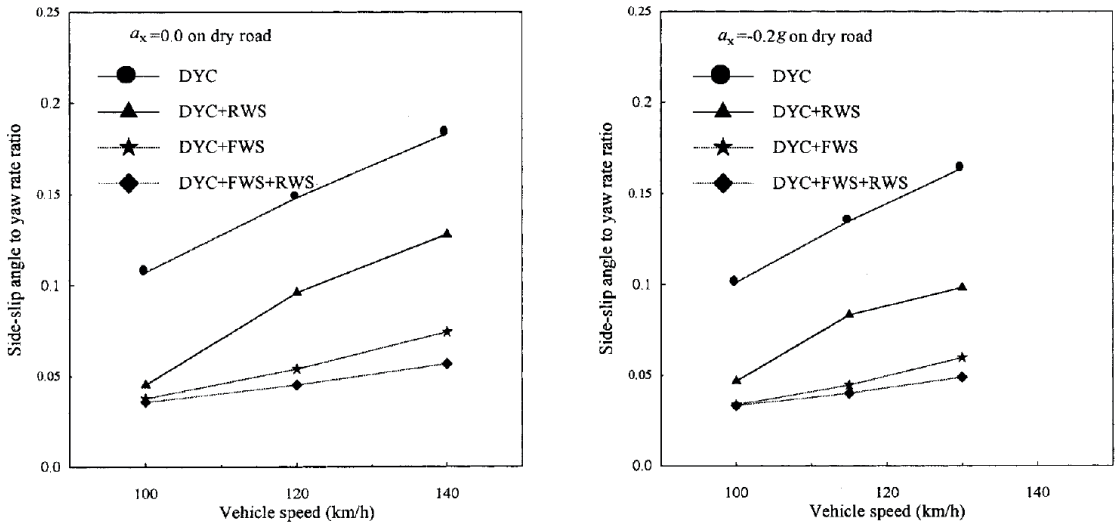

Figure 49 - Sideslip angle - yaw rate ratio versus vehicle velocity for different system configurations, DYC - direct yaw control, FWS - active front wheel steering, RWS - active rear wheel steering (reproduced from [75])

It should be noted that some studies are also considering concepts of integration of vehicle dynamics control systems with steer-by-wire instead of conventional active steering [169] [170]. An example of system integration is given on Figure 50. However, the inclusion of steer-by-wire into the control chain requires more complex implementation algorithms from viewpoint of system redundancy and fault-tolerant operation.

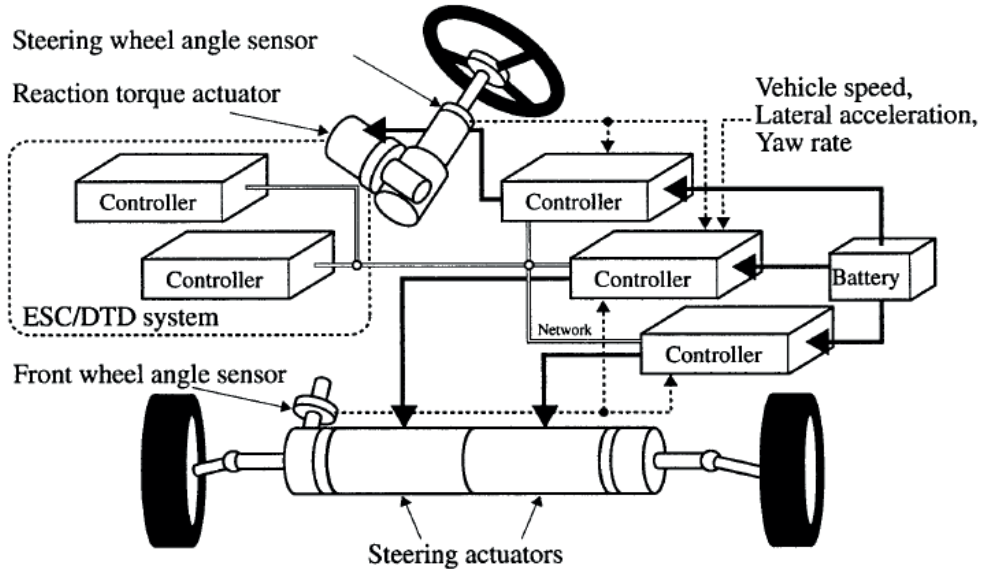

Figure 50 - Integrated control architecture with steer-by-wire system (reproduced from [170]); DTD - driving-torque distribution (torque vectoring)

Many recent investigations give special attention to more complex integration schemes with participation of several subsystems. In such cases possible conflicts between operation logic and vehicle properties can take place. In particular, Wang and his co-authors have mentioned in [164] for the integration of the active steering with the torque-based ESC systems that both participating systems can have different yaw-rate-tracking errors; as a result, a situation is possible when the active steering intends to control understeer behavior and the ESC intends to control oversteer behaviour, or vice versa. Moreover, the brake-based ESC control can correct yaw moment of the vehicle but simultaneously worsen the fulfilment of target of longitudinal acceleration tracking.

Many studies consider the active steering on only front wheels for the integration. However, such integrated systems are of interest rather for the research than for practical implementation because of minimal effect in stability improvement as compared with stand-alone yaw motion

control systems. Generally, the integration of the YMC with the AWS has more potential for enhancement both of stability and handling, especially for vehicles equipped with the steer-by-wire and for hybrid and full electric vehicles. But the complexity of the control logic is growing in this case due to high nonlinearity of the cornering dynamics of the vehicle with all steered axles.

X+Y-integration class: Active steering for braking and yaw dynamics control. This variant of integration aims at a better utilization of tyre friction in general and is efficient for specific manoeuvres as the split-μ braking. A corresponding option has been demonstrated in [171] for the coordinated operation of the active steering based on the H∞ controller and the rule-based ABS, Figure 51. The proposed system architecture has the supervisory integrated motion controller (IMC) with the event detector identifying the split-μ braking situation. When this takes place, the brake trigger disables the brake pressure attenuation, and the steering controller is activated in order to correct the yaw motion of the vehicle. The yaw dynamics control in [171] has the disturbances compensation caused by asymmetric brake pressure distribution. This method has been investigated both on the HIL test rig and the test vehicle and demonstrated a permanent reduction of the stopping distance at the split-μ braking within the initial velocity range 60...100 km/h. It should be mentioned that the improvement of the split-μ braking performance can be also achieved through integration of the active steering and torque-based yaw dynamics control. A corresponding example is given in the work [172], where a combination of the AFS and the semi-active rear differential is proposed.

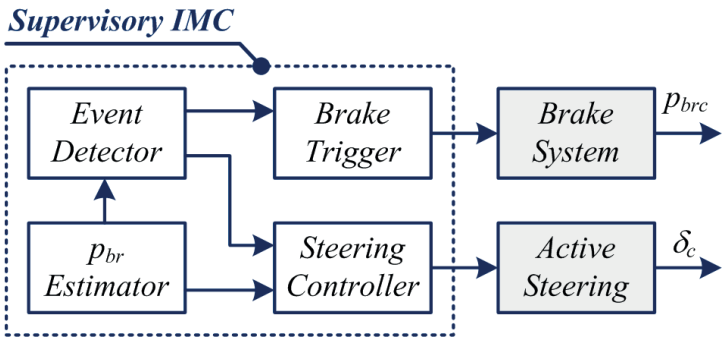

Figure 51 - Integrated active steering and brake control (adapted from [171]*)*

An important criterion indicating the performance of the systems under the X+Y integration class is the utilization of tyre friction forces both in the longitudinal and lateral domains. In this

regard several studies are demonstrated that it is reasonable to integrate the active steering and the yaw dynamics control with the consideration of tyre force allocation and constraints provided by tyre friction circle / ellipse. This statement can be illustrated with Figure 52 that explains a concept introduced by Toyota's researchers in [173], [174].

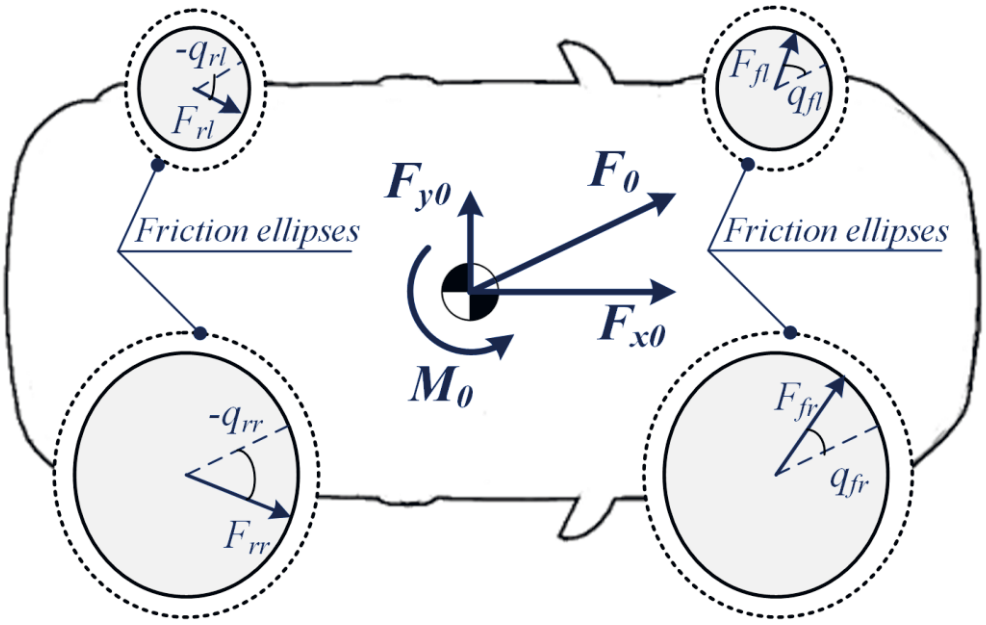

Figure 52 - Definition of target reference force and moment for integrated systems in accordance with tyre friction ellipses

In accordance with this concept, the system unites the individual active steering, the traction and braking control for each wheel and has to minimize the friction rate γ for each wheel that is calculated (using the tyre friction circle) as

$$\gamma_i = F_i / F_{\mu i} = \sqrt{F_{xi}^2 + F_{xi}^2} / F_{\mu i} \ , \tag{3.1}$$

where index "*i*" is for the front/rear left/right tyre position (*FL, FR, RL, RR*), F_{xi} and F_{yi} are the longitudinal and lateral tyre forces correspondingly, F_i is the resulting tyre force, $F_{\mu i}$ is the tyre friction force (defining the friction circle). Additional target is that the friction rate γ has to be the same for all tyres. The reference vehicle satisfying all mentioned conditions can be represented with certain target force F_0 and moment M_0. The angles q_i between the vectors F_i and F_0 are being used as the control inputs for the required task of the minimization of the γ-value. This task can be also introduced as the maximization of the following cost function:

$$J = \frac{\left(y_0 F_{x0}\right)^2 + \left(x_0 F_{y0}\right)^2 + M_{z0}}{\gamma} = y_0^2 F_{x0} \sum_i F_i \cos q_i + x_0^2 F_{y0} \sum_i F_i \sin q_i + \\ + M_{z0} \sum_i F_i \left(x_i \sin q_i - y_i \cos q_i\right)} \quad , \tag{3.2}$$

where x and y define the centres of tyre forces in relation to the centre of vehicle mass in longitudinal and lateral directions correspondingly. Using the optimal control for Eq. (3.2), the required control demands for the steering and traction/braking actuators are being defined on the next step. The simulation results presented in [174], [175] have shown that the proposed approach both improves the tyre fiction utilization and demonstrates better stability at different manoeuvres like split-μ braking, obstacle avoidance et al. as compared with non-integrated control. In particular, for single-shot sine-wave steering at the vehicle velocity of 22 m/s, the maximum resultant force was increased up to 10,5% with this method in comparison to the conventional yaw dynamics control.

Some variations of integrated systems with the optimal tyre force distribution are discussed in [176], [177], [178]. For instance, the work [176] investigated the method where the generalized control forces are defined using the sliding mode control, and their individual optimal distribution to the tyres is realized with the servo-loop part implementing the control allocation based on a constrained quadratic programming. It was illustrated with the simulation results that the corresponding integrated AWS and YMC can also sustain the vehicle stability under critical disturbances like an actuator failure and crosswind effect. Another comprehensive integration with the optimal tyre force distribution and servo-loop has been discussed in [177], where the system performance is evaluated with the normalize tyre force reserve (can be introduced as $1\text{-}\gamma$ in relation to Eq. (3.2)). The simulation of different steady-state and transient manoeuvres demonstrated that optimal coordination of the AWS and YMC reduces the normalized tyre force reserve in range 30...80% as compared with conventional systems [177].

Examination of studies investigating the systems under the X+Y integration class allows concluding that an observable effect can be expected with the use of an all-wheel steering. In many situations an integrated use of the AFS or ARS solely is not reasonable when one compares possible level of vehicle performance improvement and required complexity of the controller.

X+Y+Z integration class. In many cases the system architecture for the active safety control attributed to the X+Y+Z-integration class is not essentially different from the X+Y-, X+Z- or Y+Z-classes. But distinguishing features will be in the control logic. For example, the work [179] investigated the integration of the AFS, the AS and the WSC, where the active suspension has three control modes: (i) ride comfort (applied in normal control conditions), (ii) safety assistance (applied at emergency braking), (iii) stability assistance (applied at cornering manoeuvres). The wheel slip control has two modes: the ABS and the brake-based ESC. Depending on the vehicle motion parameters, the integrated controller identifies seven states and selects corresponding system combination, Table 7. The proposed rule-based approach can be easily implemented and ensures a certain level of robustness that was confirmed in [179] with simulation results of braking, single-lane and double-lane change manoeuvres at different road conditions. In particular, for the emergency braking, the system provided a faster wheel speed response and a better reference slip tracking due to the normal force variation by the active suspension. For cornering manoeuvres, the risk of critical situations in terms of the roll and yaw stability has been also reduced as compared with non-integrated system configurations.

Table 7: State-based IMC (adapted from [179])

Vehicle motion parameters and conditions	**Priority control task**	**System integration**
Normal driving $\lvert\delta\rvert<\delta_{th} \wedge \lvert d\psi/dt\rvert \le (d\psi/dt)_{th} \wedge \lvert a_x\rvert<a_{xth}$	Comfort	AS (ride comfort mode)
Emergency braking $\lvert\delta\rvert<\delta_{th} \wedge \lvert d\psi/dt\rvert \le (d\psi/dt)_{th} \wedge \lvert a_x\rvert \ge a_{xth}$	Braking performance	WSC (ABS mode) + AS (safety mode)
Neutral or understeer motion $\lvert\delta\rvert<\delta_{th} \wedge \lvert d\psi/dt\rvert > (d\psi/dt)_{th}$	Handling	AFS + AS (stability mode)
Neutral or oversteer motion $\lvert\delta\rvert \ge \delta_{th} \wedge V_{ch}^2>0 \wedge V_{ch}^2>V^2;\ (1<1+V^2/V_{ch}^2 \le 2)$		
Split-μ braking $\lvert\delta\rvert \ge \delta_{th} \wedge V_{ch}^2>0 \wedge 0 \le V_{ch}^2< V^2;\ (2<1+V^2/V_{ch}^2)$	Stability	WSC (ESC mode) + AFS + AS (stability mode)
Unstable motion with high understeer $\lvert\delta\rvert \ge \delta_{th} \wedge V_{ch}^2<0 \wedge \lvert V_{ch}^2\rvert \ge V^2;\ (0<1+V^2/V_{ch}^2 \le 1)$		
Unstable motion with high oversteer $\lvert\delta\rvert \ge \delta_{th} \wedge V_{ch}^2<0 \wedge \lvert V_{ch}^2\rvert < V^2;\ (1+V^2/V_{ch}^2 \le 0)$		
δ_{th} is the steering angle threshold, V_{ch} is the characteristic vehicle velocity computed according to the Hurwitz stability criterion, a_{xth} is the longitudinal acceleration threshold, $(d\psi/dt)_{th}$ is the yaw rate threshold		

The X+Y+Z-integration class can be also represented with the system architecture, when only two systems are responsible for the vehicle dynamics control in all domains (in such a case the vehicle has to be considered as multi-actuated, not over-actuated). The study [180] investigated

this case for the active suspension with the braking control, Figure 53. The control on the vehicle motion is realized through brake torques T_{brc} and suspension forces F_{zc}. In addition, the controller is synthesized using linear parameter varying (LPV) / H∞ method to address a disturbance attenuation problem. The work [180] investigated this approach by way of the double lane change simulation with variation of road surface conditions. It was observed that the proposed integration can not only ensure required stability and handling but also use efficiently dynamics of the actuators.

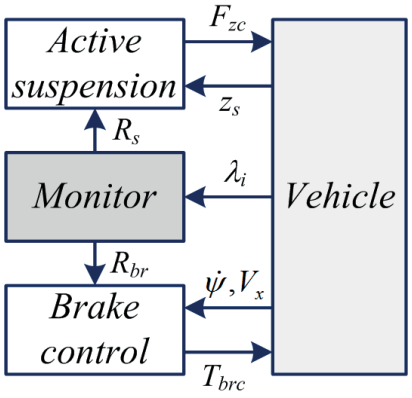

Figure 53 - Integration variant of active suspension and brake control (adapted from [180])

Several other complex control tools are investigated in various published studies dedicated to the system integration as applied to over-actuated / multi-actuated vehicles. In particular, the paper [181] proposed reinforcement learning control. The works [182], [183], [184] discussed diverse control allocation approaches. However, lack of (i) results experimentally validated in real driving conditions and (ii) benchmarking procedures for competitive control techniques does not allow to favour one or another method.

Further development of integrated systems under X+Y+Z- class is connected to X-by-wire technologies and electric vehicles. Here, essential progress was achieved in the middle of 2000s with the first prototypes and concepts of vehicles with the powertrain composed from two, three or four individual electric motors. In particular, introduction of an in-wheel motor was a key step in emerging integrated wheel corners. The relevant technologies were proposed by Siemens VDO, Michelin and Volvo [185], [186], [187]. The Autonomous Corner Module by Volvo has been investigated in different constructive variants with special attention given to the design aspects of suspension and embedding of planetary gear into the wheel hub unit.

eCorner of Siemens VDO integrated electric propulsion with active brake, damping and steering systems. An alternative wheel corner solution has been developed as Michelin Active Wheel, where similar set of active systems like eCorner is supplemented with specific tyre design. It can be expected that these concepts will receive more and more applications for future electric vehicles with mechatronic chassis.

3.2.3. Methods of system integration

The variants of active safety systems analysed in the previous section have diverse principles of the integration. Selection of the integration architecture for active safety systems depends on many factors and has to take into account response speed and energy consumption of actuators, limitations of individual systems in terms of corrective torques and forces, et al. An extended classification of available and potential integration architecture has been introduced in [188]. Following this classification, the integrated systems can be organized under (i) centralised, (ii) supervisory, (iii) hierarchical and (iv) coordinated control. However, there are no detailed recommendations in the analysed studies about the most appropriate variants of the integration architecture. For practical purposes, a simplified classification of integration methods is proposed in the presented habilitation thesis: two classes - *single-criterion* and *multi-criterion* - are conditionally designated. In the first case, the actuation or inclusion of individual systems into the control process is selected on the basis of a certain specific parameter of the vehicle dynamics. In the second case, the operation shares of all participating individual systems are defined by parameters characterizing different vehicle properties. Several most relevant examples for both cases are introduced next with particular attention given to vehicle dynamics parameters included into the decision-making process.

Single-criterion integration. A simple approach for the single-criterion architecture is to apply a rule-based coordination of individual systems, where the rules relate to one or more performance indicators of vehicle dynamics. One of the corresponding examples is introduced in the study [189] investigating the active steering, the active differential and the braking control under the Y-integration class. The control is based on the estimation of the side slip dynamics and uses β-$d\beta/dt$ phase plan to form the integration rules, Figure 54. For this architecture only active steering is initially included into the control chain. Then, when an actual driving situation becomes more critical, subsequent activations of the active driveline and the active braking take

place. Results of steer input simulations confirmed that the proposed order of the systems intervention provides a reasonable trade-off between stability and steerability and reduces a negative influence on the longitudinal vehicle dynamics [189]. The discussed method has been extended in [190] with the inclusion of the active suspension. However, simulation studies as applied to double-lane change manoeuvres with this extended configuration detected only minor improvements in the yaw rate and side slip dynamics.

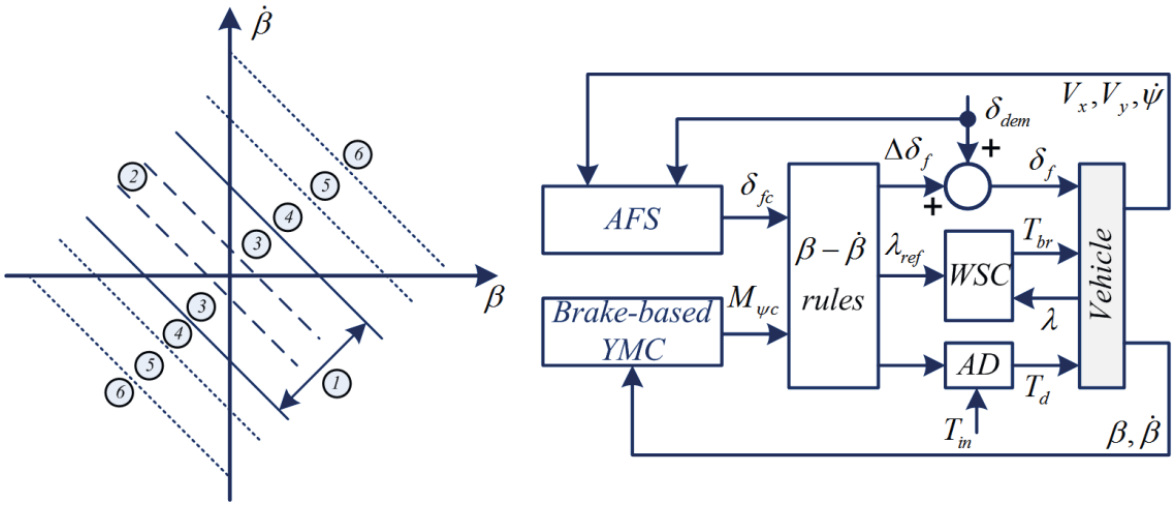

Figure 54 - Different regions in β-dβ/dt phase plan for the rule based integration scheme (reproduced from [189]); 1 - reference region for control design, 2 - active steering inclusion for steerability improvement, 3 - transitions between control tasks, 4 - active steering inclusion for stability improvement, 5 - active driveline inclusion, 6 - active braking inclusion

Other research works propose more practical and simpler methods, when the integration engages limited number of systems. In particular, the study [162] investigated the integration of the brake-based and torque-based yaw dynamics control (AD, ESC, TV) and used the state-based method as follows: (i) If the requested correcting yaw torque M_z^{req} can be generated by the active differential only, then the ESC and the TV are deactivated; (ii) If the requested correcting yaw torque M_z^{req} cannot be fully covered by the active differential, then the active differential still generates the maximum torque $M_{z,diff}^{max}$ and the rest torque $(M_z^{req} - M_{z,diff}^{max})$ is equally generated by the ESC and the TV (share of 50% for each system) under condition that the vehicle velocity should not be changed; (iii) If it is not possible to keep the vehicle velocity and to correct yaw dynamics simultaneously, the share of the ESC is increased to generate required yaw torque in spite of possible velocity reduction. Hence, such an approach considers both criterion of vehicle performance (velocity) and safety (yaw dynamics) during the control

process and tries to minimize the losses in performance (velocity reduction) by simultaneous ensuring the vehicle stability.

Another variant of rules for the integration of active steering and torque vectoring in the electric vehicle is proposed in [191]. Here the integration should follow the Gaussian activation function, Figure 55, calculated as

$$\chi_{ATVC}\left(\delta_{corr}\right)=\begin{cases}\exp\left[-\dfrac{\left(\delta_{corr}-\delta_{corr\_\max}\right)^2}{2\sigma^2}\right]\cdot 100\%, & \left|\delta_{corr}\right|\le 3^\circ\\ 100\%, & \left|\delta_{corr}\right|>3^\circ\end{cases}, \tag{3.3}$$

where χ_{AVTC} is the percentage of torque vectoring actuation, δ_{corr} is the steering angle required to correct the yaw dynamics in given driving conditions, δ_{corr_max} is the actuator range limit of the active steering controller. It can be seen that the condition (3.3) ensures gradual inclusion of the torque vectoring into the control process. From viewpoint of vehicle stability, it avoids the TV influence on driving comfort (provided by the active steering) as long as possible.

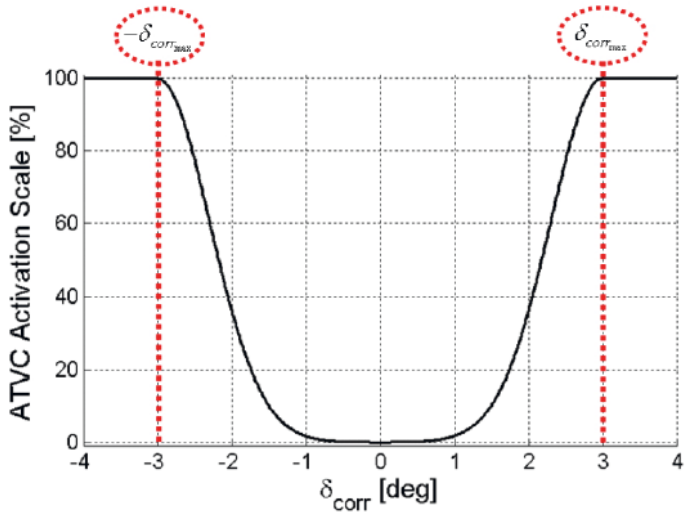

Figure 55 - Activation function used for the integration of torque vectoring and active steering (reproduced from [191]); ATVC - active torque vectoring control

Some summarized remarks can be done for the single-criterion integration principle:

- Most of relevant solutions are using the rule-based methods (including fuzzy methods) that is favourably for easier real-time implementation on the vehicle;

- Analysed single-criterion integration examples are generally considered the balance between two vehicles properties, in particular, stability vs. performance and stability vs. driving comfort; Inclusion of more vehicle attributes into the integration strategy can require more complex integration architecture.

Multi-criterion integration. Multi-criterion integrated active safety systems have mainly a multi-layer structure. To give an example, Figure 56 shows the architecture of the multi-layer vehicle dynamics control system proposed in [192] for an electric vehicle with two electric motors. The supervisory controller layer defines the reference vehicle dynamics. The upper level controller computes the actual parameters as vehicle forces and yaw moment, which are the inputs for the lower level controller determining actuator commands. The activation of participating subsystems depends on actuator constraints, which are set up by the lower level controller. For instance, as applied to the case study from [192], the supervisory controller defines firstly the control mode in accordance with Figure 57. But then the lower level controller performs the optimization of control actions by criteria of driving efficiency, minimization of allocation error, and wheel slip limits. After the optimization, the actuator commands are distributed individually to each actuator - electric motors and individual wheel brakes in the considered case. This approach has been validated by simulation of a complex manoeuvre including constant turning and several double-lane changes and confirmed better performance in terms of rollover index, minimization of the side slip and yaw rate error tracking as compared with the event-based ESC system [192].

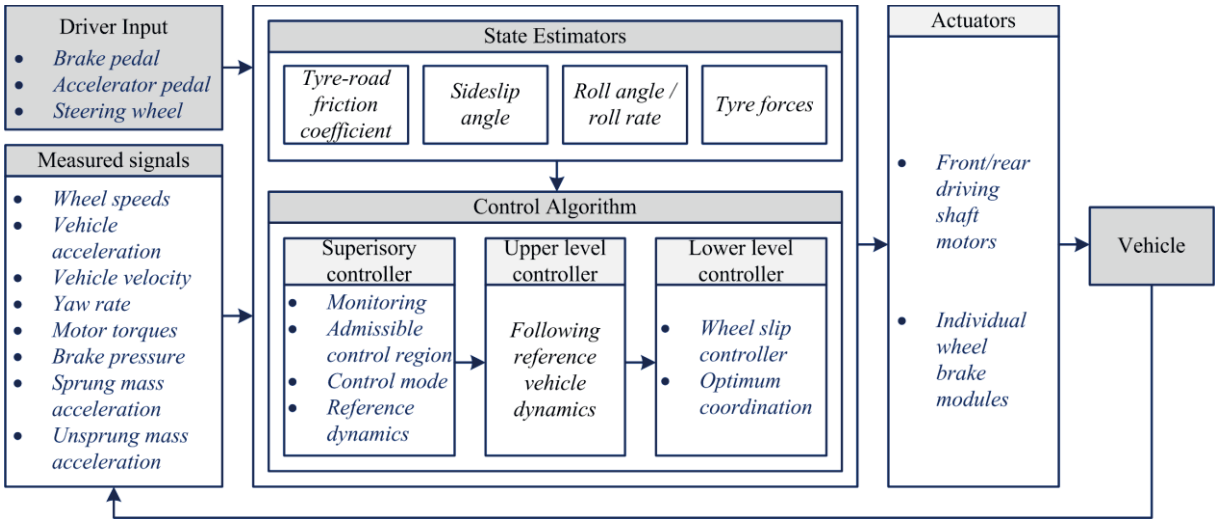

Figure 56 - Multi-layer vehicle dynamics control system (adapted from [192])

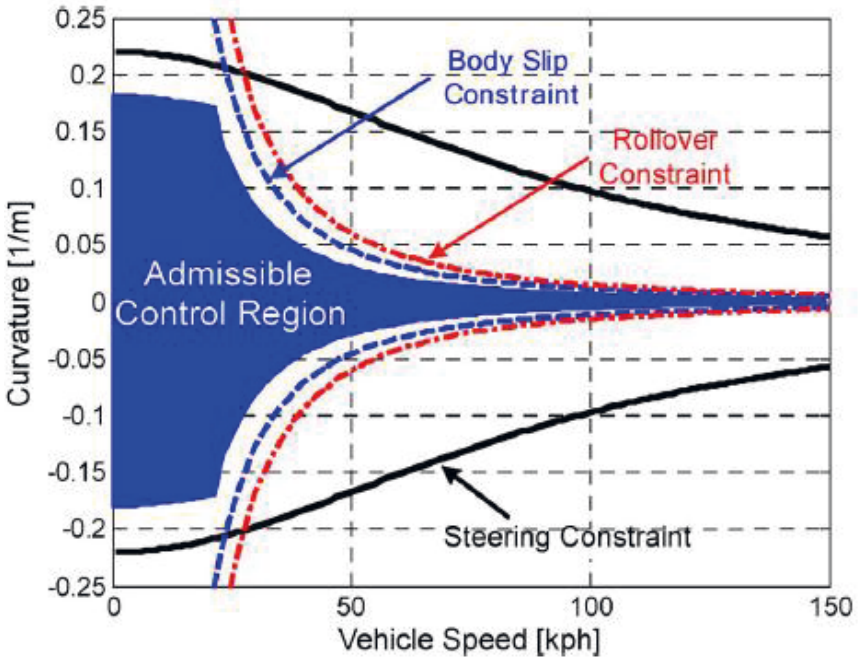

a)

Control Mode	Activation Condition	Speed Control	Yaw Rate Control
1	$(\lvert\kappa_d\rvert < \kappa_{max})$ & $(\lvert\gamma_{des} - \gamma\rvert < \gamma_{th})$	Inactive	Inactive
2	$(\lvert\kappa_d\rvert < \kappa_{max})$ & $(\lvert\gamma_{des} - \gamma\rvert \geq \gamma_{th})$	Inactive	Active
3	$(\lvert\kappa_d\rvert > \kappa_{max})$ & $(\lvert\gamma_{des} - \gamma\rvert < \gamma_{th})$	Active	Inactive
4	$(\lvert\kappa_d\rvert > \kappa_{max})$ & $(\lvert\gamma_{des} - \gamma\rvert \geq \gamma_{th})$	Active	Active

b)

Figure 57 - Example of admissible control region (a) and control activation rules (b) [192]
γ_{des} - reference yaw rate, γ - actual yaw rate, $\kappa_d=\gamma_{des}/V_x$, κ_{max} and γ_{th} - control thresholds

Many recent investigations related to the multi-criterion integration use various control allocation methods. Relevant integrated active safety systems are discussed in the works of Laine [193], Knobel [182], Shyrokau [194], and other authors. The control allocation requires optimization procedures to define the individual contribution of each individual system (actuator) to the control process. The different parameters of vehicle dynamics can be used in this regard. In particular, the study [195] has investigated a concept of the electric vehicle equipped with the motor torque control, the active steering, and the active suspension elements. The system under discussion belongs to the X+Y+Z-integration class. The operation of individual actuators is defined using the optimization problem with the following particular objectives: to minimize the tyre wear by minimizing the tyre slip angles α_i, to minimize the

energy consumption by minimizing the longitudinal tyre forces F_{xi} subjected to the tyre slip angles and wheel slip λ_i, and to minimize the utilization of the tyre friction potential:

$$\min_{\alpha_i}\left(f_1 = \sum_{i=1\ldots4} |\alpha_i| \right);\ \min_{\alpha_i,\lambda_i}\left(f_2 = \sum_{i=1\ldots4} F_{xi} \right);\ \min_{\alpha_i,\lambda_i}\left(f_3 = \max_{i=1\ldots4} \sum_{i=1\ldots4} \frac{\sqrt{F_{xi}^{\ 2} + F_{yi}^{\ 2}}}{\mu \cdot F_{zi}} \right). \tag{3.4}$$

Corresponding multi-objective optimization problem can be solved as a weighted sum of three mentioned objectives with weighting factors g_k:

$$\min_{\alpha_i,\lambda_i}\left(f = \sum_{k=1\ldots3} \left(g_k \cdot f_k \right) \right). \tag{3.5}$$

More information about the implementation of the control allocation in various active safety systems is given in [196], [197], [198]. Further Section 3.3.2 will introduce a corresponding case study. Summarizing, it can be mentioned for the multi-criterion methods of the active safety system integration with the control allocation that the complexity of problems of optimal distribution algorithms and definition of actuator constraints depends strongly from number of control systems (actuators) and objectives to be reached through the integrated control (cost functions for the optimization).

3.2.4. Summary

The presented overview of integrated active safety systems allows to conclude that they can be classified in accordance with longitudinal, lateral and vertical domains of vehicle dynamics. For the proposed classes each, various configurations of active chassis and powertrain systems are investigated in the research literature. However, a critical point for current research is the lack of clear benchmarking criteria to identify optimal or the most efficient combinations of cooperating systems. Many proposed solutions demonstrated certain effects in improvement of one or another vehicle feature as stability, braking performance, tyre friction utilization et al., but an analysis of corresponding energy consumption due to the operation of several systems for the same control tasks is often missing. It points clearly to the demand for the development of corresponding value engineering methods. Such methods are required both by designing the

integrated active safety systems and by benchmarking different system architectures by criteria of complexity, performance benefits, and robustness.

Effect from the integrated active safety control can be especially visible in the case of complex maneuvers causing critical driving situations. Proper evaluation of the system performance in such situations requires studies in new adequate procedures of validation and testing. Available testing standards use generally specific maneuvers as emergency braking, lane change et al. Therefore, advancement or development of new testing procedures for simultaneous evaluation of integrated system performance by criteria of safety, driving comfort, energy efficiency is strongly demanded.

To give several practical examples of designing integrated active safety control, the subsequent section will introduce results of two relevant case studies. These case studies were investigated at Technische Universität Ilmenau and consider applications both for conventional and electric vehicles.

3.3. Case Studies in Integrated Active Safety Control

3.3.1. Integrated stability control using the braking, steering and driveline systems

A. System architecture

The variant of integrated systems has been developed in cooperation between Technische Universität Ilmenau and Lawrence Technological University (USA) to investigate combined control on vehicle stability and performance using cooperating subsystems of driveline, brakes, and steering. Several essential results of this research are published in [199] and [200]. The developed controller has several main blocks depicted on Figure 58. Generally, the proposed algorithm of system integration can be described as follows.

Longitudinal velocity estimator calculates the vehicle speed from wheel speed sensor information ω_i and the longitudinal acceleration a_x^m using the recursive Kalman filter. The estimated velocity V_x^e, the measured acceleration a_x^m and the turning angle of the vehicle are then used in the reference vehicle model. The turning angle is resulted from the angle defined by the *driver* δ_f^m and additional angle from the active steering δ_f^{add}.

Reference vehicle model is necessary to find the control error as difference between idealized and actual vehicles parameters obtained by on-board sensors. The mathematical formulation of the reference vehicle model, used in this study, corresponds to the 12-DOF model, Figure 59. The 12-DOF model includes longitudinal (x), lateral (y), yaw (ψ) and roll (ϕ) dynamics of the vehicle and rotational dynamics of four wheels both about the spin and vertical axes. The research works carried out at Technische Universität Ilmenau confirmed a good applicability of this 12-DOF vehicle model to the development of controllers of active safety systems, especially using the hardware-in-the-loop design procedures [147]. The main output parameters of the model for subsequent processing are reference values of the yaw rate $d\psi^e/dt$, the vehicle side slip angle β^e, and the lateral acceleration a_y^e.

Using measured and calculated parameters, *boundary conditions* of the vehicle motion by the criterion of stability are defined on the next step. Because boundary conditions require inclusion

of information about *tyre-road friction* conditions, the *tyre model* is used to compute the maximum friction coefficient μ_{imax} for each wheel. The block of boundary conditions specifies errors for signals of the yaw rate, the vehicle side slip, and the lateral acceleration as the difference between the reference and measured values:

$$\Delta\dot{\psi} = \dot{\psi}^m - \dot{\psi}^e;\ \Delta\beta = \beta^m - \beta^e;\ \Delta a_y = a_y{}^m - a_y{}^e. \tag{3.6}$$

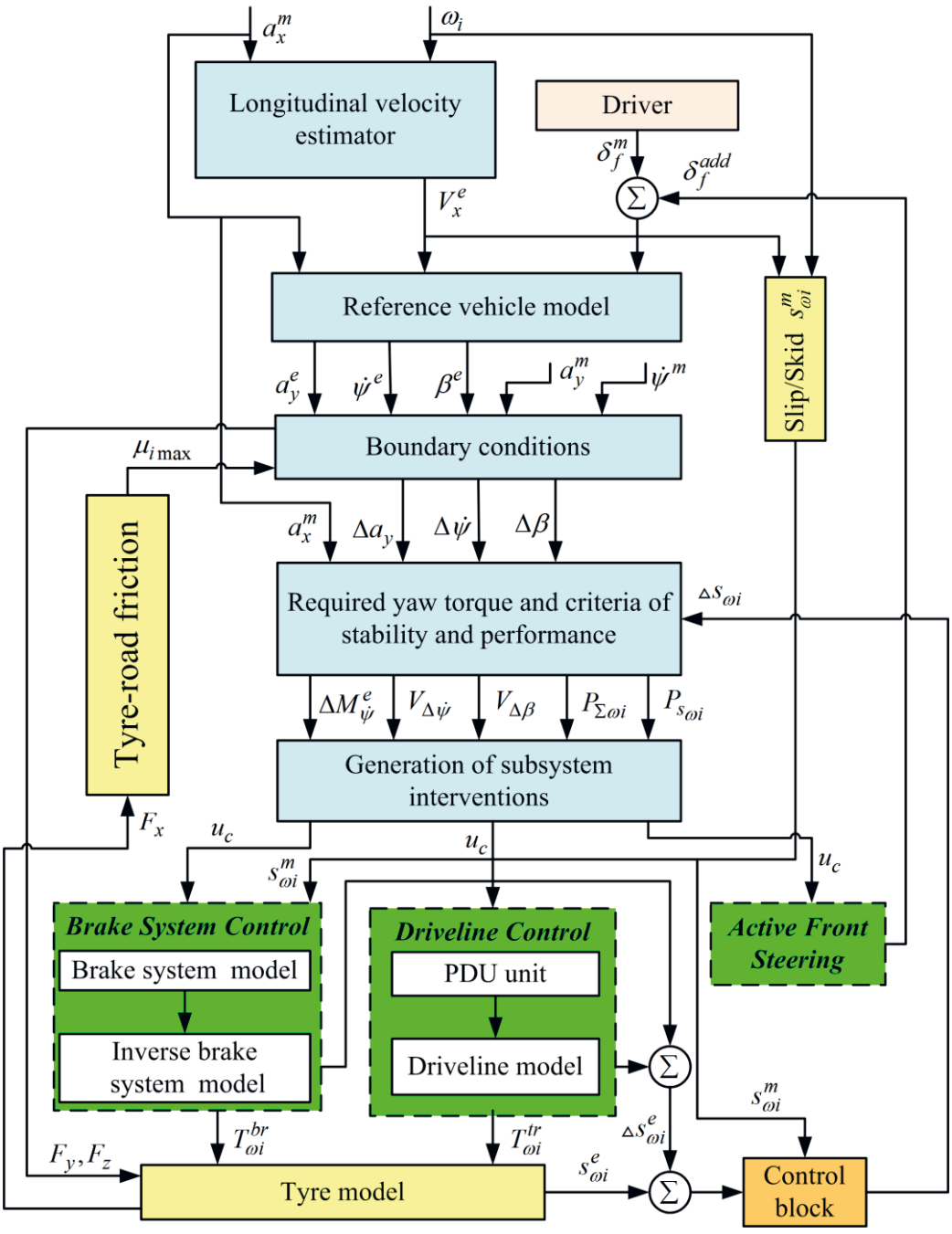

Figure 58 - Block diagram of integrated vehicle dynamics control algorithm

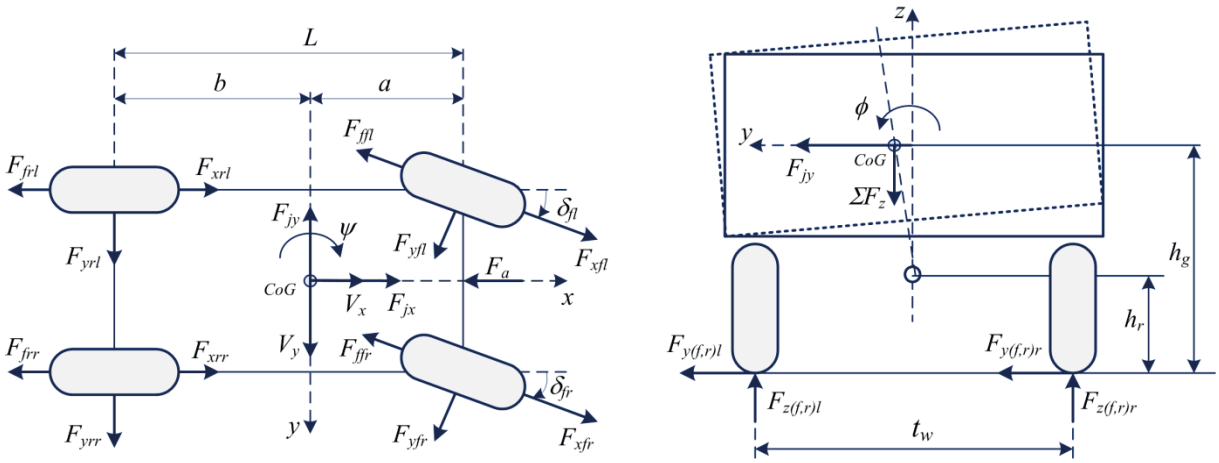

Figure 59 - 12-DOF vehicle model layout

Next block deduces *required change of the yaw torque* taking into account errors (3.6), longitudinal acceleration a_x^m and difference between the computed and measured *slip/skid factors*. This block defines also the stability and performance criteria of motion. The stability criteria are magnitudes of errors between the computed and measured yaw rate, vehicle side slip angle and lateral acceleration and the rates of error change. An objective function of the stability criteria is:

$$E_{st} = \min\left(\Delta\dot{\psi}\right) + \min\left(\Delta\beta\right) + \min\left(\Delta a_y\right) + \max\left(V_{\Delta\dot{\psi}}\right) + \max\left(V_{\Delta\beta}\right) + \max\left(V_{\Delta a_y}\right). \tag{3.7}$$

The performance criteria are instantaneous powers on wheels, positive growth of longitudinal acceleration, and slip powers. The corresponding objective function is as follows:

$$E_{perf} = \max\left(P_{\Sigma w_i}\right) + \min\left(P_{s_{wi}^m}\right) + \max\left(a_x\right). \tag{3.8}$$

The block for *generation of subsystem interventions* computes the percentage of participation of the brakes, driveline and steering subsystems in the control process. The share of participation of the brakes and driveline are introduced in the form of coefficients k_{br} and k_{tr} showing the percentage of additional positive or negative torque T_{wi}^{add}. This torque has to be applied to individual wheels to achieve simultaneously criteria of stability and driving efficiency:

$$M_{wi}^{add} = k_{bri} \cdot M_{wi}^{br} + k_{tri} \cdot M_{wi}^{tr}, \tag{3.9}$$

where T_{wi}^{br} is the additional torque from brakes, T_{wi}^{tr} is the additional torque from driveline. The contribution of active front steering subsystem is calculated as additional steering angle δ_f^{add}.

B. Results of real-time simulation of "Sine with dwell" manoeuvre: General consideration

The operation of the described integrated controller is further illustrated with the standard manoeuvre "*Sine with dwell*" performed by the passenger car (full mass 1190 kg). The "Sine with dwell" procedure is prescribed by FMVSS 126 and ECE R13H regulations as one of the tests required for the performance assessment of electronic stability control systems. Figure 60 and Figure 61 present real-time HIL simulation results for the initial vehicle velocity of *25 m/s*.

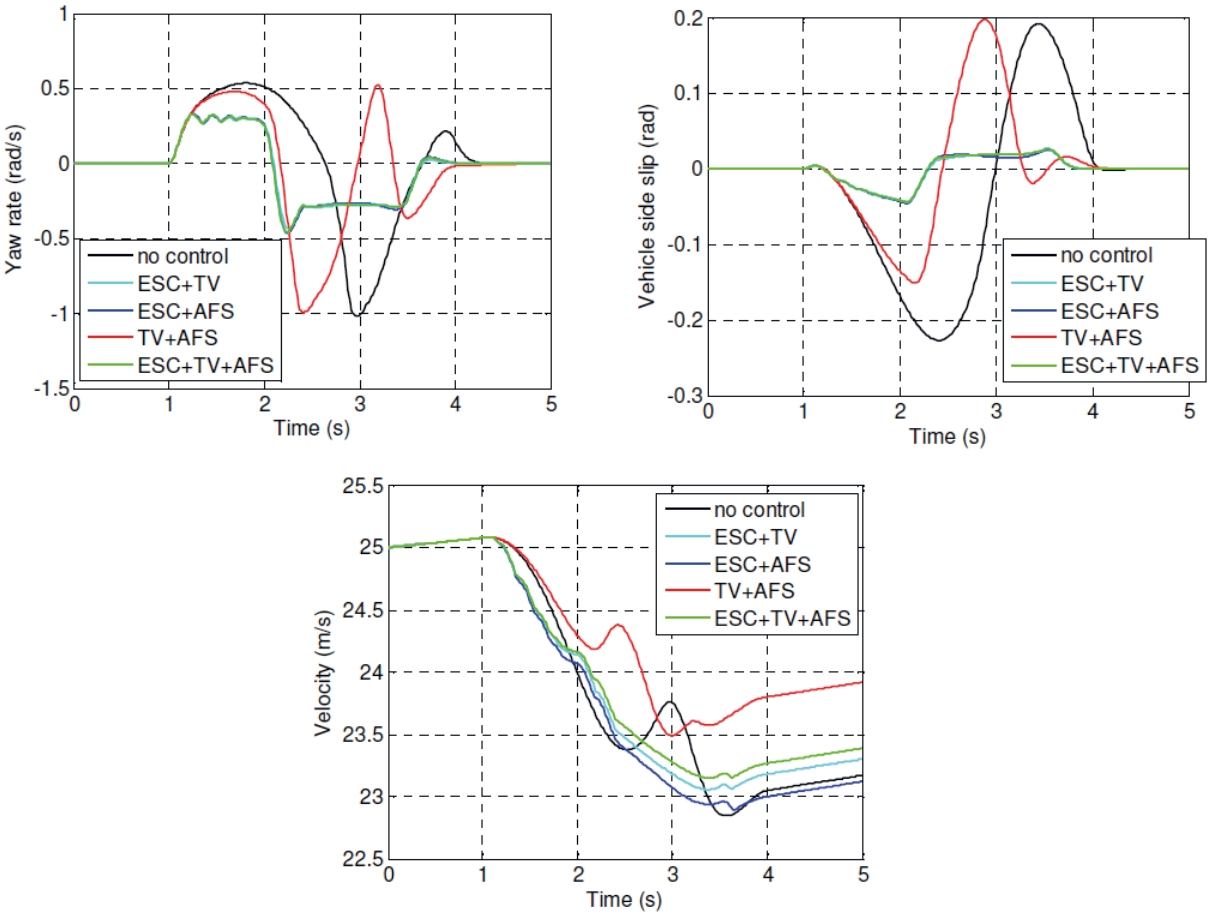

Figure 60 - "Sine with Dwell" manoeuvre for different subsystem configurations

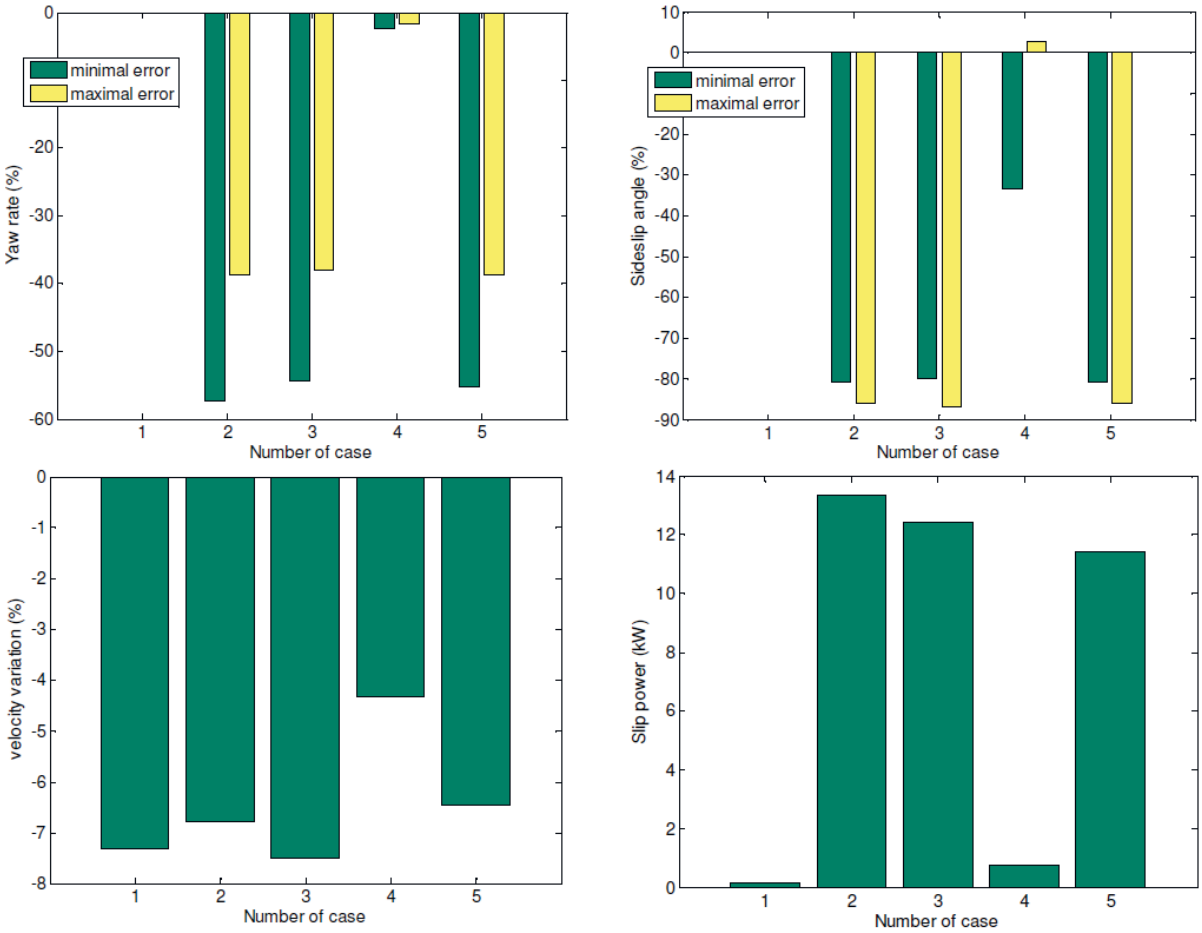

Figure 61 - Numerical indicators of system performance for "Sine with Dwell" manoeuvre; cases: 1 - no control, 2 - ESC + TV; 3 - ESC + AFS; 4 - TV+AFS; 5 - ESC+TV+AFS

It was simulated that this manoeuvre starts on the first second of vehicle motion. The car drives on dry smooth asphalt road with $\mu_{max}=0,8$. During the turning, the driver should increase the fuel feed to avoid the reduction of vehicle velocity. Next results underline the effect of an integrated control on stability and performance by various combinations of actuating subsystems. The corresponding simulation examined four combinations of subsystems as well as one mode of the vehicle motion without control actions.

The diagrams from Figure 60 show that all combinations except "*TV+AFS*" decrease the yaw rate and the side slip angle. But reduction of the vehicle velocity takes place due to partial braking of wheels. The superposition of the torque vectoring and the active steering gives no effect at high vehicle velocities that is comparable with the ESC operation. Using the maneuver without control actions as the reference case, it can be concluded that the combination of the ESC with any other subsystem ensures the step-down of amplitudes of yaw rate (on about *95%*)

and side slip (on about *165%*). The velocity losses are only within the range of *6-8%* during the maneuver. The combination of three subsystems gives the minimal velocity reduction (*6,4%*) and the minimal slip power (ca *11,5 kW*). Summarizing, three integrating subsystems show better results in stability and performance as compared with the joint operation of the ESC and one of other subsystems.

C. Results of real-time simulation of "Sine with dwell" manoeuvre: Study on system distribution

Further part of the study aims at answering the following questions: (i) How the different shares of contribution of several subsystems to the wheel torques can influence vehicle operation? (ii) Do these shares require adaptation to the vehicle velocity? These questions relate to the logic of the block "Choice of percentage participation of control systems" from Figure 58. Next real-time simulation results introduce the same maneuver with three simultaneously operating subsystems. The shares of the operation of each subsystem were calculated in reference to the yaw rate. Figure 62 and Figure 63 give results of this study.

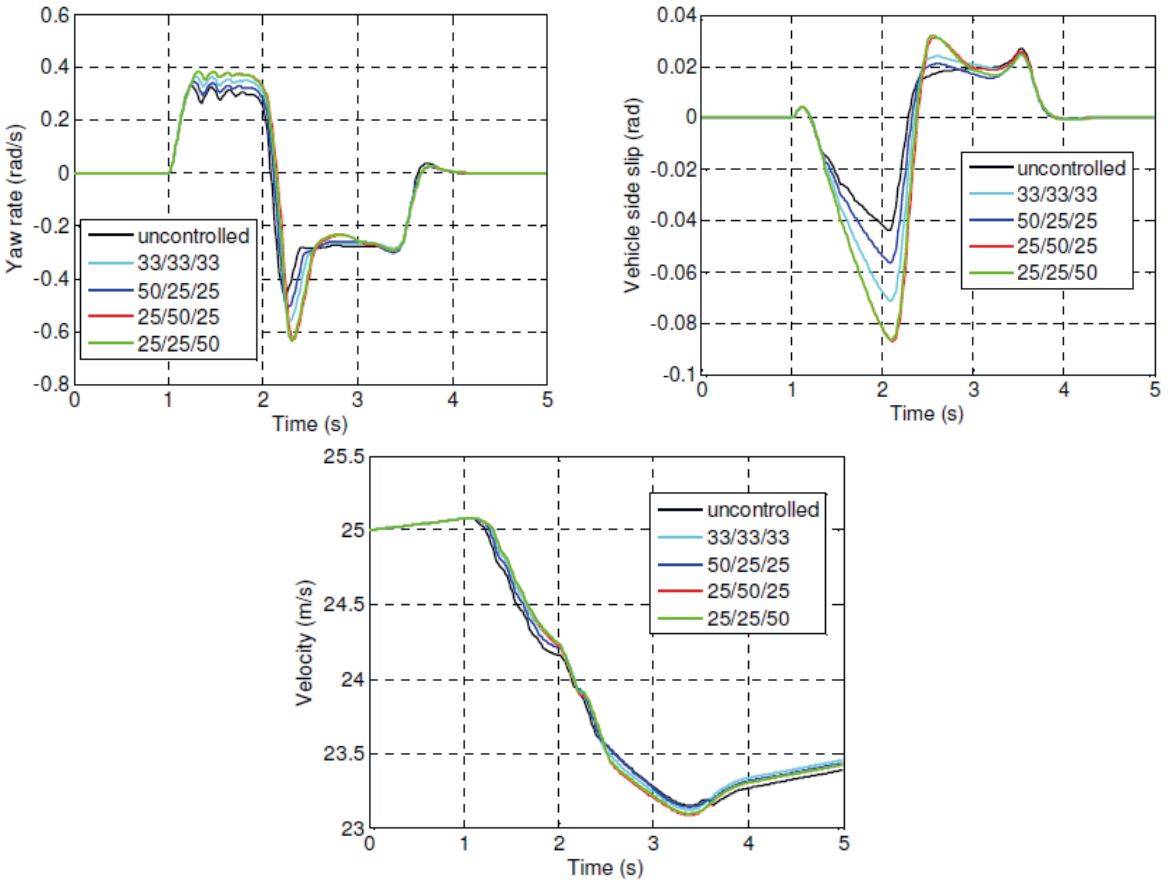

Figure 62 – Parameters of vehicle dynamics by different integration strategies

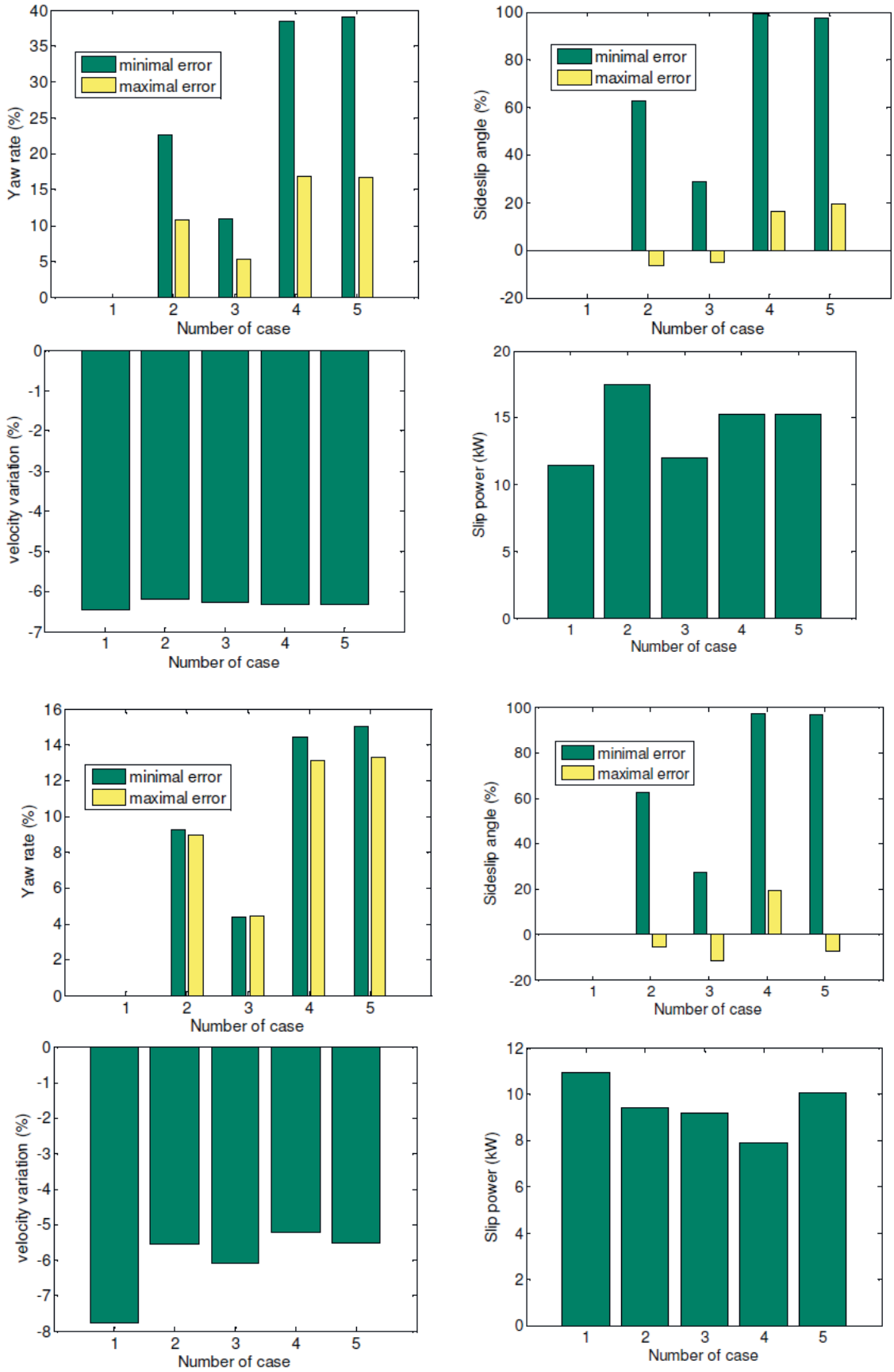

Figure 63 – Control errors for different integration strategies,
Cases: 1 - undistributed; 2 - 33/33/33; 3 - 50/25725; 4 - 25/50/25; 5 - 25/25/50

The study examined the following variants:

- Maneuver without distribution (coefficients for yaw reference signal are equal to *1* for all subsystems, shown as “uncontrolled” case on Figure 62);
- Simultaneous operation of the ESC, the TV and the AFS with the percentage participation respectively: 33/33/33; 50/25/25; 25/50/25; 25/25/50.

The different share, especially by high percentage participation of the TV and the AFS subsystems, can adversely affect the vehicle stability as compared with the "undistributed" maneuver (see "Yaw rate" on Figure 62). The vehicle velocity was insignificantly changed in all considered cases, at that the slip loss was minimum with the "undistributed" maneuver. Hence, the motion in the "undistributed" case could be considered as optimal. However, this is not true in the case of other velocities. In particular, the participation of the ESC as a correction tool should be limited by small velocities. The simulation results for the velocity of 60 km/h confirm this proposition, Figure 63. Here the maximum value of yaw rate is not so critical and the deviation from the "undistributed" case consists of 10-15%. Small slip angles can be characteristic for the driving on the high friction road. However, the third distribution variant is characterized by the velocity drop on 2% only, at that the slip power was reduced on 16% that evidences about improved vehicle performance.

3.3.2. Integrated active safety system for electric vehicle

The example of integrated vehicle control, which will be discussed in this section, is based on control allocation technique developed in Nanyang Technological University [194], [201] and experimentally validated and investigated at Technische Universität Ilmenau [202], [203], [204]. The developed concept of the integrated system is developed for the electric vehicle (full mass 1534 kg) with individually controlled in-wheel motors (max. power 20 kW, peal torque 50 Nm, maximum speed 14000 rpm) and a set of active subsystems for brakes, steering, camber angle, and tyre pressure, Figure 64. Taking into account the operation of electric motors in driving and braking modes, the presented integrated controller operates six subsystems in total.

In accordance with Figure 64, the developed control strategy includes (i) vehicle state estimator based on extended Kalman filter, (ii) high-level controller of vehicle motion, (iii) middle-level control allocation, and (iv) lower-level individual controllers of each subsystem. The high-level

control consists of reference vehicle model and vehicle dynamics controller. Here the 14-DOF vehicle model, Figure 65, is used [205]. Generalized longitudinal and yaw torque are computed in accordance with the control errors. The reference longitudinal acceleration is derived from the measured pedal force. The control demand for the vehicle dynamics controller can be calculated with different methods. In particular, the corresponding variant with the PI-formulation has been realized as follows:

$$\begin{cases} \nu_i = K_p e_i + K_i \int e_i dt \\ e_i = \begin{cases} a_x^{ref} - a_x^{mes}, & \left| a_x^{ref} - a_x^{mes} \right| > 0.1\ ms^{-2} \\ \dot{\psi}_{ref} - \dot{\psi}_{mes}, & \left| \dot{\psi}_{ref} - \dot{\psi}_{mes} \right| > 0.5^0\ s^{-1} \\ 0, & otherwise \end{cases} \end{cases}, \tag{3.10}$$

where "*ref*" relates to the reference variables and "*mes*" relates to measured parameters.

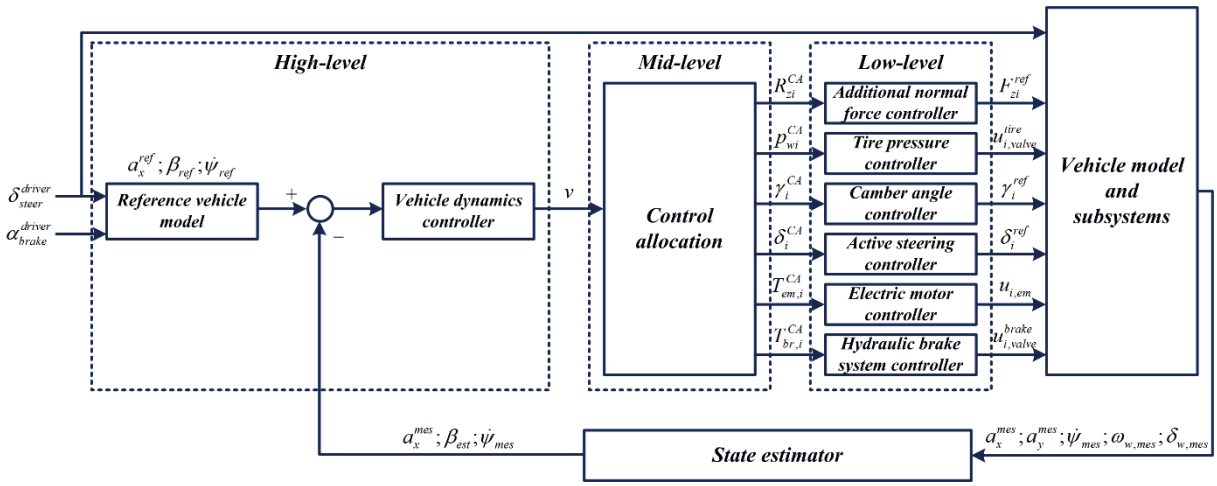

Figure 64 - Block diagram of integrated system for electric vehicle (re-edited from [204])

The middle-level control allocation takes into account that relationship between generalized forces and yaw torque from the control demand and the control inputs is nonlinear. Because of this, the feedback linearization [169] by cancelling of nonlinear term has been proposed for the realization in the middle-level block:

$$\nu^* = \nu - f(x, u_{k-1}) \approx B_{u(k-1)} u_k \tag{3.11}$$

Since the six vehicle subsystems are considered, and electric motors can develop positive (traction) and negative (brake) torques, the control input vector is given as:

$$u^{CA} = \left[\delta_{afs}^{CA}, \delta_{ars}^{CA}, M_{em,i}^{CA,pos}, M_{em,i}^{CA,neg}, M_{br,i}^{CA}, \gamma_i^{CA}, \Delta p_{wi}^{CA} \right]^T . \tag{3.12}$$

The control effectiveness matrix B_u is equal to:

$$B_u = \left[B_{steer} \quad B_{emotor}^{pos} \quad B_{emotor}^{neg} \quad B_{brake} \quad B_{\gamma} \quad B_{pw} \right] \tag{3.13}$$

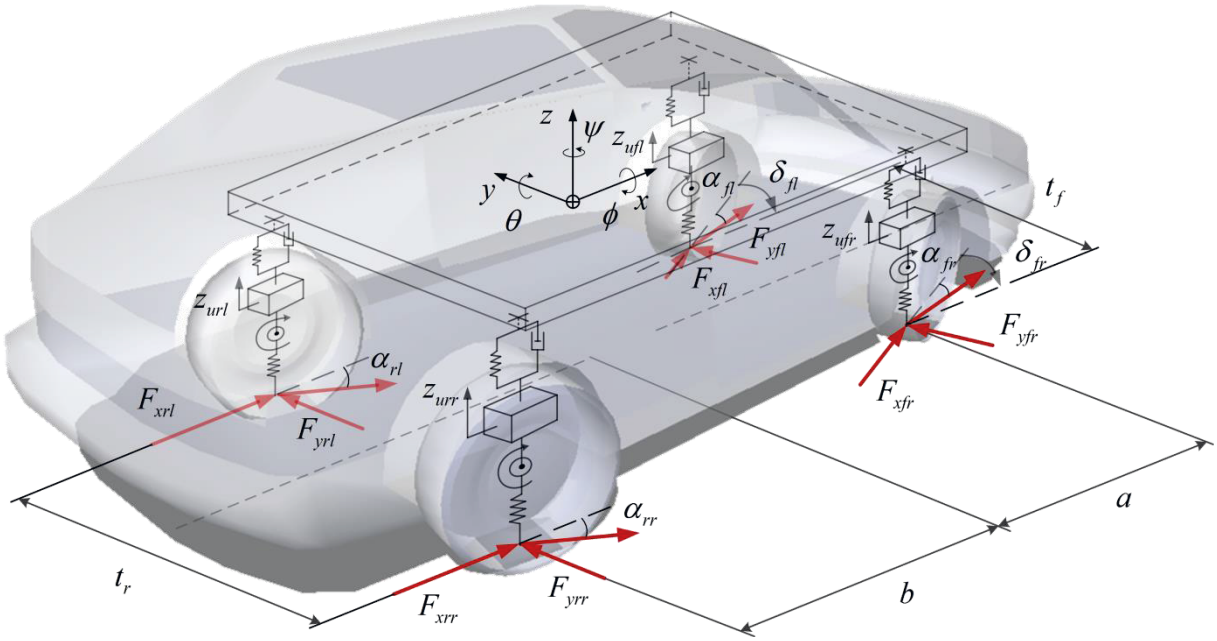

Figure 65 - 14-DOF vehicle model layout

A detailed description of control effectiveness matrices is given in [201]. The aim of control allocation is to minimize allocation error $(B_u u^{CA} - v^*)$ and energy consumption under consideration of actuator constraints. The final constraints for optimization include also tyre constraints, actuator position and rates limits. The lower-level actuator control should (i) guarantee a precise tracking of reference control signals obtained from the middle level of the controller and (ii) estimate boundary conditions for control allocation taking into account subsystem dynamics. The described concept has been tested on the advanced hardware-in-the-loop test rig at Technische Universität Ilmenau, Figure 66.

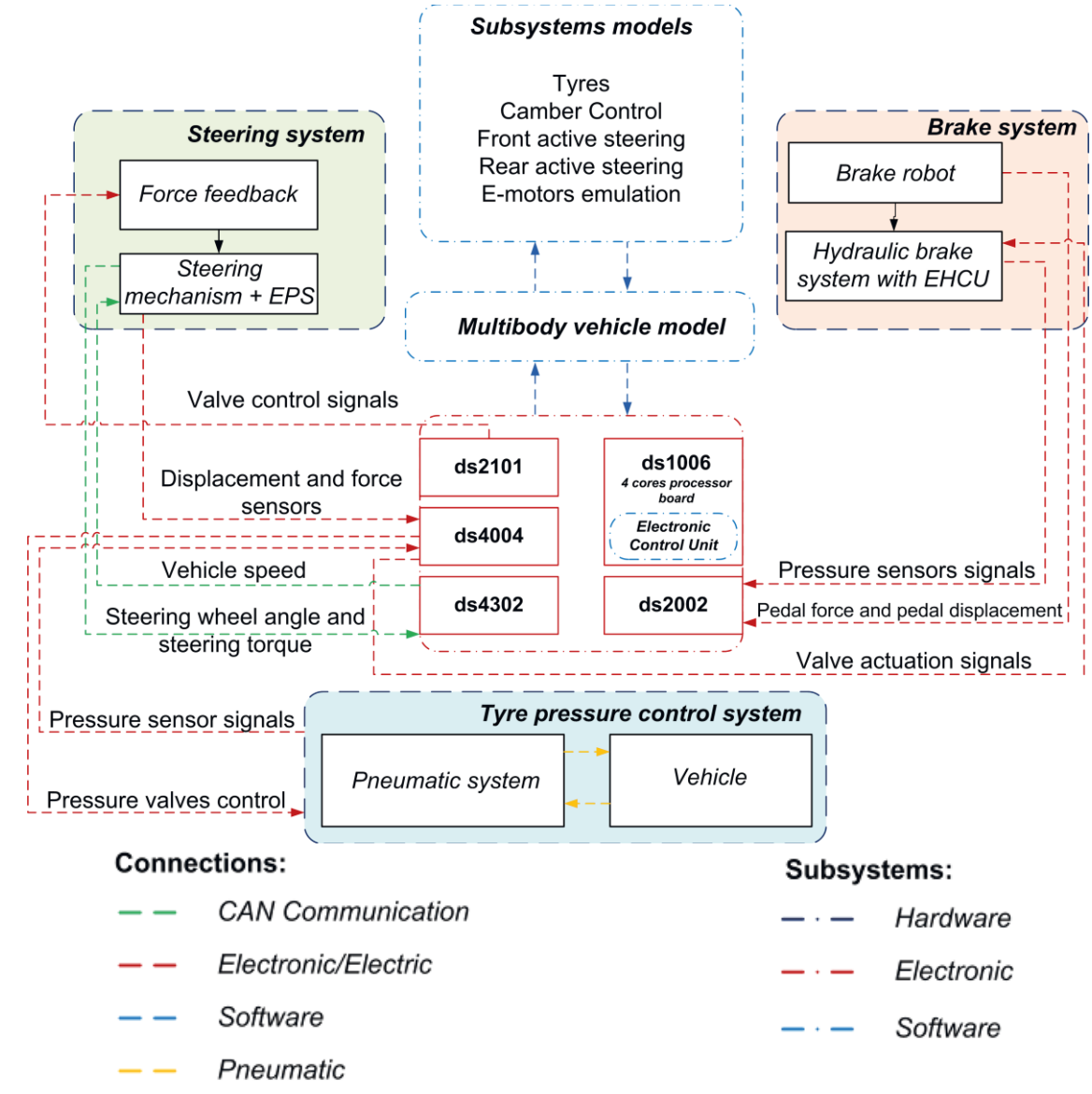

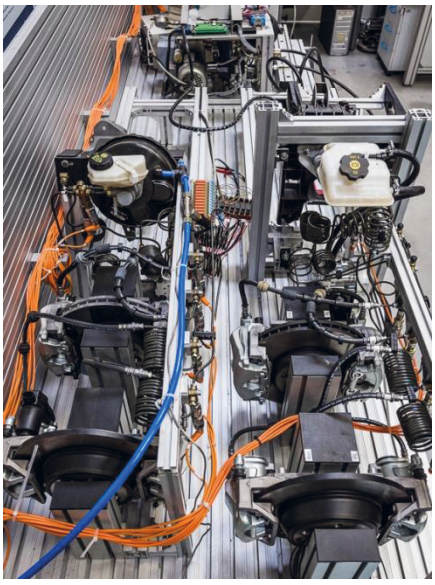

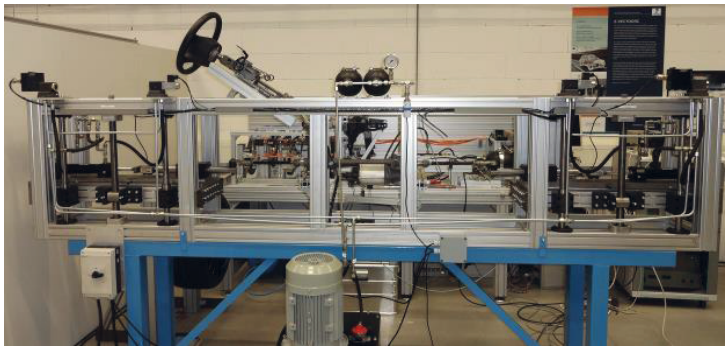

Figure 66 - Integrated HIL test rig and its components

The test platform consists of real and virtual components included into the hardware-in-the-loop architecture. The hardware subsystems are realized for the conventional electric power steering, the hydraulic brakes and the dynamic tyre pressure control. Other vehicle subsystems, the multi-body vehicle model, and the vehicle dynamics controller have software realization in MATLAB/Simulink and IPG CarMaker. The dSPACE components for digital and analogue data input/output as well as for CAN bus protocol communication compose a framework of test rig architecture. The main board (ds1006) is capable to distribute procedures between four core processors for high-performance real-time simulation. Software components of the test rig are divided in two groups related to (i) the vehicle dynamics controller and (ii) the multi-body vehicle model with a set of emulated vehicle subsystems. Several vehicle subsystems and components like electric motor, active camber mechanisms and rear active steering have software realization in MATLAB/Simulink and can communicate with the described hardware subsystems. The HIL test platform interacts with the IPG CarMaker software environment allowing the embedding of vehicle and subsystem simulators.

The functionality of the proposed integrated control system is further illustrated with a complex manoeuvre of the trajectory following in accordance with the predefined steering angle input as it is shown on Figure 67. In the test under consideration, the hardware components of the brakes, the steering and the tyre pressure control system were installed on the HIL test rig, and operation dynamics of electric motors and active camber angle subsystem had a software realization. Analysis of results obtained for an initial velocity > 105 km/h and maximum steering amplitude < 180 deg has confirmed that the developed control system demonstrates good tracking of reference yaw rate with RMSE below 3,0 deg/s. The vehicle sideslip angle does not exceed 5,0 deg. The chosen control allocation strategy also allowed optimizing energy consumption of electric motors and keeping the tyre dissipation on the low level.

As differentiated from the example shown in section 3.3.1, this integrated controller manages simultaneous operation of considerable number of active subsystems. As a result, the vehicle dynamics can be efficiently optimized not only from viewpoint of safety and performance but also with taking into account ride comfort, driveability and other vehicle properties. This approach is being advanced now at Technische Universität Ilmenau for modern concepts of conventional and electric vehicles with the use of novel X-in-the-loop testing technologies [206], [207].

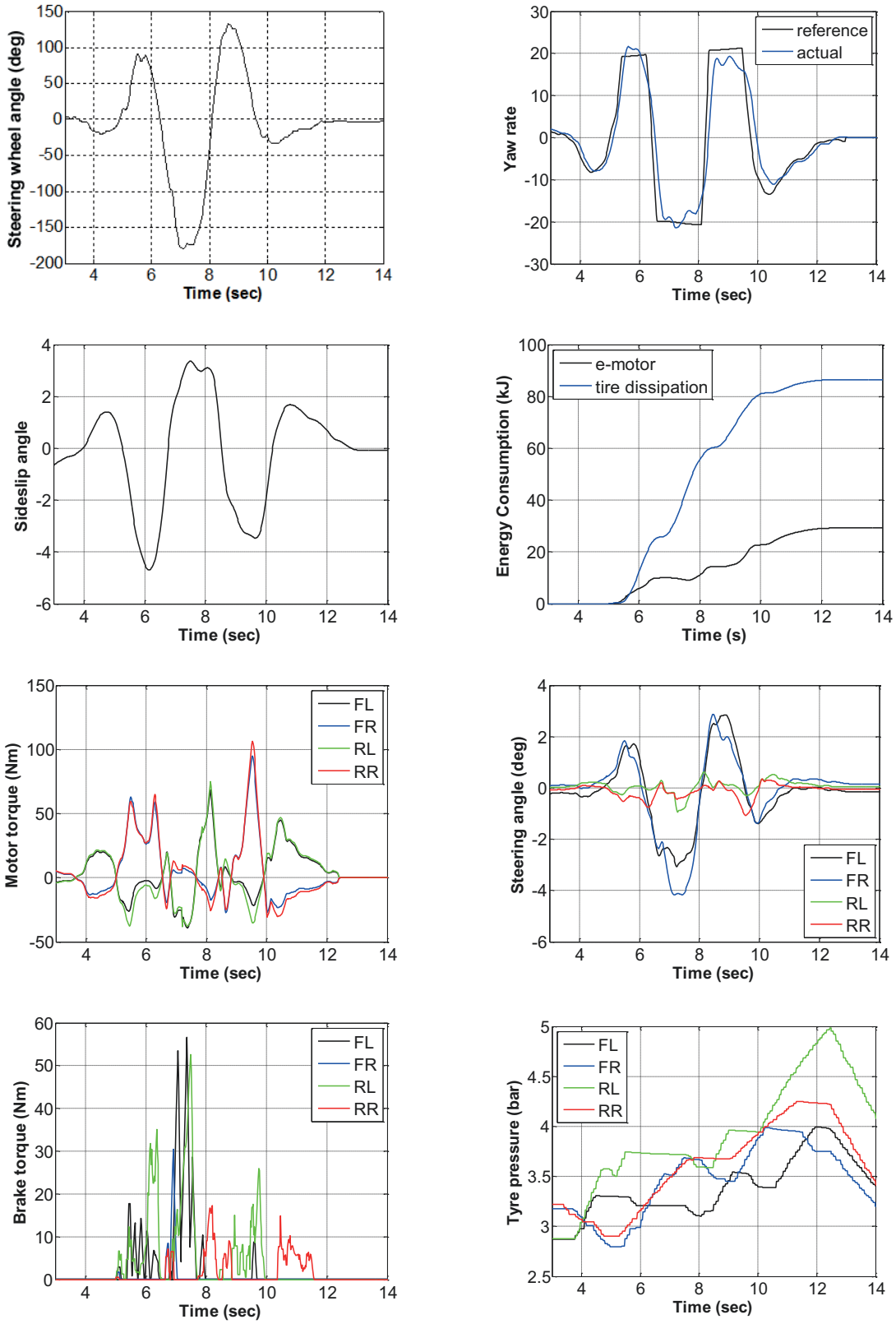

Figure 67 - Vehicle operation characteristics and subsystem actuation [204]

3.4. Chapter Summary

The presented chapter gave an overview of integrated vehicle dynamics control technologies as very important elements for the development of advanced active safety systems. It should be noted that two key factors determine the fact that the integrated active safety control receives recently more and more attention for automotive control engineering. The first factor is connected with different concepts of active wheel corners. Such concepts imply the individual integration of subsystems (e.g. brake, motor, active suspension, active camber control etc.) for each wheel. Hence, the modular, wheel-related integrated active safety control can be realized. The second factor is connected with intensive development of fully electric vehicles, especially with individually controlled electric motors. In such a case the electric motor becomes functions of actuator for the traction, braking and, partially, ride control and is the core element of the system integration. Generally, fully electric vehicles can open some new variants of designing active safety systems that will be discussed in next chapter.

4. ACTIVE SAFETY SYSTEMS FOR VEHICLES WITH ELECTRIC POWERTRAINS

4.1. Introduction

Fully electric vehicles offer new challenges not only for powertrain design but also for the chassis control and active safety systems. Alongside with conventional implementation of the braking or stability control, some variants of electric vehicle architecture provide opportunity for new design concepts for ABS, TC and ESC systems. It can be argued as follows. As compared with conventional vehicles, propulsion systems of electric vehicles can have various powertrain options differentiated by the number of driving axles and wheels, the arrangement (e.g. central, in-wheel, on-board) and the number of electric motors. Several most applicable powertrain options are depicted in Figure 68. New ABS/TC/ESC architectures are particularly feasible in the case of individually-controlled electric motors and have potentially the following benefits: (i) the reduction or even the elimination of the involvement of conventional friction brakes into the control on the wheel slip, (ii) higher bandwidth frequency, and (iii) improvement of driving comfort. Within this context, advantages of electric motor solutions are the high response time (order of milliseconds) and the possibility of dual direct control either by speed or torque, increasing the flexibility of the control of pitch-plane vehicle dynamics [208].

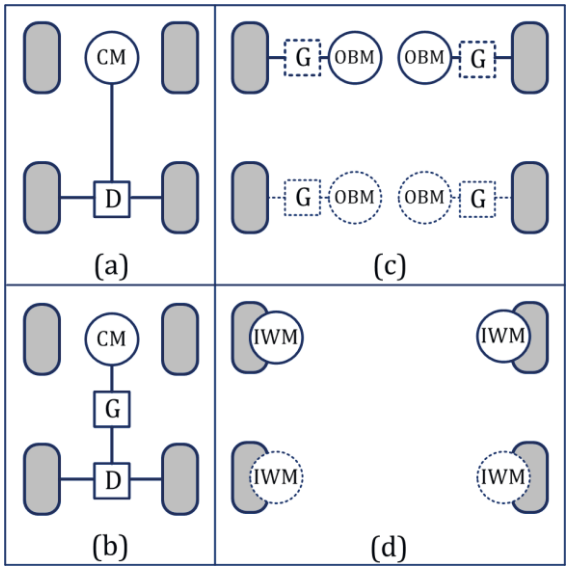

Figure 68 - Powertrain architecture of fully electric vehicles
CM - central motor, OBM - on-board motor, IWM - in-wheel motor, G - gearbox, D - differential gear
Variants: a) direct central; b) central with transmission; c) on-board with or without transmission; e) in-wheel. Variants (c) and (d) can have two- and four-wheel-drive implementation

Recently developed technologies, which are ready for implementation in mass-production cars, demonstrate the potential of active safety systems with individually-controlled electric motors. In particular, the work [209] indicates that a purely electric ABS can reduce the braking distance up to 7% on ice road as compared with a conventional hydraulic ABS. It should be noted that most of the known industrial solutions for active safety systems for fully electric vehicles are existing now on the conceptual stage. But some experimental results, like studies of Toyota and Siemens presented in [209], [210], [211], [212], allow to emphasize a number of specific features listed below, which cannot be practically realized on conventional vehicles with internal combustion engines, hybrid electric vehicles or electric vehicles with central motors:

- The individual control of the electric motors allows continuous regulation of braking / driving wheel torques and, as consequence, the braking and traction dynamics of the vehicle can be controlled seamlessly under all possible driving conditions and does not have to be restricted to emergency conditions only, as is currently employed with conventional active safety systems;
- The ABS/TC/ESC performance of full electric vehicles can be enhanced due to higher frequency (above 10 Hz) of wheel torque modulation as compared with conventional ABS/TC/ESC having average operational frequency up to max. 3...10 Hz.
- In-wheel and on-board motors as ABS/TC actuators have significantly lower actuation delay as compared, for instance, with the friction brakes for ABS or the mechanical driveline for TC. It opens the way for reduction of the slip oscillations that is beneficial not only for safety but also for driving comfort.
- As for braking mode, the integration of ABS or ESC functions and individually controlled regenerative braking for each wheel gives effect in simultaneous ensuring the vehicle safety and optimization of power consumption.

It should be noted that ESC or TV strategies for full electric vehicles with individually-controlled motors are very similar with corresponding solutions for non-electric vehicles [213], [76], [214]. However, the use of electric motors as actuators allows to propose a crucially new ABS and TC design variants. Within this context, next sections will give an overview of control techniques, which can be applied to active safety system architecture of fully electric vehicles with special attention given to the wheel slip control.

4.2. Traction Control for Vehicles with Electric Powertrains

The first research studies, which were subjected to the TC methods for full electric vehicles and have presented results obtained from validation on real cars, are dated of late 1990s. Specifically, the variant of TC system using fuzzy control has been introduced by Yoshimura et al. in [215] for an all-wheel drive electric vehicle. The variant of model-following traction control has been later introduced by Hori, Toyoda and Tsuruoka in [216]. TC systems for electric vehicles can be conditionally classified by the torque-based and slip-based controllers. This separation specifies the target control parameter of TC systems: the wheel (motor) torque or the wheel slip. Both controller variants are closely related but can use different logic and architecture.

Torque-based controllers. A simple variant of torque-based controller for the traction mode is proposed in the work [217], Figure 69. The controller logic has an assumption that the wheel skidding can be detected by an abrupt drop in the estimated wheel inertia. This effect can be traced through the estimation of the transfer function from the motor output T_{em} to the wheel velocity V_w:

$$P(s)=\begin{cases} s^{-1}\cdot\left(m_w+m\right)^{-1}, \text{ wheel slip } \rightarrow 0 \\ s^{-1}\cdot m_w{}^{-1}, \text{ wheel slip } \rightarrow 1 \end{cases} \tag{4.1}$$

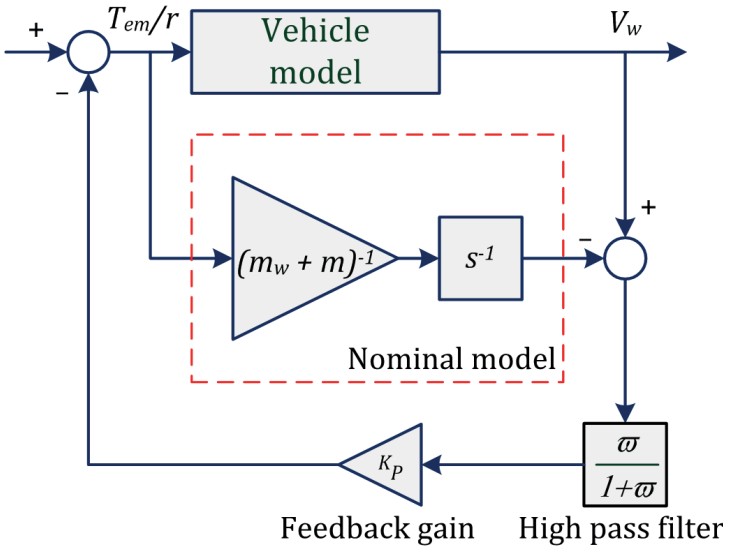

Figure 69 - Model-based traction controller (adapted from [217])

The nominal model can also take into account the back electromotive force (EMF) characteristics of the traction motors. This controller was subjected to the tests on the mini-sized vehicle (full weight of 400 kg) with the rear wheel drive (two individual permanent magnet synchronous motors) and demonstrated an improvement of acceleration dynamics: 12,5 km/h versus 10 km/h in 4 sec for the controlled acceleration as compared to the non-controlled acceleration. However, the discussed study confirmed this effect for low velocities only.

A series of studies developed the torque controller using estimates of the friction-slip derivative $d\mu/d\lambda$, assuming that this gradient parameter can be used for adaptating the control process to changes in the road surface friction. For example, the study [218] introduced a method, in which the adherence gradient controller, Figure 70, defines the electric motor torque demand T^*_{em} to be realized for the observed gradient $d\mu/d\lambda$. Two methods - fuzzy control and sliding mode control - are proposed in [218] for the control logic. In the case of the fuzzy controller, the input variables are the position of the acceleration pedal and the friction-slip-gradient, and the output variable is the demand T^*_{em}. For the sliding mode controller, the system acts in discontinuous control according to the desired sliding manifold of the gradient:

$$T_{em} = \begin{cases} \overline{T_{em}}, \text{ if } d\mu / d\lambda > 0 \\ 0, \text{ if } d\mu / d\lambda < 0 \end{cases}. \tag{4.2}$$

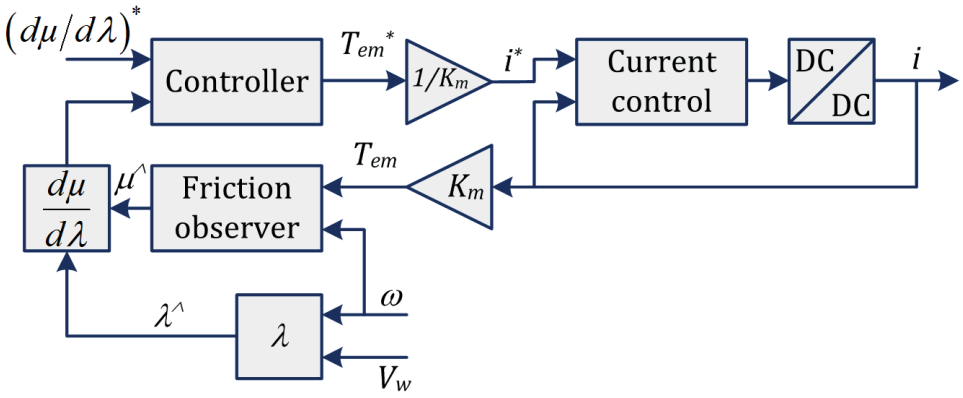

Figure 70 - Adherence gradient controller (adapted from [218])

This system has been validated via test bench experiments of the wheel torque control of a single wheel. Both fuzzy and sliding mode control showed comparable performance and a satisfactory response to an abrupt change in the wheel slip conditions.

Several other studies investigated the scenario in which the TC system is set up without information related to the vehicle velocity. This omission can potentially simplify the controller structure and reduce the computational demand. Examples of such systems are discussed below.

A method called Maximum Transmissible Torque Estimation (MTTE) has been developed in [219], [220]. This method has been realized in the controller with the basic structure depicted in Figure 69. The controller has the task to realize a maximum transmissible torque T_{max} variable defined as

$$T_{\max} = \left(\frac{I_w}{\left(\dot{V}_x / \dot{V}_w\right) mr^2} + 1 \right) \cdot r\hat{F}_x . \tag{4.3}$$

The ratio $(dV_x/dt)/(dV_w/dt)$ in Eq. (4.3) is called the relaxation factor of MTTE.

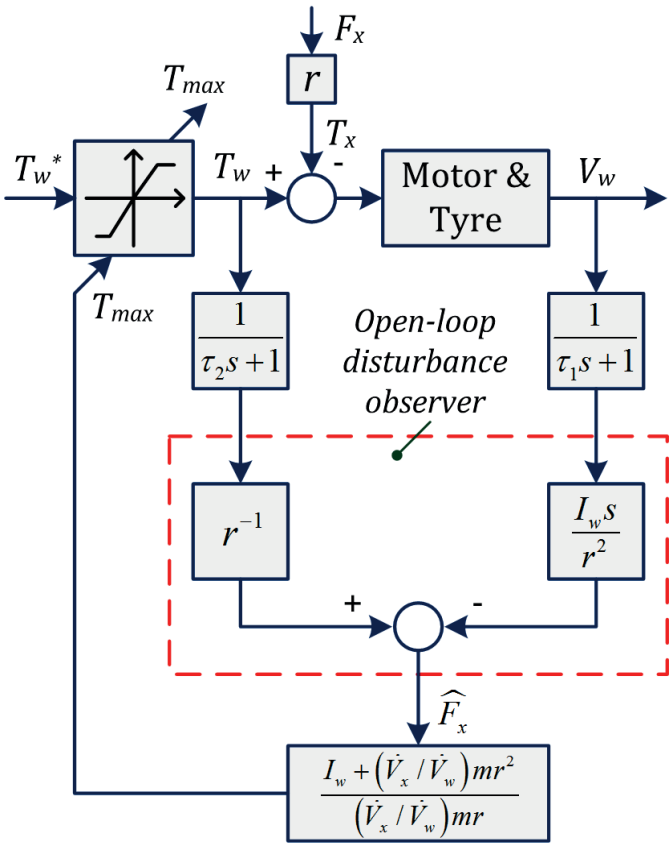

Figure 71 - Basic MTTE controller (re-edited from [219]*)*

The torque T_{max} is required to formulate demanded wheel torque T_w driven by the electric motor:

$$\begin{aligned} T_w &= T_w^* \ \text{ if } \ -|T_{\max}| < T_w^* < |T_{\max}| \\ T_w &= |T_{\max}| \ \text{ if } \ T_w^* \geq |T_{\max}| \\ T_w &= -|T_{\max}| \ \text{ if } \ T_w^* \leq -|T_{\max}| \end{aligned} \quad . \tag{4.4}$$

The structure of Figure 71 requires a saturation limiter to constrain the wheel torque by the T_{max}-value. The longitudinal tyre force F_x (which has the role of a disturbance) is computed by an open-loop force estimator with two preceding low-pass filters smoothing the noises from T_w- and V_w-signals. Since the basic approach is sensitive to wheel torque disturbances caused by the wheel inertia, advanced variants of the MTTE controller include a closed-loop observer as shown in Figure 72. This solution, realized as a PI disturbance observer, aims at (i) elimination of inaccuracies of the vehicle and tyre models and (ii) reducing sensitivity of the performance to variations in the wheel inertia. In the case of direct current motors, an additional effect can be expected in the elimination of disturbances caused by the direct current drop.

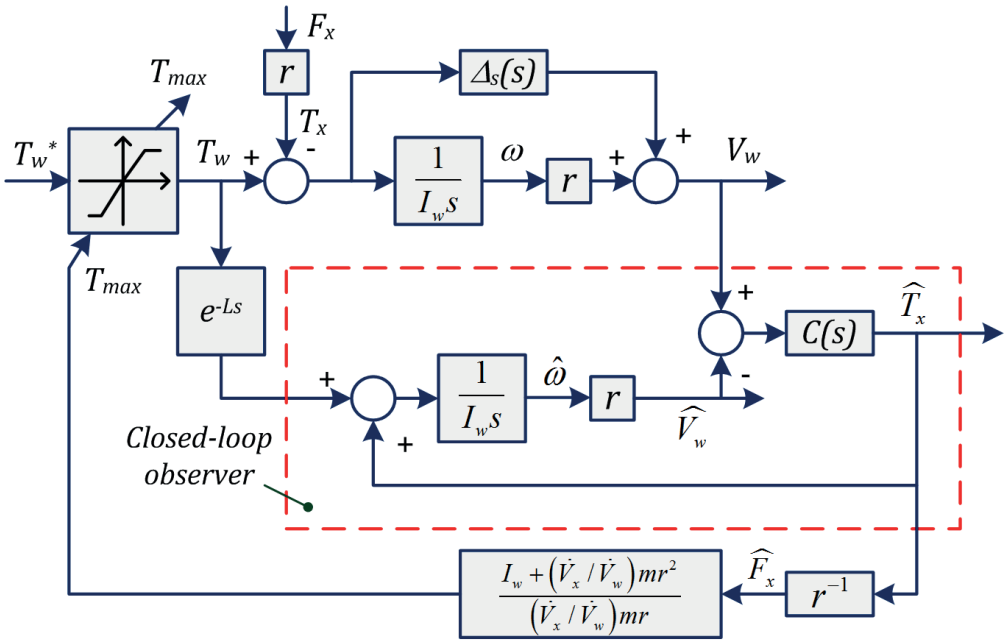

Figure 72 - Modified MTTE controller (adapted from [221])

The testing results of the MTTE controller corresponding to Figure 71 have been introduced in [219] for the experimental rear-wheel-drive vehicle (total mass 360 kg, tyre radius 220 mm).

The vehicle was equipped with two independent interior permanent magnet synchronous motors on rear wheels (maximum power 2 kW, maximum torque 100 Nm). The tests were carried out at a very low driving velocity (up to 4 m/s) on a slippery surface (wet acrylic plate) with an inertia of wheel inertia from 0,3 to 0,5 kg·m^2. The results confirm that the proposed controller considerably reduces the wheel slip for the given testing conditions and is fault-tolerant to wheel inertia disturbances.

Slip-based controllers. One of the most critical problems related to the development of the slip-based controllers is the estimation of vehicle velocity. It is especially relevant for electric vehicles with individually-controlled motors. In this case, traditional methods of vehicle velocity calculation via the wheel speed and wheel radius are not applicable. This challenge motivated a number of studies, in which slip controllers do not use directly the vehicle velocity. One of the relevant approaches is described in [222]. Figure 73 displays variants of the slip ratio observer, the slip ratio estimator and the slip controller. The structures of the slip ratio observer and estimator differ by the inclusion of the longitudinal vehicle acceleration a_x in the observer.

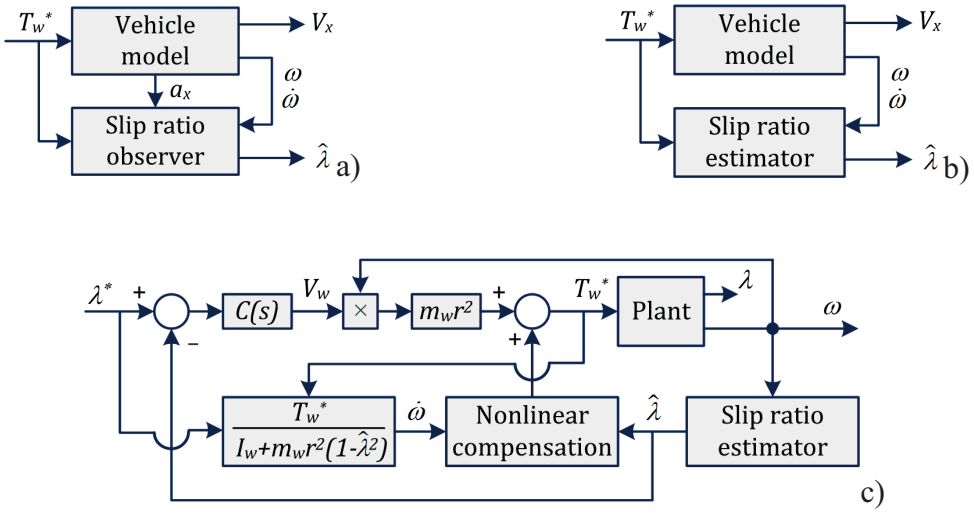

Figure 73 - Slip ratio observer (a), slip ratio estimator (b) and slip controller (c) without detection of vehicle velocity (re-edited from [222]*)*

The estimator follows the equation:

$$\dot{\hat{\lambda}} = -\frac{\dot{\omega}}{\omega}\hat{\lambda} + \left(1 + \frac{I_w}{m_w r^2}\right)\frac{\dot{\omega}}{\omega} - \frac{T_w}{m_w r^2 \cdot \omega}. \tag{4.5}$$

Using Eq. (4.5), a conclusion can be made that the estimation error *e(t)* has an offset whenever $d\omega/dt < 0$ since

$$e(t) = \lambda - \hat{\lambda};\ \frac{d}{dt}e(t) = -\frac{\dot{\omega}}{\omega}e(t). \tag{4.6}$$

Compensation of this offset can be included in the logic of the slip ratio observer through a term incorporating the longitudinal acceleration a_x and road friction μ:

$$\dot{\hat{\lambda}} = -\frac{\dot{\omega}}{\omega}\hat{\lambda} + \left(1 + \frac{I_w}{m_w r^2}\right)\frac{\dot{\omega}}{\omega} - \frac{T_w}{m_w r^2 \cdot \omega} + k\left(\hat{\lambda}\right)\cdot\left(a_x(t) - \mu\left(\hat{\lambda}\right)\cdot\frac{F_z}{m_w}\right). \tag{4.7}$$

This observer realization with fixed parameterization of the compensation term from Eq. (4.7) has been recommended for low friction road conditions [222]. The observer and estimator structures are integrated into the slip ratio controller. The generic structure of the controller is given in Figure 71c) and is based on nonlinear compensation with feedback. The results of the experiments carried out for small-sized electric vehicles (420 kg mass, fitted with electric motors of maximum power 2 kW and maximum torque 100 Nm) have shown the applicability of the controller in the case of relative high levels of reference slip ratio ($\lambda^*=0.2$).

Another control variant is introduced in [223], where the back electromotive force (EMF) is used to estimate the motor speed / wheel velocity for an electric vehicle equipped with brushless direct current motors. The controller is based on a proportional relationship between the back EMF V_{emf} and the motor speed ω as follows:

$$V_{emf} = \omega \cdot C_E \frac{1}{\tau s + 1}, \tag{4.8}$$

where C_E is the back motor EMF constant (determined by the design). Figure 74 shows the architecture of the controller. A sensible component of its design is definition of the gain *K* for the transfer function between the input and output currents i_H and i_d:

$$G_{i_H/i_d} = \frac{K}{(\tau_1 s+1)\cdot(\tau_2 s+1)-K}. \tag{4.9}$$

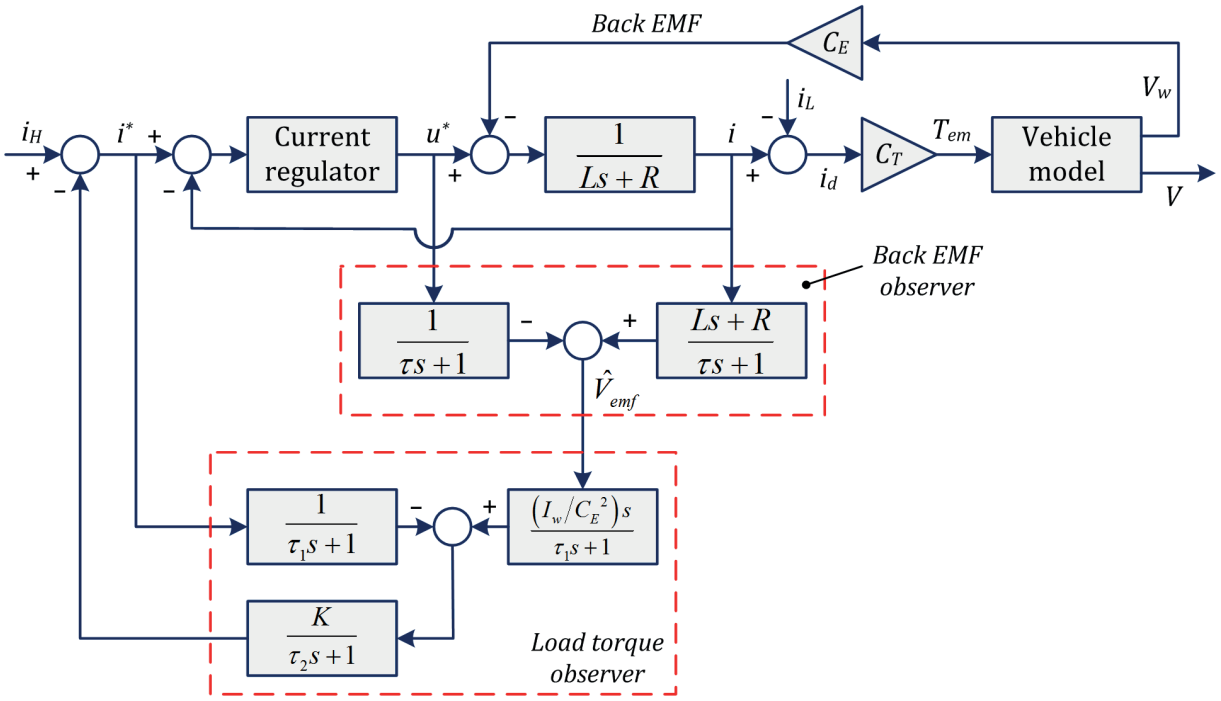

Figure 74 - Slip controller with back electromotive force (adapted from [223])

Certain electric vehicles configurations require advanced control structures due to the specific powertrain architectures employed. Specifically, TC for the powertrain layout with on-board motors connected to the wheel through the half-shaft and the gearbox requires compensation of the half-shaft torsional dynamics having a negative influence on driveability. An appropriate variant of the slip controller is proposed in [224], Figure 75.

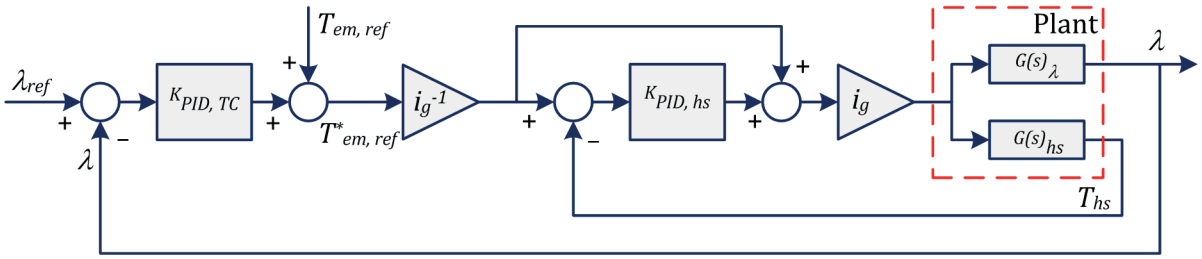

Figure 75 - Linearized traction controller (re-edited from [224]*). Indices: "ref" - reference; "TC" - traction control; "hs" - half-shaft*

The control architecture realizes direct slip control through a PID controller $K_{PID,TC}$ that computes the electric motor torque demand T_{em}. The second PID controller $K_{PID,hs}$ is included

to carry out feedback compensation of the half-shaft torque dynamics T_{hs}. The half-shaft torque level in the controller is estimated by an extended Kalman filter based on the non-linear electric powertrain model. Simulation results of the described configuration in the velocity range 20 to 90 km/h confirm that oscillations in the vehicle acceleration profile caused by the torsional dynamics are smoothed using this approach. The system also achieved a tracking capability (–3,5 dB of closed-loop response) up to a frequency of about 47 Hz. It should be mentioned that the described method requires further development for the compensation of half-shaft torsional dynamics in the case of electric motor operation in braking mode.

* * *

The presented overview of the TC system variants for fully electric vehicles reveals a diverse range of approaches to wheel torque and wheel velocity control to improve vehicle traction dynamics. In addition to the studies investigating different variants of traction controllers and TC architecture, a number of specific problems of TC for full electric vehicles can be found in publications. These problems address in particular:

- Integration of TC with chassis systems as active steering [213], [225];
- Internal controllers of electric motors with special attention to TC mode; fail-safe control [226], [227], [228];
- NVH and active vibration control of motors [229], [230].

4.3. Anti-Lock Braking Systems for Vehicles with Electric Powertrains

Many published studies in the braking control of electric vehicles address primarily adoption of conventional hydraulic / electro-hydraulic ABS. The research problems of ABS modulation through pure operation of electric motors are rarely explored in this regard. Several important works discussing design of electric ABS are recently published by researchers of Siemens and Toyota [209], [210], [211]. Relevant solutions can be also found in patent documents like [231], [232]. However, detailed methodological analysis of ABS strategies for full electric vehicles with individually controlled wheels / motors is still missing in research literature.

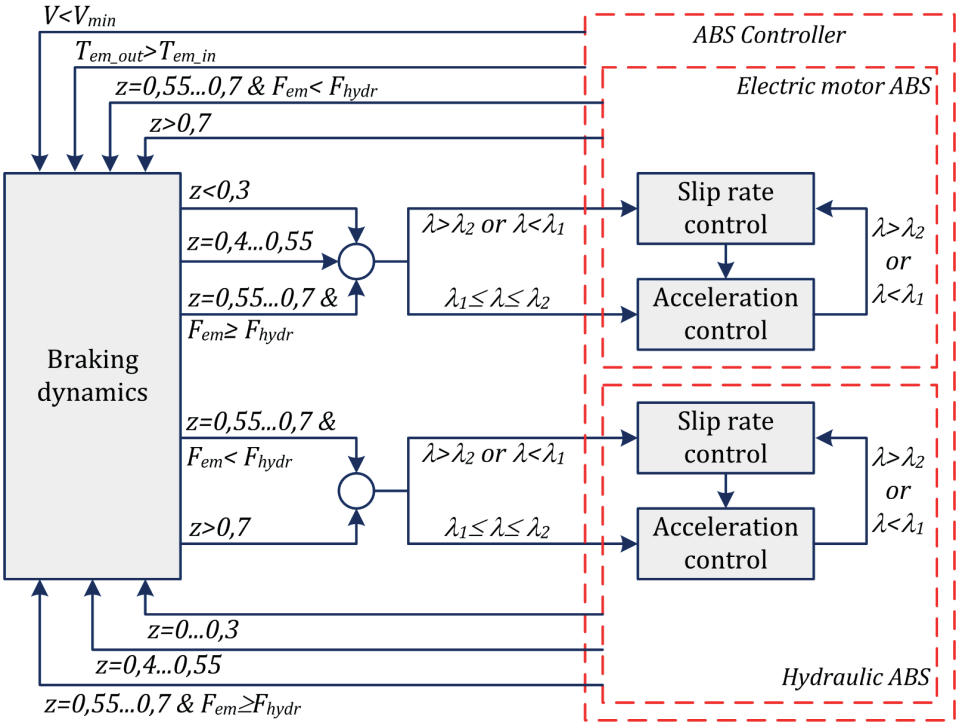

Figure 76 - Composite ABS controller (adapted from [233]*)*

Strict vehicle safety requirements define that the electric vehicle should have simultaneously both friction and motor brakes. The ABS architecture in this case can have a blended implementation [234], [235]. Simple variants of the blending between two actuating subsystems (friction brakes and electric motors) can be developed using rule-based controllers. One such ABS variant is introduced in [233] as applied to an electric vehicle with four in-wheel motors. The ABS architecture presented in Figure 76 consists of electric and hydraulic parts. Their

actuation is governed by a set of rules that operate with slip thresholds λ_1 and λ_2 and four levels of specific vehicle deceleration z. The slip thresholds assign the ABS operation mode, which is either slip ratio control (brake torque reduction) or acceleration control (brake torque increase). Four z-levels determine the transition between the electric and hydraulic ABS actuation as well as the required brake torque rate. According to the proposed control logic, pure electric ABS actuation at low torque rate is used for low friction road surfaces ($z<0,3$). At high deceleration level ($z>0,7$), purely hydraulic ABS actuation is applied. Both electric and hydraulic subsystems are simultaneously operated when braking dynamics is situated at intermediate deceleration levels.

The rule-based logic could have advantages from the viewpoint of practical ABS realization. However, results of extensive testing and validating the robustness of this approach for fully electric vehicles under different vehicle manoeuvres are not sufficiently presented in published research literature.

Aside from the studies focused on the blended ABS operation, a number of investigations concern the implementation of electric motor control for braking. For example, the work [236] introduces a method of determining the vehicle velocity and the wheel slip for electric ABS based on iterative learning, Figure 77. The proposed learning process is based on estimation of the error between the reference slip ratio $\lambda_{ref}(t)$ and the actual slip ratio $\lambda(t)$:

$$e(t) = \lambda_{ref}(t) - \lambda(t). \tag{4.10}$$

The error is used in PD algorithm, Figure 77b), with the input calculated as

$$u_{k+1}(t) = u_k(t) + \Gamma \frac{de_{k+1}(t)}{dt} + \Gamma_p e_{k+1}(t), \tag{4.11}$$

where Γ and Γ_p are learning gain matrixes. Figure 77c) gives an example of learning procedure as applied to the slip ratio λ and demanded electric motor torque T_{em_d}. This procedure is used in the control law for electric motor:

$$T_{em}(t) = b_1 \cdot \dot{V}(t) + \left(b_2 \cdot \dot{\lambda}_d(t) + b_3 \cdot e(t) + b_4 \cdot \dot{e}(t)\right) \cdot V(t), \tag{4.12}$$

where the constants b_i are deduced from the curve fitting of the torque demand on the appointed learning step (the work [236] considered five learning steps). The simulation results of the discussed ABS controller confirmed its functionality for different test conditions on homogeneous surfaces. However, additional assessment of the controller functionality is required for specific situations as braking on a μ-split surface or on a road with sudden fluctuations in the friction coefficient.

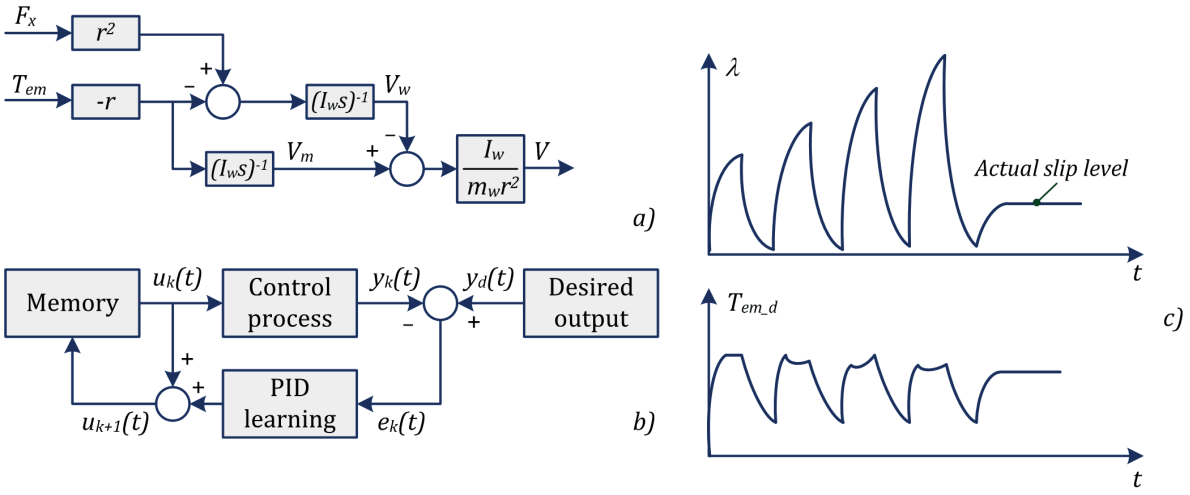

Figure 77 - Iterative learning ABS controller (adapted from [236]*);*
a) calculation of vehicle velocity; b) generic structure of iterative learning controller;
c) learning process by definition of slip ratio λ and electric motor torque demand T_{em_d}

Some results of industrial implementation of the ABS for electric vehicles can be found in already mentioned publications of Toyota and Siemens and in various patent documents. An example of the corresponding control logic can be found in the patent by Toyota [232], Figure 78. Here the ratio between the friction braking torque and electric motor torque in each wheel unit is continuously altered depending on the basic friction torque levels and the battery state of the charge. Industrial implementation of ABS and TC systems for full electric vehicles is also introduced in [209] and [210]. Figure 79 shows the design of the wheel unit with an electric motor of the test electric vehicle of Toyota with the following specifications: vehicle mass 2100 kg; maximum vehicle velocity 200 km/h; maximum wheel power 40 kW; maximum wheel torque 550 Nm. Vehicle testing confirmed a good ABS performance in the case of blended actuation of the friction brakes and electric motors. As can be seen from Figure 80, the ABS with in-wheel motors ensures a higher actuation frequency as compared with conventional ABS. The distribution of wheel slip ratio is also kept in the stable area, mainly below the level of λ=10%.

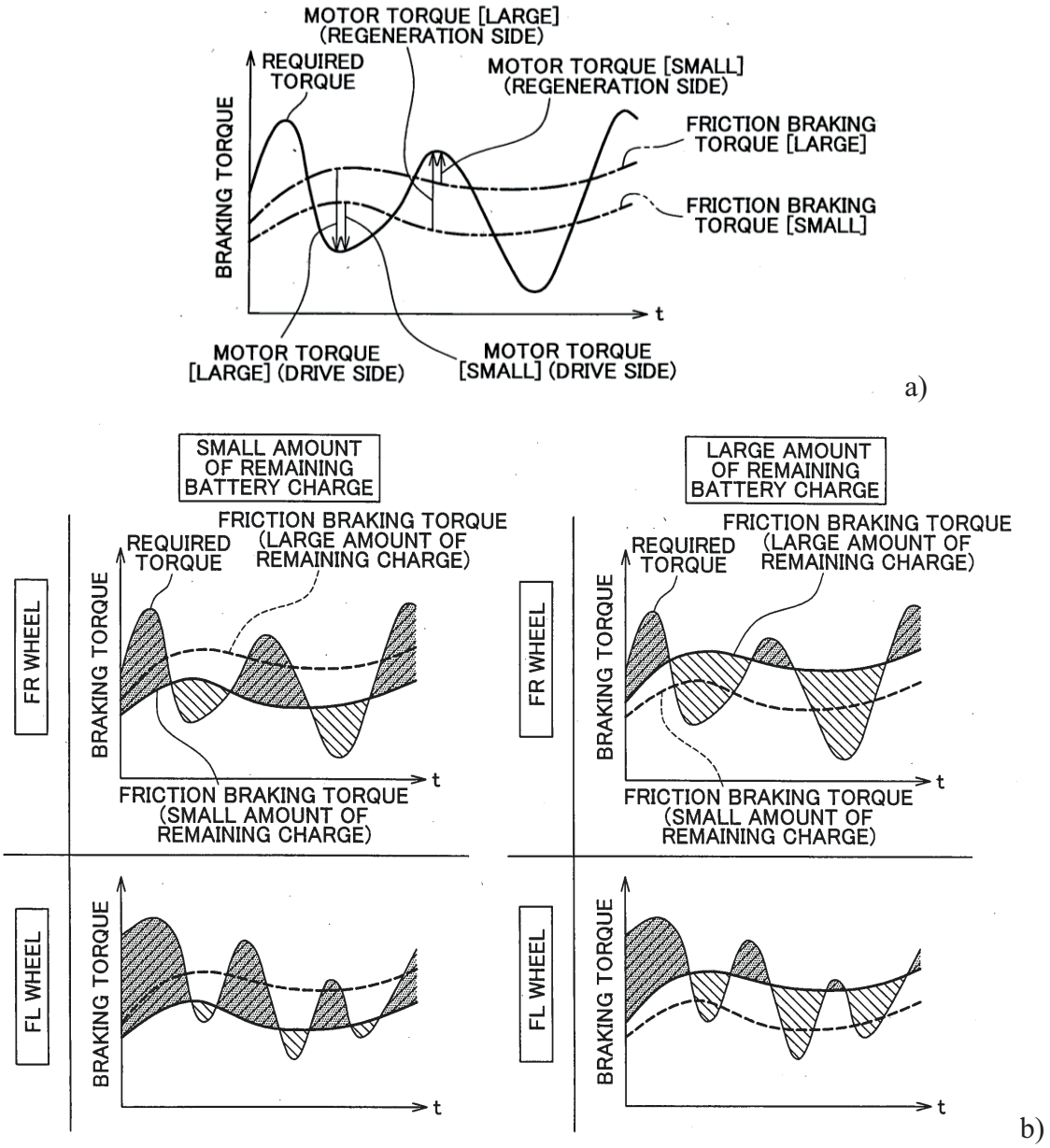

Figure 78 - Illustration to patent document US 2010/0292882; a) General diagram of electric motor torque behaviour; b) example of individual brake control

Another industrial variant of ABS with electric motors is described in [211]. This variant concerns the roadster electric vehicle (mass 1250 kg) manufactured by Roading company and equipped with wheel hub electric motors produced by Siemens, Figure 81. The motor specification is as follows: maximum continuous torque 500 Nm, maximum peak torque of 500 Nm, continuous power 73 kW and peak power 120 kW. Example of ABS braking results is shown on Figure 82. In accordance with the work [211], rear electric motors in a braking mode can guarantee the vehicle deceleration of 0,3 g at the minimum. In the case of higher deceleration demands, the front friction brakes are activated.

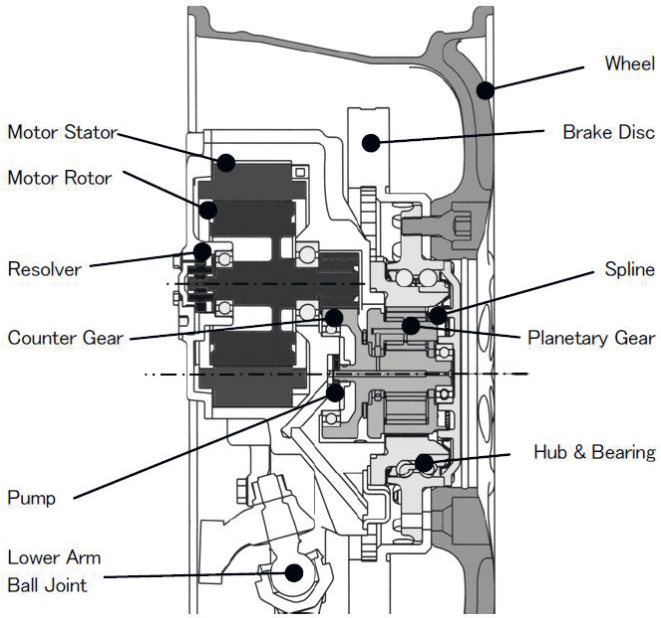

Figure 79 - Design of wheel unit with integrated electric motor [210]

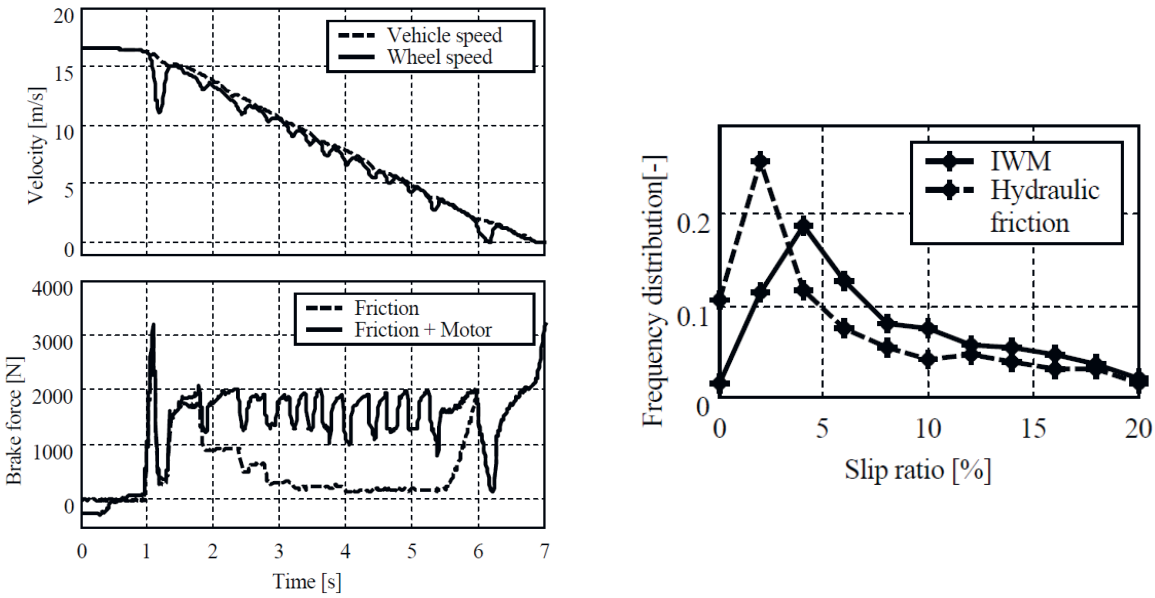

Figure 80 - Results of ABS braking on low friction road (μ=0,1) [210]

It can be mentioned that generally there are very limited number of patent documents and published industrial white papers, which have a direct relevance to the ABS functions realized through electric motors. In particular, only few control algorithms or methods are disclosed, where the specific character of the electric powertrain operation is taken into account by designing the slip controllers for electric vehicles.

Figure 81 - Installation of wheel hub electric motors on electric roadster vehicle [211]

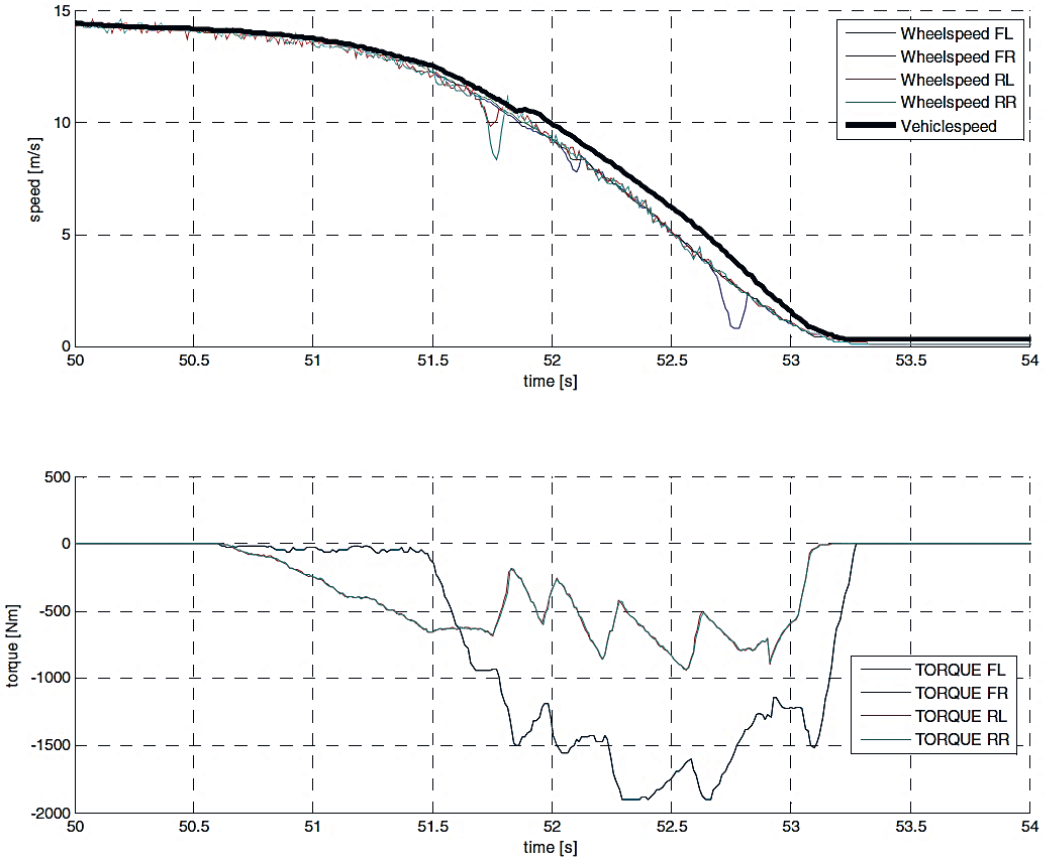

Figure 82 - Diagrams of ABS braking of electric roadster vehicle [211]

Most of known industrial solutions are existing now also on the conceptual stage. However, some experimental results, like in abovementioned studies of Toyota and Siemens, allows to appoint some targets to be used as the first benchmarks for the further development of ABS for full electric vehicles.

Besides the control methods and controller architecture, some other research topics are also of particular relevance to anti-lock braking systems for full electric vehicles. The following subjects can be especially emphasized:

- Optimization of ABS strategies for electric vehicles [237], [238];
- Integration of ABS with ESC and active chassis systems of electric vehicle [205], [239];
- Fail-safe operation of electric motors during ABS intervention [240], [241];
- Vibrations and damping methods for braking mode of electric motors [242].

It should be particularly noted that the analysis of published research and technical literature points to the limited number of studies about the methods of pure electric ABS actuation, especially validated through the road tests. To give a relevant practical example, next section introduces a corresponding case study.

4.4. Case Study: Wheel Slip Controller for Full Electric Vehicle

4.4.1. Target vehicle

The results presented in this section have been obtained at Technische Universität Ilmenau in collaboration with a number of industrial and academic partners within the framework of the European Project E-VECTOORC - Electric-Vehicle Control of Individual Wheel Torque for On- and Off-Road Conditions. The aim of the presented case study is (i) to demonstrate a possibility of integration of TC/ABS functions in a unified controller and (ii) to present results of corresponding TC/ABS operation through pure electric motor actuations validated on real vehicle with serial chassis platform. The main outcomes of the relevant ABS/TC investigations are published in [243], [244], [245], [246], [247], [248], [249] and are subjected to three patent applications.

Figure 83 - Test vehicle. Top left: overall view; top right: rear axle with electric motors; bottom left: view on the front wheel mounting; bottom right: view on battery pack and on-board control and measurement system

The case study refers to sport utility electric vehicle developed on the basis of Range Rover Evoque, Figure 83. The main technical data of the vehicle are as follows:

- Total weight 2117 kg;
- Four switched reluctance electric motors - Peak torque / power (30 sec): 200 Nm / 100 kW, Nominal torque / power: 135 Nm / 42kW, Maximum speed: 15000 m^{-1};
- Motor transmission - 2-stage reducer with helical gears, Gear ratio: 1:10,5, Half-shaft torsional stiffness: 6500 Nm/rad;
- Tyres 235/55 R 19.

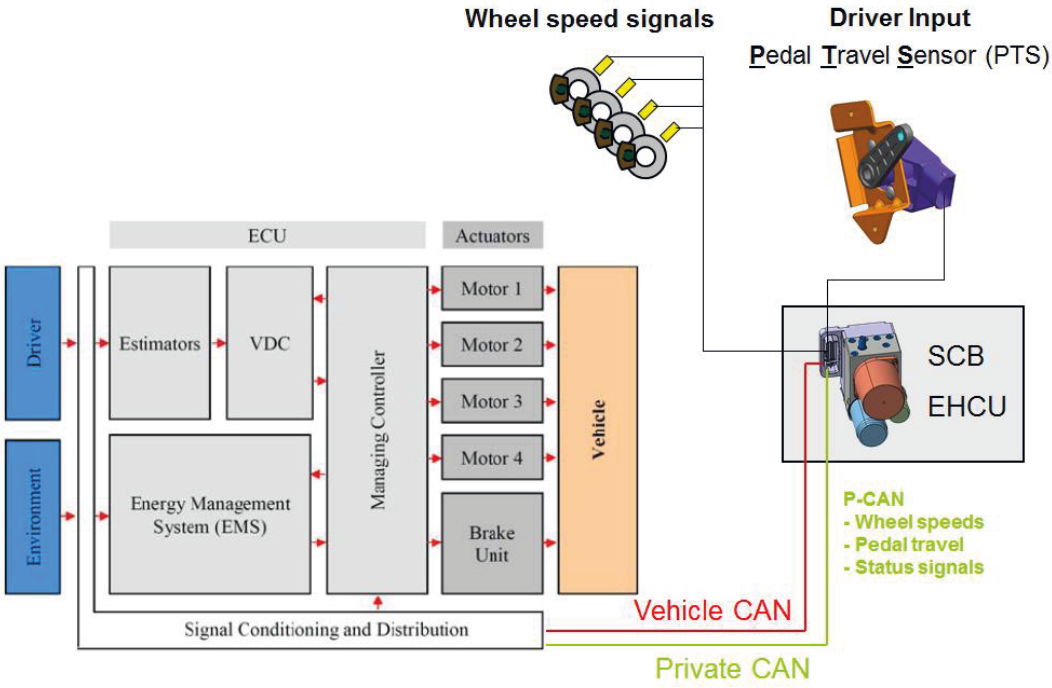

Figure 84 - Architecture of electro-hydraulic brake system ([248])

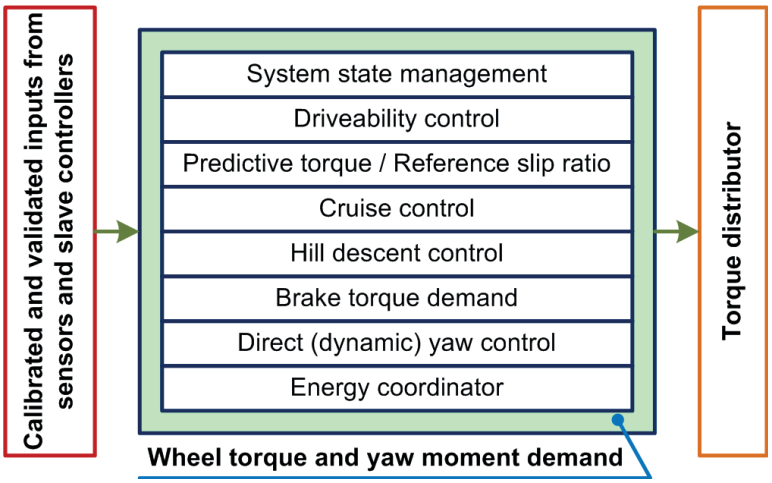

Figure 85 - Simplified structure of vehicle controller (based on [249])

The vehicle is equipped with the electro-hydraulic brake system and ABS, and the braking/ ABS functions can be also carried out by electric motors. The electro-hydraulic brake system is based on the TRW Slip Control Boost (SCB) technology. Its architecture is depicted on Figure 84. The structure of vehicle controller is presented on Figure 85.

4.4.2. Integrated TC / ABS controller

The architecture of TC / ABS, which is developed for the target vehicle, realizes the gain-scheduled proportional-integral direct slip control with feedforward and feedback slip control parts, Figure 86. In the ABS mode, the driver control action F_{driver}, estimated from the brake pedal travel, is the input of base brake controller generating the torque demand T_{dem} for each wheel, which is added up with the reactive torque T_{react}. The reactive torque is computed by the reactive torque controller, which uses the reference slip ratio λ_{ref}, the observed slip ratio λ and the vehicle velocity V_x as input parameters. In the TC mode, the torque demand is computed by bypassing the base brake controller. The actuation is realised through electric motors only. The other components and their functions are identical with the ABS controller described before.

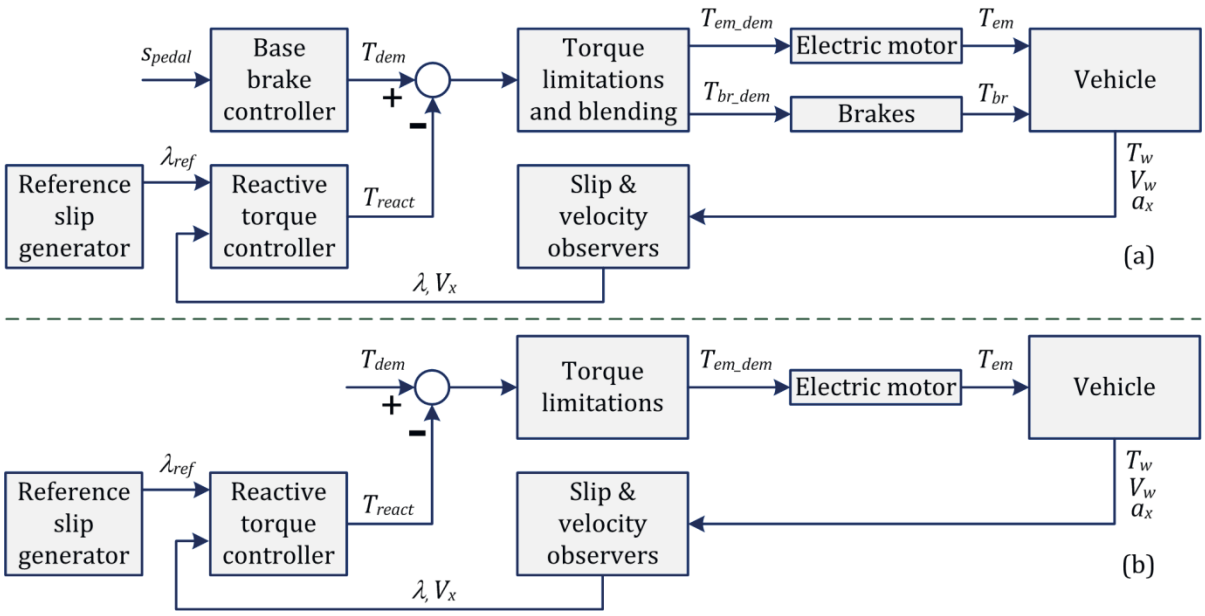

Figure 86 - Wheel slip controller architecture: (a) ABS mode; (b) TC mode

The generation of the torque demand T_{dem} is calculated from the driver control action, in particular from the brake pedal travel. In the presented study, the practical ABS realization

includes a decoupled electro-hydraulic brake system with the embedded pedal unit that is able to provide the corresponding signal of the pedal position. Preliminary the value of T_{dem_prim} is processed as function of the brake pedal travel through a lookup table (LUT). Then, this value is corrected through the predictive torque in accordance with the road conditions to prevent vehicle underbraking / overbraking. The predictive torque is defined as:

$$T_{pred} = \mu_{\max} F_z r + k_{pred} \left(\mu_{\max} F_z r \right) , \tag{4.13}$$

where μ_{max_est} is the estimated value of maximum friction coefficient for given road conditions, F_z is the estimated normal wheel load, r is the tire rolling radius, k_{pred} is the correction coefficient. It is determined for the target vehicle that k_{pred}=0.25 for front wheels and k_{pred}=0.5 for rear wheels. After the processing of the predictive torque, the torque requested by the driver is saturated as:

$$T_{dem} = \begin{cases} \min\left(T_{dem\_prim}, T_{pred} \right) \ if \ T_{dem\_prim} \geq 0 \\ \max\left(T_{dem\_prim}, T_{pred} \right) \ if \ T_{dem\_prim} < 0 \end{cases} . \tag{4.14}$$

The reference slip generator is realized in the form of a lookup table (LUT). The reference slip generator is designed to determine the reference slip λ_{ref} by means of a tyre model. The Pacejka tyre model is used in this study. Its parametrization was provided by industrial partners of the E-VECTOORC project. On the first step the reference slip is defined as

$$\lambda_{ref} = f\left(F_z, \mu_{\max} \right) . \tag{4.15}$$

Then a slip target adaptation algorithm can be applied to modify progressively the reference value obtained from the LUT, in order to be as close as possible to the maximum braking torque and to avoid under or overbraking caused either by inaccurate estimations of μ_{max} or by tire-road behavior different to the one modelled by the LUT. The general control law for reactive torque is described as:

$$\nu_{react} = \nu_{PI} \cdot \xi_{driver\_dem} , \tag{4.16}$$

where v_{PI}: is the proportional-integral control demand, and the correction factor ξ_{driver_dem} is used for the saturation of the reactive torque in order to track the driver demand and to prevent generation of wrong torques. The factor ξ_{driver_dem} is calculated depending on the driver demand computed from the brake pedal sensor.

In ABS mode, the product of the demanded T_{dem} and reactive T_{react} torques is processed in the controller module "Torque Limitations and Blending" generating as output the torque demands for the friction brake T_{br_dem} and the electric motor T_{em_dem} respectively. The individual brake torques from the friction brakes T_{br} and the electric motors T_{em} are realized by the wheels. The information about actual wheel torque T_w, the wheel velocity V_w and longitudinal acceleration / deceleration a_x is then processed in the Slip & Velocity Observers with the actual slip λ and the vehicle velocity V_x as input for the reactive torque controller. The observers use also the reference vehicle model.

Hence the feedforward slip control part is related to the generation of the predictive torque demand, the reactive torque controller is responsible for the feedback slip control part. Next sections will introduce results of experimental testing of the developed controller for the ABS mode.

4.4.3. Experimental results for ABS mode

Initial tuning of the controller gains has been done using hardware-in-the-loop test setup and then the controller has been implemented in the test vehicle, which has been instrumented as follows:

- Controller platform - dSPACE Autobox; IBM PowerPC 750GX, 1GHz; Real time software Control Desk 4.1;
- Vehicle velocity measurement - Corrsys Datron sensor: speed range 0 - 250 km/h; measurement accuracy > ± 0.2%; measurement frequency 250 Hz;
- Accelerometer - Measurement range: ± 5g; bandwidth: 50 Hz;
- Gyroscope - Measurement range: ± 300 °/s; bandwidth: 40 Hz;
- Magnetometer Measurement range: ± 1,2 Gauss; bandwidth: 5,0 Hz.

The full test program includes the braking manoeuvres on low-friction surfaces for different brake system configurations: (i) without ABS; (ii) hydraulic ABS on both axles; (iii) only electric ABS on the front axle; (iv) blended regenerative and hydraulic ABS on the front axle and hydraulic ABS on the rear axle. The low-friction surface is constituted by basalt tiles, which are continuously wetted by the sprinkler system during the vehicle tests. The surface has an inhomogeneous character with the friction coefficient of about $\mu=0,2...0,3$. To give illustrations, Figure 87, Figure 88, and Figure 89 show correspondingly the diagrams of ABS braking from 60 km/h on the low-friction surface for three system configurations: (i) electro-hydraulic ABS on both axles, (ii) electric ABS on the front axle only, (iii) blended electric and hydraulic ABS on both axles. Table 8 compares the brake distance and average deceleration for blended electric and hydraulic ABS on both axles in cases of braking without ABS and with conventional hydraulic ABS. The obtained experimental results allow a number of essential observations and conclusions to be drawn.

1) *Braking with electric ABS on the front axle only.* Even such a limited ABS configuration guarantees the required performance for the given road conditions. The average deceleration has reached the level > 1,25 m/s^2 (as for the service braking), which is considerably more than the case of braking without ABS. The initial drop of the wheel slip did not exceed the level $\lambda\sim0,2$ with the subsequent stabilization characterized by minor oscillations around the reference value $\lambda_{ref}=5\%$. Regardless of initial braking velocity, the drivetrain torque demand oscillates around 40 Nm and reached short-time peak value about of 70 Nm to the end of maneuver.

2) Braking with blended electric/hydraulic ABS on both axles. This ABS configuration demonstrated evident reduction in the brake distance compared with both non-ABS braking (>31% depending on initial braking velocity) and braking with the conventional hydraulic ABS (>6,5% depending on initial braking velocity). The absolute values of the average deceleration are also higher than the hydraulic ABS (>16,5% depending on initial braking velocity). The deceleration profile of the continuous ABS deserves special attention: it was observed that this type of ABS operation does not produce characteristic oscillations of the deceleration that enhances driving comfort.

3) Reference slip tracking. The most distinctive feature of the continuous ABS operation is accurate tracking of the reference slip ratio that was confirmed both for pure electric and

blended configurations of the anti-lock braking system. As it can be seen from Figure 88 and Figure 89, only few initial slip deviations took place during the first seconds of the brake process similar to ordinary ABS operation. To give a quantitative example, Figure 90 depicts the distribution of actual slip values during the whole duration of a single braking maneuver (blended ABS, low-friction road, braking from 50 km/h). This distribution in the form of hit percentage confirms clearly that most of the braking time all the wheels are working in the area close to the reference slip value of 5%.

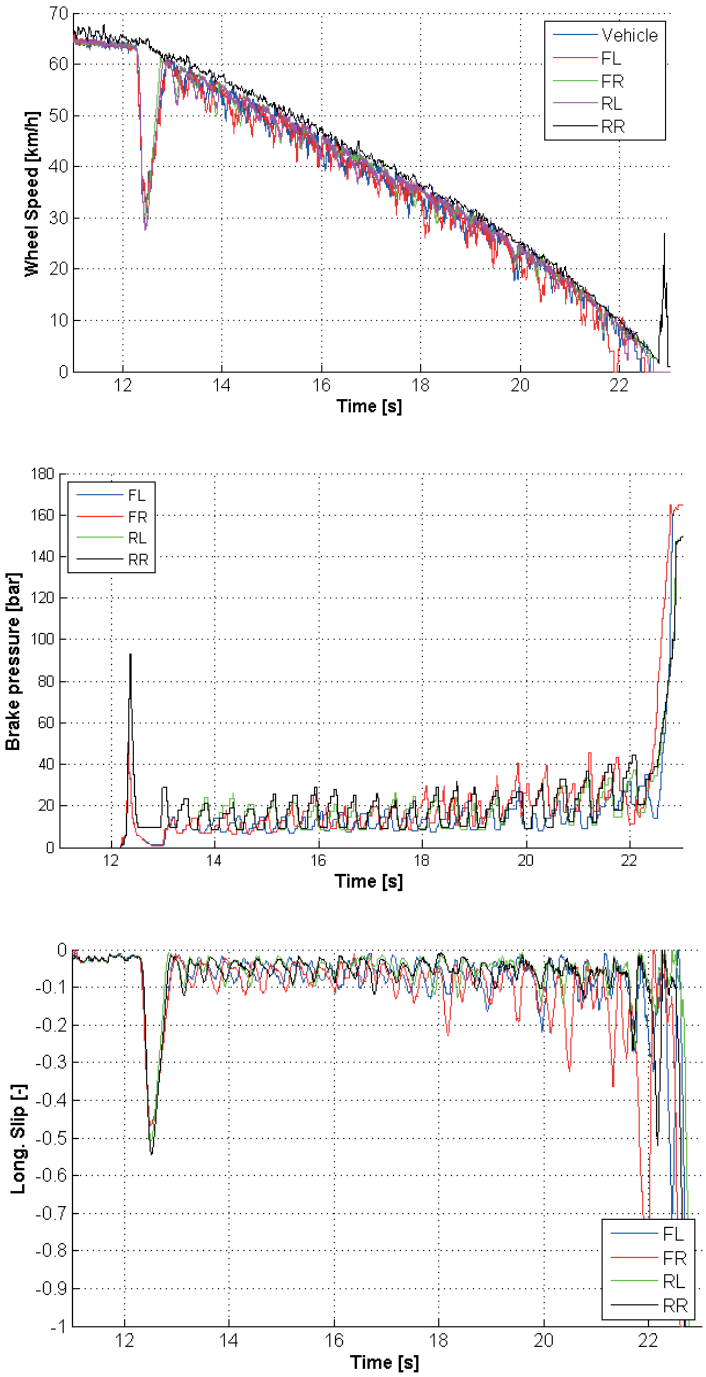

Figure 87 - Braking diagrams: Electro-hydraulic ABS on both axles

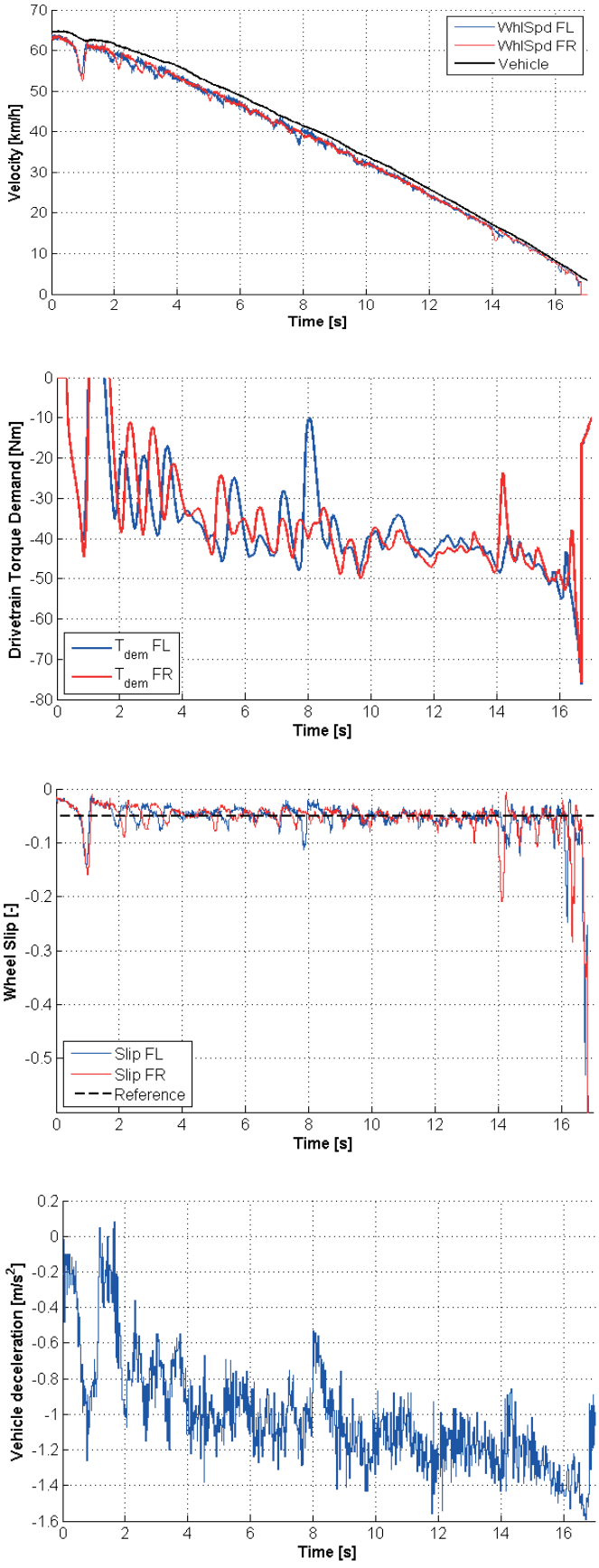

Figure 88 - Braking diagrams: Continuous regenerative ABS on front wheels only

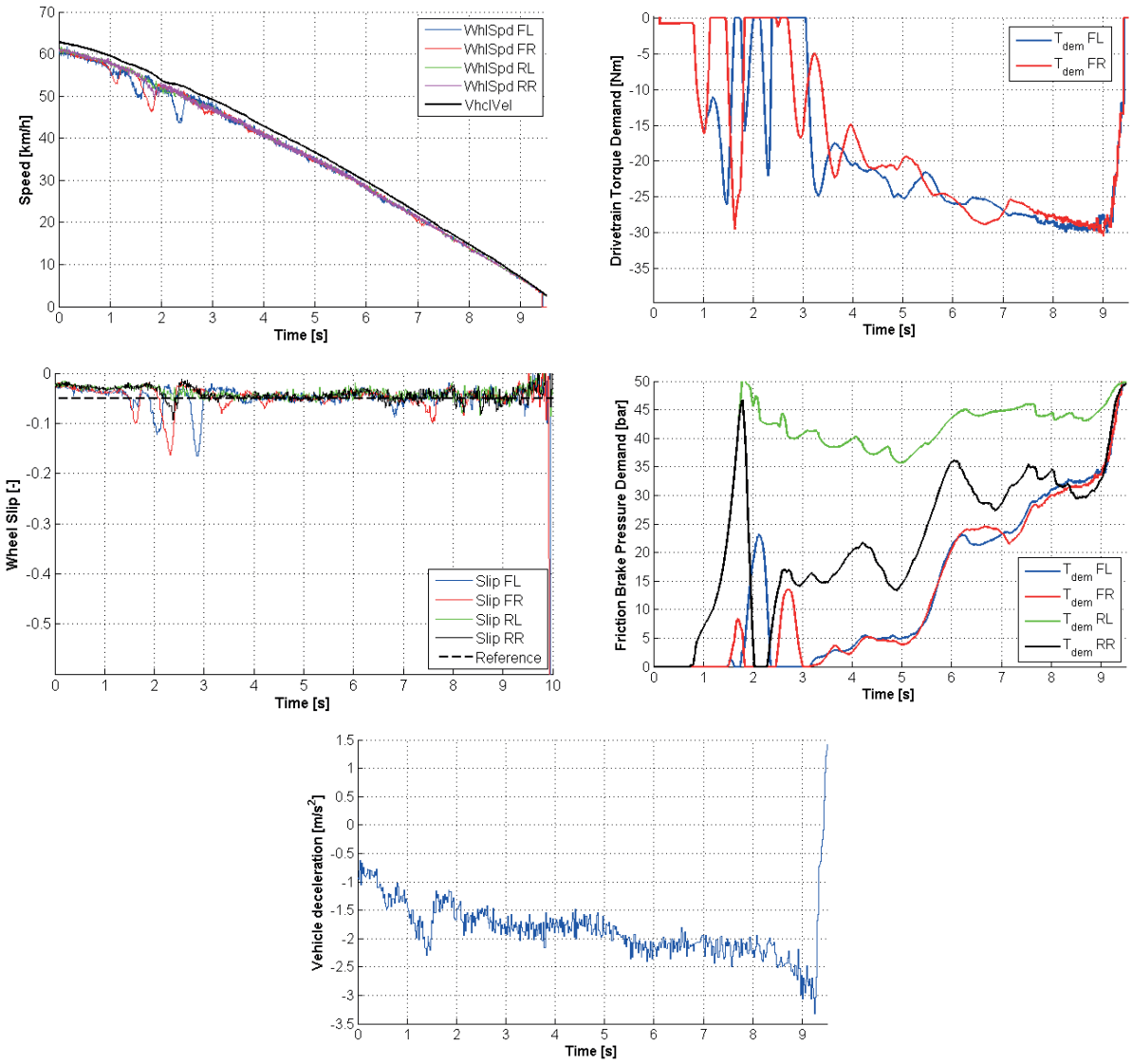

Figure 89 - Braking diagrams: Blended continuous regenerative and hydraulic ABS on front wheels, hydraulic ABS on rear wheels

Table 8: Brake distance and average deceleration

	Initial braking velocity		
	40 km/h	50 km/h	60 km/h
Braking without ABS			
Brake distance, m	68,5	96,4	153,4
Average deceleration, m/s^2	-1,10	-1,01	-1,03
Braking with conventional hydraulic ABS on both axles			
Brake distance, m	49,4	68,6	114,3
Average deceleration, m/s^2	-1,52	-1,51	-1,50
Braking with blended electric / hydraulic ABS on both axles			
Brake distance, m	44,9	64,0	105,3
Average deceleration, m/s^2	-1,81	-1,76	-1,76

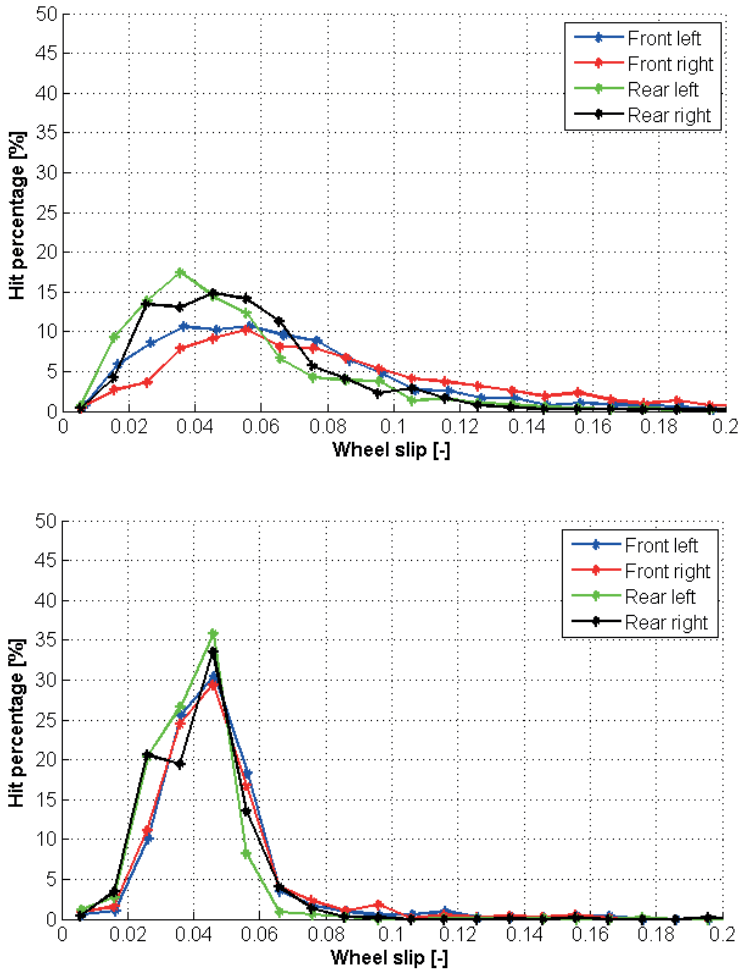

Figure 90 - Distribution of wheel slip during the braking process from 60 km/h; left - hydraulic ABS, right - blended ABS

4) Vehicle jerk. In the case of the continuous regenerative ABS on the front wheels and the blended ABS configuration, the vehicle deceleration is free from pronounced fluctuations, which are typical for conventional ABS operation. The resulting braking dynamics is characterized by the constant deceleration after reaching steady-state.

5) Adaptive properties. Adaptive properties of the ABS controller have been investigated for the braking with transition from one to another type of the road surface. Figure 91a) and b) introduces ABS diagrams for one corresponding maneuver: the vehicle starts to brake from 60 km/h on low-friction surface and then the transition to the high-friction surface takes place after 3 seconds. Figure 91c) and d) illustrates the transition braking from high-friction to low friction surface. It should be mentioned for both tests that the transition time did not exceed 200 ms and even short-time locking of the wheels was avoided. The diagrams confirm that in this case the blended continuous ABS controller properly recognized the change of road conditions.

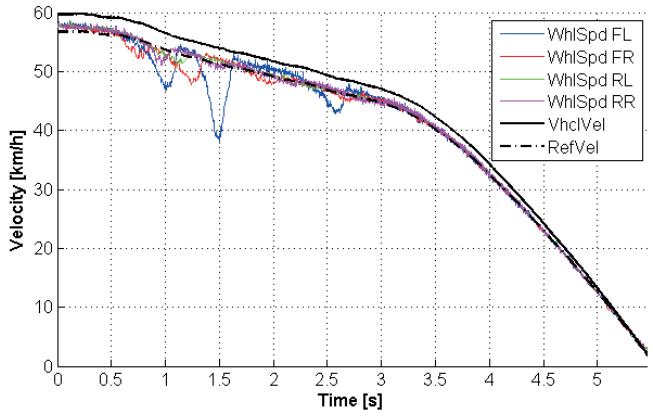

a)

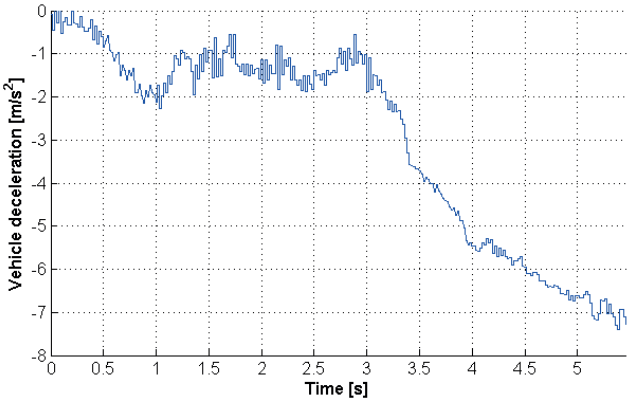

b)

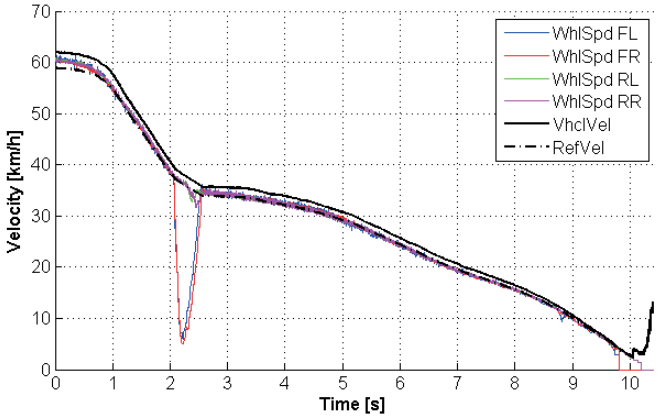

c)

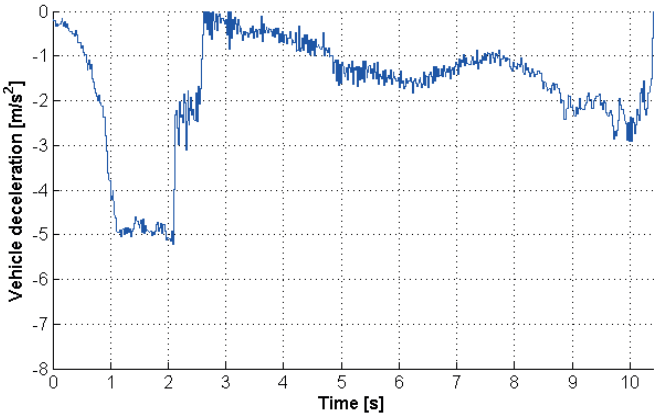

d)

Figure 91 - Diagrams of transition braking

Hence, the presented results have demonstrated an experimentally confirmed huge potential in brake distance reduction and improvement of driving comfort by the continuous ABS control realized through the actuation of individual on-board motors. Moreover, it is shown that the proposed design of the electric vehicle with the individual on-board motors connected to the wheels through the gearbox and the half-shaft can guarantee the required brake performance on the low-friction surface for the case of the brake actuation of only front wheels. Generally, the developed ABS controller both fulfils the requirements of the vehicle safety in a braking mode and also allows improving the driving comfort during the braking manoeuvres.

4.5. Chapter Summary

Analysis of active safety systems for fully electric vehicles reveals a diverse range of approaches to braking and traction control to improve electric vehicle dynamics. However, this research area has still many open questions requiring further investigations. In particular, in spite of the variety in control methods, only a few techniques have, to date, been validated and verified on full-scale vehicles. Considering electric vehicle architectures with in-wheel and on-board motors and adherent mechanical transmission elements as planetary gearboxes, most of the published studies either do not examine or only crudely take into account the oscillation processes caused by the driveline dynamics, which can fundamentally influence the control quality in real conditions. There are also few recent research publications about the controller design and testing of anti-lock braking systems using predominantly the actuation of electric motors. Nevertheless, the introduced case study has demonstrated a huge potential of electric ABS for ensuring the vehicle safety.

Finally, a number of following suggestions can be proposed for future investigations on active safety systems for full electric vehicles:

- Development of optimal traction controllers is demanded from viewpoint of simultaneous effect in vehicle agility at acceleration and minimization of electric energy consumption;
- Dynamics of electric powertrain with relatively high bandwidth is beneficial not only for safety and traction performance but also for overall driving comfort. However, unwanted drivetrain oscillations can take place by specific powertrain architectures (for example, with half-shafts between the motor and the wheel). This requires additional development of system damping mechanisms;
- Benchmarking procedures have to be developed for comparative analysis of electric ABS control variants with both continuous and cyclic actuation of electric motors;
- Advanced studies are required for the analysis of advantages, performance and functional limitations of active safety systems with regard to different variants of electric motors (brushless, switched reluctance, et al.);
- Creation of objective procedures for performance evaluation of ABS / TC of electric vehicles is strongly demanded with particular specification both for laboratory tests and road experiments.

CONCLUSIONS

The presented work covers state-of-the-art and outlooks for automotive active safety systems as complex research and technological objects on the interface between vehicle dynamics, mechatronics, mechanical and control engineering, and information technologies. Modern active safety systems demonstrate vast possibilities in reduction of road accidents or minimization of their negative consequences, however, there is still a significant gap to reach so-called "Zero-accident" level. Further progress in this area relates to a number of technologies requiring particular attention in research and industrial development. Within the framework of the introduced habilitation thesis, three corresponding topics has been discussed.

1) Identification of road conditions. An efficient operation of any active safety system depends on proper acquisition and handling of information about actual (and expected) road conditions in terms of tyre-surface friction and wheel slip. Most of up-to-date ABS, ESC and other active safety systems become such an information through estimation and observation algorithms. Known relevant procedures require minimum input data from on-board sensors but complicate the control algorithms and are sensible to various disturbances. A certain progress in this area is expected with application of new road-side sensors and inclusion of external informational channels of driving environment. Feasible effect in this regard is demonstrated in the habilitation thesis with the case study investigating the combination of the on-board and on-road identification of tyre friction. The identified tyre friction parameters can be subsequently utilized in automotive active safety systems for handling of linguistic and numerical uncertainty that improves adaptive properties of the ABS and ESC controllers. This approach is patented by the author and his collaborators (European Patent EP2089260 (A1) "Apparatus and Method for Determining the Frictional State of a Carriageway Surface and Use Thereof").

2) Integrated active safety control. A clear-cut trend today is to integrate and to coordinate the operation of various active chassis and powertrain systems to enhance efficiency and robustness of the active safety control. The integration of the brake-based / torque-based yaw motion control, the active steering, the active suspension, the torque vectoring and other automotive systems allows to reach simultaneously a better vehicle safety, driving comfort and overall energy efficiency of the vehicle. An important remark is that integrated active safety systems have a more comprehensive architecture and logic of the controller and require a careful value

analysis to find a balance between the system complexity and achievable benefits. Two relevant case studies are introduced in the habilitation work both for the conventional and the electric vehicle. They have clearly demonstrated that correct integration of the braking, steering and powertrain control improves the vehicle stability and brings additional advantage in minimization of tyre dissipation and wheel slip losses.

3) Active safety control for electric vehicles. The share of electric vehicles is continuously increased world-wide that causes a demand on better specifying their active safety control design. It is especially reasonable for electric vehicles with individual wheel motors. The motors are considered in this case both as powertrain and chassis actuators (due to operation in a regenerative, braking mode). Analysis of academic and industrial studies has identified different approaches to the realization of TC, ABS and ESC functions in the electric vehicles, and the most efficient solutions should be still specified here. Nevertheless, the first results of operation of serial electric vehicles with pure electric ABS or ESC have demonstrated an essential improvement of the control performance as compared, for example, with conventional ABS using hydraulic actuators. This statement is also confirmed with the results of case study given in this habilitation thesis for the all-wheel drive sport utility vehicle with individually controlled on-board motors. The method, introduced in the case study, is patented (German Patent DE 10 2014 003 992 A1, „System und Verfahren zur Antriebs- und Bremsmomentregelung in Elektrofahrzeugen mit Einzelradantrieb“), and is advanced in further patent application (German Patent Document DE 10 2014 017 464 A1 “System und Verfahren zur Regelung der Radbremsmomente mit gleichzeitiger Störkompensation in Elektrofahrzeugen”).

The results introduced in this work substantiate that automotive active safety systems belong to the most challenging topics in automotive engineering with wide opportunities for advanced science and implementation of novel mechatronic, vehicular and information technologies. New engineering solutions in this area are highly demanded both by industry and society, and the presented habilitation thesis makes a certain contribution in this direction.

Analysis of recent studies and innovation projects funded in industrial and public sectors allows identifying the following promising directions, where further application areas of active safety systems and corresponding research demand are expected:

- New mechatronic chassis and powertrain actuators allowing better dynamics of active safety control and characterized by miniaturization of components (beneficial for modular and in-wheel design), reduced power consumption, and energy harvesting;
- Further inclusion of driver parameters into the active safety control circuit in order to enlarge functionality of advanced driver assistance systems with functions of training the driver in hazard perception;
- Adaptation of active safety control to the conditions of automated driving, especially for transient operation of the vehicle between semi-autonomous and autonomous modes;
- Advanced methods for vehicle state and parameter estimation for the active safety controllers with the use of sensor fusion technique, on-road information, and new sensor technologies for detection and measurement of road and vehicle parameters;
- Novel procedures and testing methods, which are required for development design of active safety systems and validation and verification of their functionality and based on X-in-the-loop technologies that allows shared and distributed experiments for simultaneous real-time studies in control performance, loading modes, and reliability both on component, system, and vehicle levels.

The listed technological areas are not only important for active safety systems approaching to zero-accident level but also influential in creation of new vehicle and mobility paradigms. Their proper consideration should be essential by establishing innovative educational and research concepts in Automotive Engineering.

PERSONAL CONTRIBUTION OF THE AUTHOR TO HABILITATION TOPICS

The case studies of the presented habilitation thesis are based on long-term works of the author not only in the form of individual investigations but also in collaboration with other scientists, professionals and institutions. To give a proper acknowledgement to all collaborative studies, the personal contributions of the author and his colleagues are summarized below.

1) Case study from Section 2.2

Personal contribution: Development of three-layer cascade architecture of tyre friction identification and corresponding fuzzy models; Design of HIL experiments.

Relevant projects: "Fuzzy Environment of Tyre-Surface Interaction" by Alexander von Humboldt Foundation; "INTYRE: Interface of Intelligent Control Philosophy and Mechatronics Technology for Tyre-Surface Interaction" by the European Commission.

Contribution of collaborators: Prof. Dr.-Ing. Klaus Augsburg (TU Ilmenau) - support in the tyre model specification and definition of HIL test rig architecture; Dr. Barys Shyrokau (former TU Ilmenau, now TU Delft) - development of 12-DOF vehicle model, realization of HIL experiments.

Relevant publications: [147], [148], [149], [150], [152], [153], [154], [157].

2) Case study from Section 3.3.1

Personal contribution: Specification of integrated active safety system controller and related sub-controllers; Definition of integration rules and benchmarking criteria.

Relevant projects: "Integration of Inverse Dynamics and Fuzzy Sets for Control Processes in Mechatronic Systems" by DFG.

Contribution of collaborators: Dr. Barys Shyrokau (former TU Ilmenau and Nanyang Technological University, now TU Delft) - development of sub-controllers of ESC, TV and AFS; realization of software and HIL simulation. Prof. Dr.-Ing. Klaus Augsburg (TU Ilmenau) - support in integrated controller specification. Prof. Vladimir Vantsevich (former Lawrence Technological University, now University of Alabama) - development of inverse vehicle model.

Relevant publications: [199], [200].

3) Case study from Section 3.3.2

Personal contribution: Design of HIL test rig architecture for investigation on integrated active safety control; Development of benchmarking criteria.

Relevant projects: Research Group "PORT Powertrain-Radiotrain" funded by the European Social Fund.

Contribution of collaborators: Dr. Barys Shyrokau (former TU Ilmenau and Nanyang Technological University, now TU Delft) - development of the integrated controller based on the control allocation method; development of 14-DOF vehicle model. Prof. Dr.-Ing. Klaus Augsburg (TU Ilmenau) - support in specification of real-time HIL experiments. Dipl.-Ing. Dzmitry Savitski, Dipl.-Ing. Lukas Heidrich, Dipl.-Ing. Kristian Höpping (all - TU Ilmenau) - organization and carrying out of HIL tests.

Relevant publications: [44], [203], [204].

4) Case study from Section 4.4

Personal contribution: Specification and co-development of integrated TC/ABS controller; Specification and carrying out of test procedures on the HIL test rig and the vehicle demonstrator; Design of experiment.

Relevant projects: "E-VECTOORC: Electric-vehicle control of individual wheel torque for on- and off-road conditions" by the European Commission

Contribution of collaborators: Dr. Barys Shyrokau (former TU Ilmenau and Nanyang Technological University, now TU Delft) - co-development of integrated TC/ABS controller; Dipl.-Ing. Dzmitry Savitski - co-development of the integrated TC/ABS controller; carrying out of test procedures on the HIL test rig and the vehicle demonstrator; Prof. Dr.-Ing. Klaus Augsburg (TU Ilmenau), Dr. Aldo Sorniotti (University of Surrey) - general supervising and consulting during the TC/ABS development process. Dr.-Ing. Thomas Pütz (TRW Automotive), Dr. Phil Barber (Jaguar Land Rover) - support of tests on the HIL and vehicle demonstrator. Dr. Javier Orus, Ing. Ruben Meneses Bouso, Ing. José Manuel Rodríguez Fortún (ITAINNOVA / Instituto Tecnológico de Aragón) - co-development of integrated TC/ABS controller. Ing. Johan Theunissen, Ing. Jasper De Smet, Ing. Karel Janssen, Ing. Dirk Steenbeke (Flanders Make) - tests on the vehicle demonstrators.

Relevant publications: [52], [243], [244], [245], [246], [247], [248].

REFERENCES

[1] P. Lepercq, "A World Free of Road Crash Death and Injury," in *FISITA Summit*, Mainz, Germany, 2010.

[2] European Commission, "Towards a European road safety: policy orientations on road safety 2011-2020," Brussels, 2010.

[3] M. Aga and A. Okada, "Analysis of vehicle stability control (VSC)'s effectiveness from accident data," in *Proc. of the 18th International Technical Conference of the Enhanced Safety of Vehicles*, Nagoya, Japan, 2003.

[4] NHTSA, "Statistical analysis of the effectiveness of electronic stability control (ESC) systems - Final report," U.S. Department of Transportation, Washington, DC, 2007.

[5] R. Frampton and P. Thomas, "Effectiveness of electronic stability control systems in Great Britain," VSRC, Loughborough University, Loughborough, 2007.

[6] J. Scully and S. Newstead, "Followup evaluation of electronic stability control effectiveness in Australasia," Monash University Accident Research Centre, Victoria, 2010.

[7] A. Erke, "Potential effects of Electronic Stability Control (ESC) on accidents," Association for European Transport and contributors, Henley-in-Arden, UK, 2006.

[8] S. K. Clark, Mechanics of pneumatic tires, Washington: U.S. Government Printing Office, 1971.

[9] K. Grosch, "The relation between the friction and visco-elastic properties of rubber," *Proceedings A of the Royal Society,* pp. 21-39, 25 June 1963.

[10] H. Kummer, Unified theory of rubber and tire friction, University Park, PA: Pennsylvania State University, 1966.

[11] D. F. Moore, The friction of pneumatic tyres, Amsterdam: Elsevier Scientific Pub. Co., 1975.

[12] B. Persson, "Rubber friction and tire dynamics," *Journal of Physics: Condensed Matter,* p. 015003, 2011.

[13] H. Kummer and W. Meyer, "New theory permits better frictional coupling between tire and road," in *Proc. of FISITA World Automotive Congress*, Munich, Germany, 1966.

[14] H. Kummer and W. Meyer, "Verbesserter Kraftschluss zwischen Reifen in Fahrbahn - Ergebnisse einer neuen Reibungstheorie," *Automobiltechnische Zeitschrift,* pp. 245-251, 382-386, 1967.

[15] R. Gnadler, H.-J. Unrau, H. Fischlein and M. Frey, "Ermittlung von µ-Schlupf-Kurven an Pkw-Reifen," FAT-Schriftenreihe, Frankfurt am Main, 1995.

[16] M. Gothié, T. Parry and P. Roe, "The relative influence of the parameters afecting road surface friction," in *Proceedings of the 2nd International Colloquium on Vehicle Tyre Road Interaction*, Florence, Italy, 2001.

[17] R. Gnadler, H.-J. Unrau, H. Fischlein and M. Frey, "Umfangskraftverhalten von Pkw-Reifen bei unterschiedlichen Fahrbahnzuständen," *Automobiltechnische Zeitschrift,* September 1996.

[18] I. Besselink, A. Schmeitz and H. Pacejka, "An improved Magic Formula/Swift tyre model that can handle inflation pressure changes," *Vehicle System Dynamics,* pp. 337-352, December 2010.

[19] W. Gengenbach, "Experimentelle Untersuchungen von Reifen auf nasser Fahrbahn," *Automobiltechnische Zeitschrift,* pp. 83-90, 288-293, 310-316, 1968.

[20] X. Clayes, J. Yi, L. Alvarez, R. Horowitz, C. Canudas de Wit and L. Richard, "Tire Friction Modeling under Wet Road Conditions," in *Proceedings of the American Control Conference*, Arlington, VA, 2001.

[21] M. Salaani, G. Heydinger and P. Grygier, "Measurement and modelling of tire forces on a low coefficient surface," *SAE Technical Paper Series,* pp. 2006-01-0559, 2006.

[22] R. Weber, "Reifen auf Glatteis," *Automobiltechnische Zeitschrift,* pp. 1-9, 146-150, Januar, April 1972.

[23] M. Mizuno, H. Sakai, K. Oyama and Y. Isomura, "Development of a tyre force model incorporating the influence of the tyre surface temeprature," *Vehicle System Dynamics,* pp. 395-402, January 2005.

[24] G. Heinrich and M. Klüppel, "Rubber Friction and Tire Traction," in *VDI-Berichte Nr. 2014*, Düsseldorf, VDI, 2007, pp. 341-360.

[25] W. Blythe and T. Day, "Single vehicle wet road loss of control: Effect of tire tread depth and placement," *SAE Technical Paper Series,* pp. 2002-01-0553, 2002.

[26] E. Fiala, "Seitenkräfte am rollenden Luftreifen," *VDI-Zeitschrift,* pp. 973-979, 1954.

[27] H. B. Pacejka, Tire and Vehicle Dynamics, Third Edition, Oxford: Butterworth-Heinemann, 2012.

[28] C. Peng, P. Cowell, C. Chisholm and J. Lines, "Lateral tyre dynamics characteristics," *Journal of Terramechanics,* pp. 395-414, 1994.

[29] H. Sakai, "Study on Cornering Properties of Tire and Vehicle," *Tire Science and Technology,* pp. 136-169, July-September 1990.

[30] L. Segel, "Force and Moment Response of Pneumatic Tires to Lateral Motion Inputs," *Journal of Engineering for Industry,* pp. 37-44, 01 February 1966.

[31] U. Kiencke and L. Nielsen, Automotive Control Systems, Berlin - Heidelberg: Springer-Verlag, 2005.

[32] J. Reimpell, H. Stoll and J. W. Betzler, The Automotive Chassis: Engineering Principles, Oxford: Butterworth-Heinemann, 2001.

[33] H. Dörrie, C. Schröder and B. Wies, "Winter Tires: Operating Conditions, Tire Characteristics and Vehicle Driving Behaviour," *Tire Science and Technology,* pp. 119-136, April-June 2010.

[34] H. Kim and P. I. Ro, "A Tire Side Force Model by Artificial Neural Network," *SAE Technical Paper Series,* 1995.

[35] D. Karnopp, Vehicle Dynamics, Stability, and Control, Boca Raton, FL: CRC Press, 2013.

[36] M. Mitschke, Dynamik der Kraftfahrzeuge - Band C: Fahrverhalten, Berlin: Springer-Verlag, 1990.

[37] Z. A. Zomotor, Fahrwerktechnik: Fahrverhalten, Würzburg: Vogel Buchverlag, 1987.

[38] W. F. Milliken and D. L. Milliken, Race car vehicle dynamics, Warrendale: SAE International, 1995.

[39] J. Y. Wong, Theory of ground vehicles, New York: John Wiley Sons, Inc., 2001.

[40] A. G. Ulsoy, H. Peng and M. Cakmakci, Automotive Control Systems, New York: Cambridge University Press, 2012.

[41] A. Trächtler, "Integrierte Fahrdynamikregelung mit ESP, aktiver Lenkung und aktivem Fahrwerk," *at – Automatisierungstechnik,* vol. 53, no. 1, pp. 11-19, 2005.

[42] M. Horiguchi, A. Mizuno, M. Jones and K. Futamura, "Active Camber Control," *Lecture Notes in Electrical Engineering,* vol. 198, pp. 247-256, 2013.

[43] K. Augsburg, V. Ivanov, K. Kruchkova, K. Höpping, S. Gramstat, M. Bogdevicius and P. Kiss, "Project Adtyre: Towards dynamic tyre inflation control," *Lecture Notes in Electrical Engineering,* vol. 198, pp. 185-198, 2013.

[44] B. Shyrokau, D. Wang, L. Heidrich and K. Höpping, "Analysis of subsystems coordination for electric vehicle during straigh-line braking and brake-in-turn," in *IEEE Symposium on Computational Intelligence for Engineering Solutions*, Singapore, 2013.

[45] Bosch Automotive Handbook, 8 ed., Warrendale: SAE International, 2011, p. 1266.

[46] W. Pasillas-Lépine, "Hybrid modelling and limit cycle analysis for a class of five-phase anti-lock brake algorithms," *Vehicle System Dynamics,* vol. 44, no. 2, pp. 173-188, 2006.

[47] K. Bill and B. Breuer, Brake Technology Handbook, Warrendale: SAE International, 2008.

[48] J. Ahn, K. Jung, D. Kim, H. Jin, H. Kim and S. Hwang, "Analysis of a Regenerative Braking System for Hybrid Electric Vehicles Uisng an Electro-Mechanical Brake," *International Journal of Automotive Technology,* vol. 10, no. 2, pp. 229-234, 2009.

[49] T. Strutz, "Use of Brake by Wire - Example EHCB in Audi R8 Etron," in *Eurobrake 2013*, Dresden, Germany, 2013.

[50] T. Johansen, I. Petersen, J. Klakkuhl and J. Lüdemann, "Gain-scheduled wheel slip control in automotive brake systems," *IEEE Transactions on Control Systems Technology,* vol. 11, no. 6, pp. 799-811, 2003.

[51] F. Sun, K. Lolenko and J. Rudolph, "Nonlinear observer design for state estimation during anti-lock braking," in *The 13th Mechatronics Forum International Conference*, Linz, Austria, 2012.

[52] D. Savitski, V. Ivanov, K. Augsburg, B. Shyrokau, R. Wragge-Morley, T. Pütz and P. Barber, "The new paradigm of anti-lock braking system for full electric vehicle: experimental investigation and bencmarking," *Proc. of IMechE, Part D: Journal of Automobile Engineering,* 2015.

[53] A. Hac and M. D. Simpson, "Estimation of vehicle side slip angle and yaw rate," *SAE Technical Paper Series,* no. 2000-01-0696, 2000.

[54] Q. Cheng, A. C. Victorino and A. Charara, "A new nonlinear observer of the sideslip angle and the road bank angle using the particle filter," in *The 11th International Symposium on Advanced Vehicle Control*, Seoul, Korea, 2012.

[55] M. Abe, A. Kato, K. Suzuki, Y. Kano, Y. Furukawa and Y. Shibahata, "Estimation of vehicle side-slip angle for DYC by using on-board-tire-model," in *The 4th International Symposium on Advanced Vehicle Control AVEC*, Nagoya, Japan, 1998.

[56] K. Sawase and Y. Sano, "Application of active yaw control to vehicle dynamics by utilizing driving/breaking force," *JSAE Review,* vol. 20, pp. 289-295, 1999.

[57] K. Sawase and K. Inoue, "Classification and characteristic analysis of right-and-left torque vectoring mechanisms based on velocity diagram," *VDI-Berichte,* no. 2014, pp. 121-134, 2007.

[58] D. Piyabongkarn, J. Lew, R. Rajamani and J. Grogg, "Active driveline torue-management systems," *IEEE Control Systems Magazine,* pp. 86-102, August 2010.

[59] F. Cheli, L. Kakalis and A. Zorzutti, "A torque vectoring control logic for active high performance vehicle handling improvement," in *The ASME 2007 International Design Engineering Technical Conferences & Computers and Information in Engineering Conference*, Las Vegas, Nevada, USA, 2007.

[60] G. Kaiser, F. Holzmann, B. Chretien and M. Korte, "Torque vectoring with a feedback and feed forward controller - applied to a through the road hybrid electric vehicles," in *IEEE Intelligent Vehicles Symposium*, Baden-Baden, Germany, 2011.

[61] J. Webb, S. Boltshauser and J. Quentin, "Introduction to IDIADA's torque vectoring technology for electric vehicles," in *EAEC European Automotive Congress*, Valencia, Spain, 2011.

[62] L. De Novellis, A. Sorniotti and P. Gruber, "Wheel torque distribution criteria for electric vehicles with torque-vectoring differentials," *IEEE Transactions on Vehicular Technology,* vol. 63, no. 4, pp. 1593-1602, 2013.

[63] K. Shimada and Y. Shibahata, "Comparison of three active chassis control methods for stabilizing yaw moments," *SAE Technical Paer Series,* no. 940870, 1994.

[64] J. Yamakawa and K. Watanabe, "A method of optimal wheel torque determination for independent wheel drive vehicles," *Journal of Terramechanics,* vol. 43, no. 3, pp. 269-285, 2006.

[65] J. Song and W. S. Che, "Comparison and evaluation of brake yaw motion controllers with an antilock brake system," *Proc. IMechE Part D: Journal of Automobile Engineering,* vol. 222, pp. 1273-1288, 01 July 2008.

[66] M. Nagai, M. Shino and F. Gao, "Study on integrated control of active front steer angle and direct yaw moment," *JSAE Review,* vol. 23, pp. 309-315, 2002.

[67] W. Klier and W. Reinelt, "Active front steering (Part 1): Mathematical modeling and parameter estimation," *SAE Technical Paper Series,* no. paper 2004-01-1102, 2004.

[68] S. Tanizaki and T. Yamanaka, "The effect of active rear steer system," in *International Symposium on Advanced Vehicle Control*, Nagoya, Japan, 1998.

[69] M. Abe, "Vehicle dynamics and control for improving handling and active safety: from four-wheel steering to direct yaw moment control," *Proc. of the IMechE, Part K: Journal of Multi-Body Dynamics,* vol. 213, no. 12, pp. 87-101, 1999.

[70] N. Bajcinca, M. Hauschild and L. Bose, "Steer-by-Wire Lenkung: Algorithmen, Aktuatorik und Rapid-Control-Prototyping," in *Tagung Aktive Sicherheit durch Fahrerassistenz*, München, 2004.

[71] J. Foth, Ü. Gazyakan, P. Dominke and G. Ruck, "Steering systems for future requirements," in *European Automotive Congress EAEC*, Barcelona, Spain, 1999.

[72] W. Cho, J. Yoon, K. Yi and T. Jeong, "An investigation into unified chassis control based on correlation with longitudinal/lateral tire force behavior," *SAE Technical Paper Series,* no. 2009-01-0438, pp. 1-8, 2009.

[73] W. Cho, H. Heo and K. Yi, "Unified chassis control for the improvement of agility, maneuverability, and lateral stability," *IEEE Transactions on Vehicular Technology,* vol. 61, no. 3, pp. 1008-1020, 2012.

[74] M. Abe and O. Mokhiamar, "An integration of vehicle motion controls for full drive-by-wire vehicle," *Proc. of IMechE, Part K: J. Multi-body Dynamics,* vol. 221, pp. 117-127, 2007.

[75] O. Mokhiamar and M. Abe, "Active wheel steering and yaw moment control combination to maximize stability as well as vehicle responsiveness during quick lane change for active vehicle handling safety," *Proc. of the IMechE, Part D: Journal of Automobile Engineering,* vol. 216, pp. 115-124, 1 February 2002.

[76] D. Kim, S. Hwang and H. Kim, "Vehicle stability enhancement of four-wheel-drive hybrid electric vehicle uisng rear motor control," *IEEE Transactions on Vehicular Technology,* vol. 57, no. 2, pp. 727-735, 2008.

[77] H. Fujimoto and Y. Yamauchi, "Advanced motion control of electric vehicle based on lateral force observer with active steering," in *IEEE International Symposium on Industrial Electronics (ISIE)*, Bari, Italy, 2010.

[78] H. Nagase, T. Inoue and Y. Hori, "Decoupling control of beta and gamma for high performance AFS and DYC of 4 wheel motored electric vehicle," in *Proc. of 6th International Symposium on Advanced Vehicle Control AVEC*, Hiroshima, Japan, 2002.

[79] C. March and T. Shim, "Integrated control of suspension and front steering to enhance vehicle handling," *Proc. IMechE, Part D: Automobile Engineering,* vol. 221, pp. 377-391, 2007.

[80] H. Deiss, M. Eickhoff, G. Karch, H. Krimmel and C. Pelchen, "Networled driveline, steering and chassis systems," in *Proc. of the 31st FISITA World Automotive Congress*, Yokohama, Japan, 2006.

[81] H. Her, K. Yi, J. Suh and C. Kim, "Development of integrated control of electronic stability control, continuous damping control and active anri-roll bar for vehicle yaw stability," in *Proc. of the 7th IFAC Symposium on Advances in Automotive Control*, Tokyo, Japan, 2013.

[82] R. Tchamna, E. Youn and I. Youn, "Combined control effects of brake and active suspension control on the global safety of a full-car nonlinear model," *Vehicle System Dynamics: International Journal of Vehicle Mechanics and Mobility,* vol. 52, no. sup. 1, pp. 69-91, 2014.

[83] A. Hac and M. Bodie, "Improvements in vehicle handling through integrated control," *Int. J. of Vehicle Design,* vol. 29, no. 1-2, pp. 23-50, 2002.

[84] A. Alleyne, "Improved vehicle performance using combined suspension md braking forces," in *Proc. 1995 American Control Conference (ACC)*, Seattle, WA, USA, 1995.

[85] M. Reul and H. Winner, "Enhanced braking performance by integrated ABS and semi-active damping control," in *Proc. the 21st Enhanced Safety of Vehicles ESV Conference*, Stuttgart, Germany, 2009.

[86] H. Hamersma and P. Els, "Improving the brake performance of a vehicle with ABS and a semi-active suspension system on a rough road," *Journal of Terramechanics,* vol. 56, pp. 91-101, 2014.

[87] S.-B. Lu, Y.-N. Li and S.-B. Choi, "Contribution of chassis key subsystems to rollover stability control," *Proc. IMechE, Part D: Journal of Automobile Engineering,* vol. 226, pp. 479-493, 2012.

[88] S. Yim and K. Yi, "Design of an active roll control system for hybrid four-wheel-drive vehicles," *Proc. IMechE, Part D: Journal of Automobile Engineering,* vol. 227, no. 2, pp. 151-163, 2013.

[89] S.-J. Park and J.-H. Sohn, "Effects of camber angle control of front suspension on vehicle dynamics behaviors," *Journal of Mechanical Science and Technology,* vol. 26, no. 2, pp. 307-313, 2012.

[90] M. Wiesentahl, H. Collenberg and H. Krimmel, "Aktive Hinterachskinematk AKC - ein Beitrag zu Fahrdynamik, Sicherheit und Komfort," in *17. Aachener Kolloquium Fahrzeug- und Motorentechnik*, Aachen, Germany, 2008.

[91] C. Carlson and J. Gerdes, "Identifying tire presure variation by nonlinear estimation of longitudinal stiffness and effective radius," in *Proc. of AVEC 2002 6th International Symposium of Advanced Vehicle Control*, Hiroshima, Japan, 2002.

[92] J. Svendenius, "Tire modelling and friction estimation - PhD Thesis," University Lund, Lund, Sweden, 2007.

[93] M. Al-Solihat, S. Rakheja and A. Ahmed, "Influence of tyre pressure on an urban bus transient and steady state handling performance," *Proc. of IMechE, Part D: Journal of Automobile Engineering,* vol. 224, pp. 893-908, 2010.

[94] P. Fancher, Descriptive parameters used in analyzig the braking and handling of heavy trucks - measurements of the longitudinal and lateral traction properties of truck tyres, vol. 3, Univ of Michigan, Highway Safety Research Institute, 1981.

[95] E. Kasprzak, K. Lewis and D. Milliken, "Inflation pressure effects in the nondimensional tire model," *SAE Technical Paper,* no. 2006-01-3607, 2006.

[96] H. Bloecher, J. Dickmann and M. Andres, "Automotive active safety & comfort functions using radar," in *Proc. of IEEE International Conference on Ultra-Wideband (ICUWB)* , Vancouver, BC, Canada, 2009.

[97] J. Breuer, A. Faulhaber, P. Frank and S. Gleissner, "Real world safety benefits of brake assistance systems," in *Proc. 20th International Technical Conference on the Enhanced Safety of Vehicles Conference (ESV)*, Lyon, France, 2007.

[98] J. McCall and M. Trivedi, "Driver behavior and situation aware brake assitance for intelligent vehicles," *Proceedings of IEEE,* vol. 95, no. 2, pp. 374-387, 2007.

[99] A. Eckert, B. Hartmann, M. Sevenich and P. Rieth, "Emergency steer & brake assist - a systematic approach for system integration of two complementary driver assistance systems," in *Proceedings of the 22nd International Technical Conference on the Enhanced Safety of Vehicles (ESV)*, Washington, DC, USA, 2011.

[100] M. Rüder, W. Enkelmann and R. Garnitz, "Highway lane change assistant," in *Proc. of IEEE Intelligent Vehicle Symposium*, Versailles, France, 2002.

[101] S. Habenicht, H. Winner, S. Bone, F. Sasse and P. Korzenietz, "A maneuver-based lane change assistance system," in *Proc. of IEEE Intelligent Vehicle Symposium*, Baden-Baden, Germany, 2011.

[102] R. Bishop, Intelligent vehicle technology and trends, Norwood, MA: Artech House Inc., 2005.

[103] T. Kosch, C. Schroth, M. Strassberger and M. Bechler, Automotive inter-networking, Chichester: John Wiley & Sons, 2012.

[104] M. Imran, Y. Hassan and D. Patterson, "GPS-GIS-based procedure for tracking vehicle path on horizontal alignments," *Computer-Aided Civil and Infrastructure Engineering,* vol. 21, pp. 383-394, 2006.

[105] M. Jokela, M. Kutila, J. Laitinen, F. Ahlers, N. Hautiere and T. Schendzielorz, "Optical road monitoring of the future smart roads - preliminary results," *International Journal of Computer and Information Science and Engineering,* vol. 1, no. 4, pp. 240-245, 2007.

[106] C. Nwagboso, P. Georgakis and N. Rangwala, "Architectural design of integrated external speed adaptation with collision avoidance system for intelligent trucks," *International Journal of Vehicle Autonomous Systems,* vol. 2, no. 1/2, pp. 104-125, 2004.

[107] C. Lex, A. Eichberger and W. Hirschberger, "Metoden zur Ermittlung des Reifen-Fahrbahn-Kraftschlusspotenzials für Fahrerasstenzsysteme," *Automobiltechnische Zeitschrift,* vol. 113, no. 12, pp. 992-997, 2011.

[108] L. Li, F.-Y. Wang and Q. Zhou, "Integrated longitudinal and lateral tire/road friction modeling and monitoring for vehicle motion control," *IEEE Transactions on Intelligent Transportation Systems,* vol. 7, no. 1, pp. 1-19, 2006.

[109] G. Rill, Simulation von Kraftfahrzeugen, Wiesbaden: Vieweg Verlag, 1994.

[110] P. Dahl, "Solid friction damping of mechanical vibrations," *AIAA Journal,* vol. 14, no. 12, pp. 1675-1682, 1976.

[111] C. Canudas de Wit and P. Tsiotras, "Dynamic tire friction models for vehicle traction control," in *Proc. IEEE Conf. Decision and Control*, Phoenix, AZ, USA, 1999.

[112] B. Breuer, V. Eichorn and J. Roth, "Measurement of tyre/road friction ahead of car and inside the tyre," in *Proc. Int. Symposium Advanced Vehicle Control AVEC*, Yokohama, Japan, 1992.

[113] E. Ono, S. Hosoe, H. Tuan and S. Doi, "Bifurcation in vehicle dynamics and robust front wheel steering control," *IEEE Transactions on Control Systems Technology,* vol. 6, no. 3, pp. 412-420, 1998.

[114] F. Gustafsson, "Slip-based tire-road friction estimation," *Automatica,* vol. 33, no. 6, pp. 1087-1099, June 1997.

[115] S. Müller, M. Uchanski and K. Hedrick, "Estimation of the maximum tire-road friction coefficient," *ASME J. Dyn. Syst. Meas. Control,* vol. 125, no. 4, pp. 607-617, Dec. 2003.

[116] W. Sienel, "Estimation of the tire cornering stiffness and its application to active car steering," in *Proc. IEEE Conf. Decision and Control*, San Diego, CA, USA, 1997.

[117] A. Porcel, P. Laurence, M. Basset and G. Gissinger, "Tyre model for vehicle simulation: Overview and real time solution for critical situations," in *Proceedings of the 2001 IEEE International Conference on Control Applications*, Mexico City, Mexico, 2001.

[118] K. Guo and L. Ren, "A non-steady and non-linear tire model under large lateral slip condition," *SAE Technical Paper Series,* no. 2000-01-0358, pp. 1-8, 2000.

[119] M. Sawada, E. Ono, K. Asano, M. Sugai, S. Ito, M. Yamamoto and Y. Yasui, "Estimation of friction force characteristics between tire and road using wheel velocity and application to braking control," in *Proc. of AVEC Symposium*, Hiroshima, Japan, 2002.

[120] T. Umeno, "Estimation of tire-road friction by tire rotational vibration model," *R&D Review of Toyota,* vol. 37, no. 3, pp. 53-58, 2006.

[121] R. Rajamani, G. Phanomchoeng, D. Piyabongkarn and J. Lew, "Algorithms for real-time estimation of individual wheel tire-road friction coefficients," *IEEE/ASME Transactions on Mechatronics,* vol. 17, no. 6, pp. 1183-1195, December 2012.

[122] A. Daiß, "Model based calculation of friction curves between tyre and road surface," in *Proc. of the 4th IEEE Conference on Control Applications*, Albany, NY, USA, 1995.

[123] C. Lee, K. Hedrick and K. Yi, "Real-time slip-based estimation of maximum tire-road friction coefficient," *IEEE/ASME Transactions on Mechatronics,* vol. 9, no. 2, pp. 454-458, June 2004.

[124] J. Ninomiya, M. Minakawa, Y. Orimoto and J. Nakahara, "Measurement technique of the force transmitted from road surface to tire during actual driving, and its application," in *Proc. of AVEC International Symposium of Advanced Vehicle Control*, Nagoya, Japan, 1998.

[125] A. Andrieux, R. Lengelle, P. Beauseroy and C. Chabanon, "A novel approach to real time tire-road frip and slip monitoring," in *Proc. of the 17th IFAC World Congress* , Seoul, Korea, 2008.

[126] C. Hartung, C. Nuthong and F. Svaricek, "Stochastic models for tyre force estimation: An overview about recent developments and trends," in *Proc. of The 6th IFAC Symposium Advances in Automotive Control*, Munich, Germany, 2010.

[127] M. Doumiati, A. Charara, A. Victorino and D. Lechner, Vehicle dynamics estimation using Kalman filtering, London: John Wiley & Sons, Inc., 2013.

[128] T. Shim and D. Margolis, "Model-based road friction estimation," *Vehicle System Dynamics,* vol. 41, no. 4, pp. 249-276, 2004.

[129] J. Villagra, B. d'Andrea-Novel, M. Fliess and H. Mounier, "A diagnosis-based approach for tire-road forces and maximum friction estimation," *Control Engineering Practice,* vol. 19, pp. 174-184, 2011.

[130] M. Tanelli, L. Piroddi and S. Savaresi, "Real-time identification of tire-road friction conditions," *IET Control Theory and Applications,* vol. 3, no. 7, pp. 891-906, 2009.

[131] C.-S. Liu and H. Peng, "Road friction coefficient estimation for vehicle path prediction," *Vehicle System Dynamics,* vol. Suppl., pp. 413-425, 1996.

[132] J. Matusko, I. Petrovic and N. Peric, "Application of the RBF neural networks for tire-road friction force estimation," in *Proc. of the ISIE'03 - IEEE International Symposium on Industrial Electronics*, Rio de Janeiro, Brazil, 2003.

[133] W. Pasterkamp and H. Pacejka, "Application of neural networks in the estimation of tire/road friction using the tire as sensor," *SAE Technical Paper Series,* no. 971122, pp. 1-7, 1997.

[134] N. Patel, C. Edwards and S. Spurgeon, "Tyre/road friction estimation - a comparison of two observers," in *Proc. of the 16th IEEE International Conference on Control Applications*, Singapore, 2007.

[135] H. Imine, N. M'Sirdi and Y. Delanne, "Sliding-mode observers for systems with unknown inputs: application to estimating the road profile," *Proc. IMechE, Part D: J. Automobile Engineering,* vol. 219, pp. 989-997, 2005.

[136] L. Ray, "Nonlinear tire-force estimation and road friction identification: Field test results," *SAE Technical Paper Series,* no. 960181, pp. 1-9, 1996.

[137] Z. Deng, Z. Qi, Z. Dong, P. He, C. Han and S. Ren, "A road surface identification method for a four in-wheel-motor drive electric vehicle," in *Proc. of the 19th International Conference on Mechatronics and Machine Vision in Practice*, Auckland, New Zealand, 2012.

[138] J. Alonso, J. Lopez, I. Pavon, M. Recuero, C. Asensio, G. Arcas and A. Bravo, "On-board wet road surface identification using tyre-road noise and Support Vector Machines," *Applied Acoustic,* vol. 76, pp. 407-415, 2014.

[139] K. Biligri and K. Kaloush, "Prediction of pavement materials' impedance using ultrasonic pulse velocity," *Road Materials and Pavement Design,* vol. 10, no. 4, pp. 767-787, 2009.

[140] A. Bystrov, M. Abbas, E. Hoare and T.-Y. Tran, "Remote road surface identification using radar and ultrasonic sensors," in *Proc. 11th European Radar Conference*, Rome, Italy, 2014.

[141] J. Paulo, E. Freitas and J. Bento Coelho, "Texture and noise features for road pavement identification and classification," in *Proc. of the 39th International Congress and Exposition on Noise Control Engineering*, Lisbon, Portugal, 2010.

[142] J. Lu, R. Zhou, J. Ding and S. Wu, "Road characteristic identification based on wavelet neural network," in *Proc. of IEEE Intelligent Vehicles Symposium*, Xi'an, China, 2009.

[143] M. Mizuno, T. Takahashi and M. Hada, "Magic Formula tire model using the measured data of a vehicle running on actual roads," in *Proc. of the 4th International Symposium for Advanced Vehicle Control AVEC*, Nagoya, Japan, 1998.

[144] M. Yamada, K. Ueda, I. Horiba and N. Sugie, "Discrimination of the road condition toward understanding of vehicle driving environments," *IEEE Transactions on Intelligent Transportation Systems,* vol. 2, no. 1, pp. 26-31, March 2001.

[145] J. Casselgren, M. Sjödahl, S. Woxneryd and M. Sanfridsson, "Calssification of road conditions - to improve safety," in *Advanced Microsystems for Automotive Applications*, Berlin, Springer-Verlag, 2007, pp. 47-59.

[146] B. Heimann, N. Bouzid and A. Trabelsi, "Road-wheel interaction in vehicles - A mechatronic view of friction," in *Proc. of IEEE International Conference on Mechatronics*, Budapest, Hungary, 2006.

[147] V. Ivanov, B. Shyrokau, K. Augsburg and S. Gramstat, "Advancement of vehicle dynamics control with monitoring the tire rolling environment," *SAE International Journal of Passenger Cars - Mechanical Systems,* vol. 3, no. 1, pp. 199-216, 2010.

[148] V. Ivanov, K. Augsburg and B. Shyrokau, "lterbale fuzzy computing for monitoring tire parameters," in *Proc. of AVEC'08 / International Symposium of Advanced Vehicle Control*, Kobe, Japan, 2008.

[149] V. Ivanov, B. Shyrokau and K. Augsburg, "Handling tyre parameters by uncertain condiions," in *Proc. of The 21st International Symposium on Dynamics of Vehicles on Roads and Tracks IAVSD*, Stockholm, Sweden, 2009.

[150] V. Ivanov and B. Shyrokau, "Fuzzy architecture of safety-relevant vehicle systems," in *Proc. of the 4th International Workshop on Reliable Engineering Computing*, Singapore, 2010.

[151] V. Ivanov, "Fuzzy methods in ground vehicle engineering: state-of-the-art and advanced applications," in *Proc. of the 8th International Conference on Structural Dynamics*, Leuven, Belgium, 2011.

[152] B. Shyrokau and V. Ivanov, "Alterable fuzzy sets in automotive control applications," *International Journal of Modelling, Identification and Control,* vol. 3, no. 3, pp. 305-317, 2008.

[153] V. Ivanov, B. Shyrokau, K. Augsburg and V. Algin, "Fuzzy evlautaion of tyre-surface interaction parameters," *Journal of Terramechanics,* vol. 47, no. 2, pp. 113-130, 2010.

[154] V. Ivanov, K. Augsburg and B. Shyrokau, "Apparatus and method for determimimg the frictional state of a carriageway surface and use thereof". EU Patent EP2089260 (A1), 27 02 2013.

[155] V. Ivanov, "Fuzzy architecture of systems with alterbale information: case study for tyre-ground friction estimators," *International Journal of Reliability and Safety,* vol. 5, no. 3/4, pp. 398-419, 2011.

[156] U. Sandberg, "Relation between tyre/road friction and road texture," Swedish Road and Traffic Research Institute, Linköping, 1990.

[157] V. Ivanov, "Investigation into tyre-road interaction based on fuzzy logic methods," *International Journal of Vehicle Autonomous Systems,* vol. 3, no. 2/3/4, pp. 198-215, 2005.

[158] R. Fruechte, A. Karmel, J. Rillings, N. Schilke, N. Boustany and B. Repa, "Integrated vehicle control," in *Proc. of the 39th IEEE Vehicular Technology Conference*, San Francisco, CA, USA, 1986.

[159] S. Sato, H. Inoue, M. Tabata and S. Inagaki, "Integrated chassis control system for improved vehicle dynamics," in *Proc. of the 1st Advanced Vehicle Control Symposium AVEC*, Yokohama, Japan, 1992.

[160] M. Yamamoto, "Active control strategy for improved handling and stability," *SAE Technical Paper Series,* no. 911902, pp. 1-13, 1991.

[161] J. Wei, Z. Yu and L. Zhang, "Integrated chassis control system for improving vehicle stability," in *Proc. of IEEE International Conference on Vehicular Electronics and Safety ICVES*, Beijing, China, 2006.

[162] M. Velardocchia and A. Vigliani, "Control systems integration for enhanced vehicle dynamics," *The Open Mechanical Engineering Journal,* vol. 7, pp. 58-69, 2013.

[163] J. Zuurbier and P. Bremmer, "State estimation for integrated vehicle dynamics control," in *Proc. of the 7th Advanced Vehicle Control Symposium AVEC*, Hiroshima, Japan, 2002.

[164] J.-X. Wang, N. Chen, D.-W. Pi and G.-D. Yin, "Agent-based coordination framework for integrated vehicle chassis control," *Proc. of the IMechE, Part D: Journal of Automobile Engineering,* vol. 223, pp. 601-621, 1 May 2009.

[165] A. Trächtler, "Integrated vehicle dynamics control using active brake, steering and suspesnion systems," *International Journal of Vehicle Design,* vol. 36, no. 1, pp. 1-12, 2004.

[166] T. Miura, Y. Ushiroda, K. Sawase, N. Takahashi and K. Hayashikawa, "Development of intgegrated vehicle dynamics control systems "S-AWC"," *Mitsubishi Motors Technical Review,* no. 20, pp. 21-25, 2008.

[167] M. Schiebahn, P. Zegelaar and O. Hofmann, "Yaw torque control for vehicle dynamics systems: Theoretical generation of additional yaw torque," in *VDI-Berichte*, Düsseldorf, Germany, VDI-Verlag, 2007, pp. 101-119.

[168] V. Ivanov and D. Savitski, "Systematization of integrated motion control of ground vehicles," *IEEE Access,* vol. 3, pp. 2080-2099, 2015.

[169] A. Hac, D. Doman and M. Oppenheimer, "Unified control of brake- and steer-by-wire systems using optimal control allocation methods," *SAE Technical Paper Series,* no. 2006-01-0924, pp. 1-14, 2006.

[170] R. Hayama, H. Yoshimoto, S. Kawahara, S. Nakano and H. Kumamoto, "Steer-by-wire system integrated with active braking and driving-torque distribution," *Journal of the Japan Society for Precision Engineering,* vol. 76, no. 3, pp. 343-348, 2010.

[171] M. Ahn, B. Kim and M. Lee, "Modeling and control of an anti-lock brake and steering system for cooperative control on split-mu surfaces," *International Journal of Automotive Technology,* vol. 13, no. 4, pp. 571-581, 2012.

[172] R. Marino and S. Scalzi, "Integrated active front steering and semiactive rear differential control in rear wheel drive vehicles," in *Proc. 17th IFAC World Congress*, Seoul, Korea, 2008.

[173] E. Ono, K. Takanami, N. Iwama, Y. Hayashi, Y. Hirano and Y. Satoh, "Vehicle integrated control for steering and traction systems by μ-synthesis," *Automatica,* vol. 30, no. 11, pp. 1639-1647, 1994.

[174] E. Ono, Y. Hattori, Y. Muragishi and K. Koibuchi, "Vehicle dynamics integrated control for four-wheel-distributed steering and four-wheel-distributed traction/braking systems," *Vehicle System Dynamics: International Journal of Vehicles Mechanics and Mobility,* vol. 44, no. 2, pp. 139-151, 2006.

[175] E. Ono, Y. Hattori and Y. Muragishi, "Estimation of tire friction circle and vehicle dynamics integrated control for four-wheel distributed steering and four-wheel distributed traction/braking systems," *R&D Review of Toyota CRDL,* vol. 40, pp. 7-13, 2005.

[176] D. Li, B. Li, F. Yu, S. Du and Y. Zhang, "A top-down integration approach to vehicle stability control," in *Proc. IEEE International Conference on Vehicular Electronics and Safety*, Beijing, China, 2007.

[177] H. Peng, R. Sabahi, S.-K. Chen and N. Moshchuk, "Integrated vehicle control based on tire force reserve optimization control," in *Proc. ASME 2011 International Mechanical Engineering Congress and Exposition*, Denver, CO, USA, 2011.

[178] P. Song, M. Tomizuka and C. Zong, "A novel integrated chassis controller for full drive-by-wire vehicles," *Vehicle System Dynamics: International Journal of Vehicles Mechanics and Mobility,* pp. 1-22, 2015.

[179] S.-B. Lu, S.-B. Choi, Y.-N. Li, M.-S. Seong and J.-S. Han, "Global integrated control of vehicle suspension and chassis key subsystems," *Proc. IMechE, Part D: Journal of Automobile Engineering,* vol. 224, no. 4, pp. 423-441, 2010.

[180] C. Poussot-Vassal, O. Sename, L. Dugard, P. Gaspar, Z. Szabo and J. Bokor, "Attitude and handling improvements through gain-scheduled suspensions and brakes control," *Control Engineering Practice,* vol. 19, no. 3, pp. 252-263, 2011.

[181] J. Villagra, V. Milanes, J. Perez, J. Godoy, E. Onieva, J. Alonso, C. Gonzalez, T. de Pedro and R. Garcia, "A reinforcement learning modular control architecture for fully automated vehicles," *Lecture Notes in Computer Science,* vol. 6928, pp. 390-397, 2012.

[182] C. Knobel, A. Pruckner and T. Bünte, "Optimited force allocation - a general approach to control and to investigate the motion of over-actuated vehicles," in *Proc. of the 4th IFAC Symposium on Mechatronic Systems*, Heidelberg, Germany, 2006.

[183] H. Heo, E. Joa, K. Yi and K. Kim, "Integrated chassis control for enhancement of high speed cornering performance," *SAE International Journal of Commercial Vehicles,* vol. 8, no. 1, pp. 102-109, 2015.

[184] B. Shyrokau, D. Wang and M. Lienkamp, "Integrated vehicle dynamics control based on control allocation with subsystem coordination," in *Proc. 23rd IAVSD International Symposium on Dynamics of Vehicles on Roads and Tracks*, Qingdao, China, 2013.

[185] M. Johansson, S. Zetterstrom and A. Stensson Trigell, "Autonomous corner modules as an enabler for new vehicle chassis solutions," in *Proc. of FISITA World Automotive Congress*, Yokohama, Japan, 2006.

[186] S. Birch, "eCorner is the wheel thing for Siemens," *Automotive Engineering International,* p. 20, March 2007.

[187] "Michelin Active Wheel: the reinvented wheel," [Online]. Available: http://michelin.com.

[188] T. Gordon, M. Howell and F. Brandao, "Integrated control methodologies for road vehicles," *Vehicle System Dynamics,* vol. 40, no. 1, pp. 157-190, 2003.

[189] J. He, D. Crolla, M. Levesley and W. Manning, "Coordination of active steering, driveline, and braking for integrated vehicle dynamics control," *Proc. IMechE, Part D: Automobile Engineering,* vol. 220, pp. 1401-1421, 2006.

[190] C. Rengaraj, D. Crolla, G. Hilton and A. Wheatley, "Integration of active driveline, active steering, active suspension and active brake for an improved vehicle dynamic performance," in *Proc. 21st IAVSD International Symposium on Dynamics of Vehicles on Roads and Tracks*, Stockholm, Sweden, 2009.

[191] K. Jalali, T. Uchida, S. Lambert and J. McPhee, "Development of an advanced torque vectoring control system for an electric vehicle with in-wheel motors using soft computing techniques," *SAE International Journal of Alternative Powertrains,* vol. 2, no. 2, pp. 261-278, 2013.

[192] J. Kang, J. Yoo and K. Yi, "Driving control algorithm for maneuverability, lateral stability, and rollover prevention of 4WD electric vehicles with independently driven front and rear wheels," *IEEE Transactions on Vehicular Technology,* vol. 7, pp. 2987-3001, 2011.

[193] L. Laine and J. Fredriksson, "Traction and braking of habrid electric vehicles using control allocation," *Interntaional Journal of Vehicle Design,* vol. 48, no. 3/4, pp. 271-298, 2008.

[194] B. Shyrokau and D. Wang, "Control allocation with dynamic weight scheduling for two-task integrated vehicle control," in *Proc. of the 11th International Symposium on Advanced Vehicle Control*, Seoul, Korea, 2012.

[195] P. Reinold and A. Traechtler, "Closed-loop control with optimal tire-force distribution for the horizontal dynamics of an electric vehicle with single-wheel chassis actuators," in *Proc. American Control Conference (ACC)*, Washington, DC, USA, 2013.

[196] J. Wang and R. Longoria, "Coordinated and reconfigurable vehicle dynamics control," *IEEE Transactions on Control Systems Technology,* vol. 17, no. 3, pp. 723-732, 2009.

[197] S. Yim, J. Choi and K. Yi, "Coordinated control of hybrid 4WD vehicles for enhanced maneuverability amd lateral stability," *IEEE Transactions on Vehicular Technology,* vol. 61, no. 4, pp. 1946-1950, 2012.

[198] M. Schiebahn, P. Zegelaar, M. Lakehal-Ayat and O. Hofmann, "The yaw torque influence of active safety systems and smart actuators for coordinated vehicle dynamics control," *Vehicle System Dynamics,* vol. 48, no. 11, pp. 1269-1284, 2010.

[199] V. Ivanov, K. Augsburg, B. Shyrokau, D. Wang and V. Vantsevich, "Advanced agent-based vehicle dynamics control," in *Proc. of the Europena Automotive Congress EAEC*, Valencia, Spain, 2011.

[200] V. Ivanov, B. Shyrokau, K. Augsburg and V. Vantsevich, "System fusion in off-road vehicle dynamics control," in *Proc. of the Joint 9th Asia-Pacific ISTVS Conference*, Sapporo, Japan, 2010.

[201] B. Shyrokau and D. Wang, "Coordination of steer angles, tyre inflation pressure, brake and drive torques for vehicle dynamics control," *SAE International Journal of Passenger Cars - Mechanical Systems,* vol. 6, no. 1, pp. 241-251, 2013.

[202] B. Shyrokau, D. Wang, L. Heidrich and K. Hoepping, "Analysis of subsystems coordination for electric vehicle during straight-line braking and brake-in-turn," in *IEEE Symposium Series on Computational Intelligence*, Singapore, 2013.

[203] B. Shyrokau, D. Savitski, D. Wang, V. Ivanov and K. Augsburg, " Analysis of coordination and novel blending strategy between friction brake system and electric motors," in *Dresden, Germany*, 2013, Proc. of the Eurobrake Conference.

[204] L. Heidrich, B. Shyrokau, D. Savitski, V. Ivanov, K. Augsburg and D. Wang, "Hardware-in-the-loop test rig for integrated vehicle control systems," in *Proc. of the 7th IFAC Symposium on Advances in Automotive Control*, Tokyo, Japan, 2013.

[205] B. Shyrokau, D. Wang, D. Savitski and V. Ivanov, "Vehicle dynamics control with energy recuperation based on control allocation for independent wheel motors and brake system," *International Journal of Powertrains,* vol. 2, no. 2/3, pp. 153-181, 2013.

[206] K. Augsburg, S. Gramstat, R. Horn, V. Ivanov, H. Sachse and B. Shyrokau, "Test-rig-in-the-loop (TRIL) application to controllable brake processes," in *Proc. EuroBrake 2012 Conference*, Dresden, Germany, 2012.

[207] K. Augsburg, S. Gramstat, R. Horn, V. Ivanov, H. Sachse and B. Shyrokau, "Investigation of brake control using test rig-in-the-loop technique," *SAE Technical Paper Series,* no. paper 2011-01-2372, 2011.

[208] D. Crolla and D. Cao, "The impact of hybrid and electric powertrains on vehicle dynamics, control systems and energy regeneration," *Vehicle System Dynamics,* vol. 50, no. supl, pp. 95-109, 2012.

[209] S. Murata, "Innovation by in-whhel-motor drive unit," *Vehicle System Dynamics,* vol. 50, no. 6, pp. 807-830, 2012.

[210] D. Akaho, M. Nakatsu, E. Katsuyama, K. Takakuwa and K. Yoshizue, "Development of vehicle dynamics control system for in-wheel-motor vehicle," in *Proc. of the JSAE Annual Congress (Spring)*, Yokohama, Japan, 2010.

[211] G. Freitag, M. Gerlich, D. Bergmann, G. Pais and B. Fischer, "Replacement of the friction brake by a wheel hub drive," in *Proc. of the 3rd International Munich Chassis Symposium chassi.tech plus*, Munich, Germany, 2012.

[212] G. Freitag, M. Klopzig, K. Schleicher, M. Wilke and M. Schramm, "High-performance and highly efficient electric wheel hub drive in automotive design," in *Proc. of the 3rd International Electric Drive Production Conference (EDPC)*, Nuremberg, Germany, 2013.

[213] J. Wang, Q. Wang, L. Jin and C. Song, "Independent wheel torque control of 4WD electric vehicle for differential drive assisted steering," *Mechatronics,* vol. 21, pp. 63-76, 2010.

[214] L. De Novellis, A. Sorniotti, P. Gruber and A. Pennycott, "Comparison of feedback control techniques for torque-vectoring control of fully electric vehicles," *IEEE Transactions on Vehicular Technology,* vol. 63, no. 8, pp. 3612-3623, 2014.

[215] T. Yoshimura, H. Uchida, H. Nasu, J. Hino and R. Ueno, "Traction force control of an electric vehicle in 2WS-4WD using fuzzy reasoning," *International Journal of Vehicle Design,* vol. 18, no. 5, pp. 442-454, 1997.

[216] Y. Hori, Y. Toyoda and Y. Tsuruoka, "Traction control of electric vehicle: basic experimental results using the test EV "UOT electric march"," *IEEE Transactions on Industry Applications,* vol. 34, no. 5, pp. 1131-1138, 1998.

[217] T. Akiba, R. Shirato, T. Fujita and J. Tamura, "A study of novel traction control method for electric motor driven vehicle," in *Proc. of the PCC'07 Power Conversion Conference*, Nagoya, Japan, 2007.

[218] V. Delli Colli, G. Tomassi and M. Scarano, “"Single Wheel" longitudinal traction control for electric vehicles,” *IEEE Transactions on Power Electronics,* vol. 21, no. 3, pp. 799-808, 2006.

[219] D. Yin and Y. Hori, “A new approach to traction control of EV based on maximum effective torque estimation,” in *Proc. of the 34th Annual Conference of IEEE Industrial Electronics IECON*, Orlando, FL, USA, 2008.

[220] D. Yin, S. Oh and Y. Hori, “A novel traction control for EV based on maximum transmissible torque estimation,” *IEEE Transactions on Industrial Electronics,* vol. 56, no. 6, pp. 2086-2094, 2009.

[221] J. Hu, D. Yin and Y. Hori, “Fault-tolerant traction control of electric vehicles,” *Control Engineering Practice,* vol. 19, no. 2, pp. 204-213, 2011.

[222] K. Fujii and H. Fujimoto, “Traction control based on slip ratio estimation without detecting vehicle speed for electric vehicle,” in *Proc. of the PCC'07 Power Conversion Conference*, Nagoya, Japan, 2007.

[223] L. Li, S. Kodama and Y. Hori, “Back-EMF-absed slip prevention controller for EV simulated by DC motor system,” in *Proc. of the 23rd Chinese Control Conference*, Shanghai, China, 2004.

[224] F. Bottiglione, A. Sorniotti and L. Shead, “The effect of half-shaft torsion dynamics on the performance of a traction control system for electric vehicles,” *Proc. of zje IMechE, Part D: Journal of Automobile Engineering,* vol. 226, no. 9, pp. 1145-1159, 2012.

[225] T. Weiskircher and S. Müller, “Control performance of a road vehicle with four independent single-wheel electric motors and steer-by-wire system,” *Vehicle System Dynamics,* vol. 50, no. suppl. 1, pp. 53-69, 2012.

[226] Y.-P. Yang and C.-P. Lo, “Current distribution control of dual driven wheel motors for electric vehicles,” *Control Engineering Practice,* vol. 16, pp. 1285-1292, 2008.

[227] N. Mutoh, T. Kazama and K. Takita, “Driving characteristics of an electric vehicle system with independently driven front and rear wheels,” *IEEE Transactions on Industrial Electronics,* vol. 53, no. 3, pp. 803-813, 2006.

[228] W. Sung, J. Shin and Y.-S. Jeong, “Energy-efficient and robust control for high-performance induction motor drive with an application in electric vehicles,” *IEEE Transactions on Vehicular Technology,* vol. 61, no. 8, pp. 3394-3405, 2012.

[229] G. Götting and R. De Doncker, “Active drive control of electric vehicles using a modal state observer,” in *Proc. of the 35th Annual IEEE Power Electronics Specialists Conference*, Aachen, Germany, 2004.

[230] R. J.M., R. Meneses and J. Orus, “Active vibration control for electric vehicle compliant drivetrains,” in *Proc. of IECON 2013 Conference of the IEEE Industrial Electronics Society*, Vienna, Austria, 2013.

[231] C. Maini, P. Ramaraju, S. Veerabetappa Munirangiah, B. Paul and S. Hameed, “Antilock braking for vehicles”. WO Patent 2010/049945 A1, 2010.

[232] S. Murata, “Vehicle behavior control device, and vehicle behavior control method”. USA Patent US 2010/0292882, 2010.

[233] C. Song, J. Wang and L. Jin, “Study on the composite AVS control of vehicles with four electric wheels,” *Journal of Computers,* vol. 6, no. 3, pp. 618-626, 2011.

[234] S.-I. Sakai and Y. Hori, “Advantage of electric motors for anti skid control of electric vehicle,” *European Power Electronics and Drives Journal,* vol. 11, no. 4, pp. 26-32, 2001.

[235] T. Bera, K. Bhattacharya and A. Samantaray, "Bond graph model-based evaluation of a sliding mode controller for a combined regenerative and antilock braking system," *Proceedings of the IMechE, Part I: Journal of Systems and Control Engineering,* vol. 226, no. 8, pp. 1060-1076, 2012.

[236] C. Mi, H. Lin and Y. Zhang, "Iterative learning control of antilock braking of electric and hybrid vehicles," *IEEE Transactions on Vehicular Technology,* vol. 54, no. 2, pp. 486-494, 2005.

[237] P. Khatun, C. Bingham and P. Mellor, "Comparison of control methods for electric vehicle antilock braking / traction control systems," *SAE Technical Paper Series,* no. 2001-01-0596, 2001.

[238] J. Zhang, D. Kong, L. Chen and X. Chen, "Optimization of control strategy for regenerative braking of an electrified bus equipped with an anti-lock braking system," *Proc. IMechE, Part D: Journal of Automobile Engineering,* vol. 226, no. 4, pp. 294-506, 2012.

[239] H. Ha, J. Kim and J. Lee, "VDC of in-wheel EV simulation based on precise wheel torque control," *Lecture Notes in Computer Science (including subseries Lecture Notes in Artificial Intelligence and Lecture Notes in Bioinformatics,* vol. 8102, no. 1, pp. 153-181, 2013.

[240] M. Ellims, H. Monkhouse, D. Harty and T. Gade, "Using vehicle simulation to investigate controllability," *SAE International Journal of Alternative Powertrains,* vol. 2, no. 1, pp. 18-36, 2013.

[241] N. Mutoh and Y. Nakano, "Dynamics of front-and-rear-wheel-independent-drive-type electric vehicles at the time of failure," *IEEE Transactions on Industrial Electronics,* vol. 59, no. 3, pp. 1488-1499, 2012.

[242] M. Rosenberger, R. Uhlig, T. Koch and M. Lienkamp, "Combining regenerative braking and anti-lock braking for enhanced braking performance and efficiency," *SAE Technical Paper Series,* no. 2012-01-0234, 2012.

[243] V. Ivanov, J. Orus, T. Pütz, F. Brungs, D. Savitski and B. Shyrokau, "Electric and friction braking control systems for AWD electric vehicles," in *Proc. of FISITA 2014 World Automotive Congress*, Maastricht, The Netherlands, 2014.

[244] V. Ivanov, D. Savitski, K. Augsburg, B. Knauder, P. Barber and J. Zehetner, "Wheel slip control for all-wheel drive electric vehicle," in *Proc. of the 18th Conference of the International Society for Terrain-Vehicle Systems ISTVS*, Seoul, Korea, 2014.

[245] V. Ivanov, B. Shyrokau, D. Savitski, J. Orus, R. Meneses, J. Rodriguez, J. Theunissen and K. Janssen, "Design and testing of ABS for electric vehicles with individually controlled on-board motor drives," *SAE International Journal of Passenger Cars – Mechanical Systems,* vol. 7, no. 2, pp. 902-913, 2014.

[246] V. Ivanov, D. Savitski and B. Shyrokau, "A survey of traction control and anti-lock braking systems of full electric vehicles with individually-controlled electric motors," *IEEE Transactions on Vehicular Technology,* October 2014.

[247] D. Savitski, V. Ivanov, B. Shyrokau, J. De Smet and J. Theunissen, "Experimental study on continuous ABS operation in pure regenerative mode for full electric vehicle," *SAE International Journal of Passenger Car - Mechanical System,* vol. 8, no. 1, 2015.

[248] D. Savitski, V. Ivanov, L. Heidrich, K. Augsburg and T. Pütz, "Experimental investigation of braking dynamics of electric vehicle," in *Proc. of Eurobrake 2013 Conference*, Dresden, Germany, 2013.

[249] J. Theunissen, K. Verhaege, S. van Aalst, O. Cruyt, J. De Smet, S. Battain, R. Verdaasdonk, D. Seenbeke and J. de Clercq, “Powertrain architecture of electric vehicles with individually controlled switched reluctance motors,” in *Proc. of FISITA 2014 World Automotive Congress*, Maastricht, The Netherlands, 2014.